THE UNIVERSITY OF OXFORD

Department of Cardiovascular Medicine

Cardiovascular Manifestations of Marfan Syndrome: Insights from Advanced Cardiovascular Magnetic Resonance

Doctor of Philosophy Thesis

Alex Pitcher
New College
Michaelmas 2012

ABSTRACT

Marfan syndrome (MFS) is the commonest inherited disorder of connective tissue and is associated with a high risk of potentially life-threatening complications, including aortic aneurysm, dissection and rupture, and, perhaps, ventricular disease. This work describes the prospective application of advanced cardiovascular magnetic resonance techniques to the aorta and heart of consecutive, unselected subjects with MFS, and to appropriately matched control populations.

Comprehensive 3D visualisation of blood flow in the entire thoracic aorta of subjects with MFS was achieved using a time-resolved phase-contrast magnetic resonance technique with 3-directional velocity encoding (4D flow), demonstrating a high prevalence of major flow disturbance (87 ± 12%), compared to controls (28 ±18%), localising to those regions of the aorta known to be most prone to aortic dissection (sinuses of Valsalva and proximal descending aorta). Wall shear stress, recently identified as a potentially important determinant of aneurysm progression and rupture, was interrogated in these datasets at the sinuses of Valsalva (SOV), ascending aorta (AA), arch, and proximal (PDA) and distal descending aorta (DDA), using the 4D flow datasets, and was shown to be significantly reduced at each location (SOV -15%; AA -12%; Arch -17%; PDA -18%; and DDA -14%, $p<0.05$ for each), in subjects with MFS compared to healthy subjects.

4D flow datasets were used to generate relative pressure maps in healthy subjects and in subjects with several aortic diseases. A novel method for the separate evaluation of the components of relative pressure was applied, revealing marked differences in the relative contribution of the components of pressure (unsteady > convective >> viscous), and characteristic differences between subjects in overall relative pressure, and its components. Left ventricular volumes and function were evaluated in subjects with MFS, and did not differ significantly from healthy subjects in the absence of significant valvular regurgitation and / or shunt. Left ventricular end-diastolic volume varied markedly with degree of regurgitation ($r=0.75$, $p=0.0001$). The mechanistic implications of these findings, and the potential role of these techniques in the evaluation of cardiovascular disease, are discussed.

ACKNOWLEDGEMENTS

I would like to express my sincere thanks to the many people who have helped me to undertake my research over the last four years, many of whom are world leaders in their field and I am very humbled that they would give their advice and discuss ideas with me so willingly.

Prof. Stefan Neubauer and Dr Steffen Petersen have been superb, inspiring supervisors, and I am very grateful for their mentorship, which I hope will continue. I have benefitted enormously from interactions with and expert advice from many colleagues locally, particularly Dr Edward Blair, Dr Colin Forfar, Dr Paul Leeson, Prof. Hugh Watkins, and Prof. Paul Wordsworth, to whom I extend my great thanks. I am grateful to Mrs Jane Francis for her help with scanning, for teaching me so much about CMR and for everything else, and to Mrs Hayley Harvey for her hard work and loyalty. I am also grateful to my colleagues in OCMR, too numerous to name here, who have made my time in OCMR very memorable, but particular thanks to Sacha, Joe, Vanessa, and Banjo.

I am very grateful to my collaborators: Prof. Nic Smith, Dr Sebastian Krittian and Dr Pablo Lamata in the UK; Prof. Michael Markl and Dr Alex Barker in Chicago; Dr Ramona Lorenz, Dr Jelena Bock and Dr Bernd Jung in Freiburg; Dr Carl-Johan Carhäll, Prof. Tino Ebbers, and Dr Petter Dyverfeldt in Linköping. I am grateful to the 4D Flow team, for valuable discussions and technical expertise, including Dr Saul Myerson and Dr Malenka Bissell and to the physics team, Dr Aaron Hess, Dr Elizabeth Tunnicliffe, Dr Stefan Piechnik, Dr Luca Biassiolli, and Dr Matthew Robson.

Thanks are due to my students, Luke Granger, Anisha Ramessur, Alec Maynard, and Margaret Neher, and to Tom Cassar in particular, who knows how much I owe him (literally and figuratively), and to my patients with Marfan syndrome and Loeys-Dietz syndrome, in particular to those who agreed to participate in this study, whose patience and generosity is much appreciated. Finally, I would like to thank my family, and Kathleen.

DECLARATION

The work described in this thesis is my own. Prof. Stefan Neubauer and Dr Steffen Petersen contributed to the design of the project and gave advice throughout. Dr Forfar, Dr Blair, Prof. Wordsworth and Dr Kohler supported recruitment of subjects with Marfan syndrome. Mrs Jane Francis assisted with data acquisition. Dr Michael Markl and colleagues provided training and physics support for the 4D flow implementation. Mr Tom Cassar assisted with 4D flow data analysis for Chapters 3, 4 and 5. Dr Sebastian Krittian developed the finite-element approach to non-invasive pressure estimation based on 4D flow data, and Dr Pablo Lamata and I together developed the methods for the analysis, visualisation and interpretation of components of pressure estimation, described in Chapter 5, and Dr Malenka Bissell provided the dataset of a subject with bicuspid aortic valve disease discussed in this chapter. Mr Luke Granger assisted with data analysis for Chapter 6, and Dr Joanna D'Arcy and Dr Bernard Prendergast provided all data on patients with mitral regurgitation but no features of Marfan syndrome from the OxValve project, used in Chapter 6. Where figures have been reproduced from published work, the permission of the copyright holder has been granted.

MANUSCRIPTS ARISING FROM THIS WORK

Pitcher A, Lamata P, Krittian S, Forfar JC, Blair E, Wordsworth BP, Markl M, Smith N, Petersen SE, Neubauer S. Towards a comprehensive description of the haemodynamics of the aorta in Marfan syndrome. Manuscript in preparation.

Lamata P*, **Pitcher A***, Krittian S, Nordsletten D, Bissell M, Cassar T, Barker AJ, Markl M, Neubauer S, Smith NP. Aortic relative pressure components in health and disease derived from 4D flow cardiovascular magnetic resonance. *Journal of Cardiovascular Magnetic Resonance* (submitted). (*=both authors contributed equally to this work).

Krittian SB, Lamata P, Michler C, Nordsletten DA, Bock J, Bradley CP, **Pitcher A**, Kilner PJ, Markl M, Smith NP. A finite-element approach to the direct computation of relative cardiovascular pressure from time-resolved MR velocity data. Med Image Analysis. 2012 Jul;16(5):1029-37.

Pitcher A, Ashby D, Elliott P, Petersen SE. Cardiovascular MRI in clinical trials: expanded applications through novel surrogate endpoints. Heart. 2011 Aug; 97(16):1286-92.

ABSTRACTS ARISING FROM THIS WORK

Pitcher A* Lamata P*, Krittian SB, Nordsletten D, Bissell MM, Francis, Cassar TE, Barker AJ, Markl M, Neubauer S, Smith N. Towards a comprehensive description of relative aortic pressure: insights from 4D flow CMR. SCMR 2013**.**

Pitcher A, Ramessur A, Cassar T, Blair E, Wordsworth P, Leeson P, Francis JM, Bock J, Lorenz R, Barker A, Forfar JC, Markl M, Petersen SE, Neubauer S. Aortic blood flow disturbance and wall shear stress in Marfan syndrome: insights from 4D phase-contrast CMR. AHA 2011.

Pitcher A, Cassar TE, Leeson P, Francis JM, Blair E, Wordsworth P, Forfar JC, Petersen SE, Markl M, Neubauer S. Aortic dissection: visualisation of aortic blood flow and quantification of wall shear stress using time-resolved, 3D phase-contrast MRI. SCMR 2011.

Pitcher A, Cassar TE, Suttie J, Francis JM, Leeson P, Blair E, Wordsworth BP, Forfar JC, Myerson SG, Markl M, Neubauer SN, Petersen SE. Visualisation of aortic flow disturbance in Marfan syndrome by 4D phase-contrast CMR. SCMR 2011.

Pitcher A, Leeson P, Forfar C, Trevitt C, Francis J, Neubauer S and Petersen SE. Aortic distensibility decreases during exercise in normal volunteers *from* 13th Annual SCMR Scientific Sessions Phoenix, AZ, USA. 21-24 January 2010 *Journal of Cardiovascular Magnetic Resonance* 2010, 12(Suppl 1):P136

Pitcher A, Cassar TE, Leeson P, Francis JM, Blair E, Wordsworth BP, Forfar JC, Petersen SE, Markl M, Neubauer S. Visualisation and quantification of aortic root blood flow and wall shear stress using time-resolved, 3D phase-contrast MRI. British Heart Foundation Centre for Research Excellence Symposium, Oxford, September 2010.

CONTENTS

Abstract 2
Acknowledgements 3
Declaration 4
Manuscripts arising from this work 5
Abstracts arising from this work 6
Contents 7
List of abbreviations 11
List of figures 13
Chapter 1 13
Chapter 3 13
Chapter 4 13
Chapter 5 14
Chapter 6 15
List of tables 16
Chapter 3 16
Chapter 4 16
Chapter 5 16
Chapter 6 16
1.1. Overview 18
1.2. Marfan syndrome 19
1.2.1. Epidemiology and clinical features 19
1.2.2. Historical background 19
1.2.3. Diagnosis 20
1.2.4. Molecular pathogenesis 20
1.2.5. Cardiovascular manifestations of Marfan syndrome 24
1.2.6. Prognosis 24
1.2.7. Current role of cardiovascular imaging 25
1.2.8. Current role of cardiovascular magnetic resonance in patient management 26
1.2.9. Therapeutic options 26
1.2.10. Need for improved imaging strategies for risk stratification 28
1.3. Cardiovascular magnetic resonance 29
1.3.1. Basic principles of cardiovascular magnetic resonance 29
1.3.2. Phase-contrast principle 30
1.4. Aims 37
2.1. Ethics 39
2.2. Subject recruitment 39
2.3. Study eligibility 39
2.4. Study design 39

2.5. Study protocol 40
2.6. CMR data acquisition 41
2.6.1. CMR hardware 41
2.6.2. CMR protocols 41
2.6.3. Ventricular volumes and function 41
2.6.4. Phase-contrast CMR acquisitions 42
2.6.5. Phase-contrast data pre-processing and visualisation 43
2.6.6. Phase-contrast data post-processing 43
2.7. Statistical methods 43
2.7.1. Descriptive statistics 43
2.7.2. Parametric tests 43
2.7.3. Non-parametric tests 44
3.1. Abstract 46
3.1.1. Background 46
3.1.2. Methods 46
3.1.3. Results 46
3.1.4. Conclusions 47
3.2. Introduction 48
3.3. Methods 49
3.3.1. Subjects 49
3.3.2. Study protocol 49
3.3.3. CMR data acquisition and pre-processing 49
3.3.4. Data post-processing 51
3.3.5. Aortic visualisation and evaluation 52
3.3.6. Intra-observer reproducibility methods 54
3.4. Results 55
3.4.1. Baseline characteristics 55
3.4.2. Analysable segments 55
3.4.3. Inter-rater agreement 55
3.4.4. Prevalence of any flow disturbance 55
3.4.5. Prevalence of major flow disturbance 58
3.5. Discussion 61
3.5.1. Summary of findings 61
3.5.2. Aspects of study methodology 62
3.5.3. Mechanisms 63
3.6. Conclusions 64
4.1. Abstract 66
4.1.1. Background 66
4.1.2. Methods 66
4.1.3. Results 66

4.1.4. Conclusions 67
4.2. Introduction 68
4.2.1. Aim 68
4.3. Methods 69
4.3.1. Subjects and protocol 69
4.3.2. Wall shear stress analysis 69
4.3.3. Definition of an analysable segment 71
4.3.4. Accuracy of segmentation 71
4.3.5. Reproducibility of WSS estimation 71
4.4. Results 73
4.4.1. Baseline characteristics 73
4.4.2. Analysability of imaging planes 73
4.4.3. Accuracy of segmentation 73
4.4.4. Reproducibility of WSS estimates 73
4.4.5. Mean WSS at aortic locations 73
4.5. Discussion 79
4.6. Conclusions 82
5.1. Abstract 84
5.1.1. Background 84
5.1.2. Methods 84
5.1.3. Results 84
5.1.4. Conclusions 85
5.2. Introduction 86
5.2.1. Aim 87
5.3. Methods 88
5.3.1. Computational methods 88
5.3.2. Case selection 88
5.3.3. CMR data acquisition 90
5.3.4. CMR data pre-processing 90
5.3.5. Pressure estimation 90
5.3.6. Visualisation and calculation of spatio-temporal maps of relative pressure 91
5.4. Results 92
5.4.1. Healthy volunteers 92
5.4.2. Diseased subjects 95
5.5. Discussion 99
5.5.1. Summary of findings 99
5.5.2. Aspects of study design and methodology 99
5.5.3. Relationship to other methodologies 100
5.5.4. Mechanistic implications of findings 102
6.1. Abstract 105

6.1.1. Background 105
6.1.2. Methods 105
6.1.3. Results 105
6.1.4. Conclusions 106
6.2. Introduction 107
6.3. Methods 109
6.3.1. Subjects 109
6.3.2. Protocol 109
6.3.3. CMR data acquisition 109
6.3.4. CMR data analysis 110
6.3.5. Assessment of shunt and valvular regurgitation 110
6.4. Results 111
6.4.1. Baseline characteristics 111
6.4.2. Left and right ventricular volumes and systolic function 111
6.4.3. Relationship between LVEDV and regurgitation and/or shunt 111
6.4.4. Relationship between LVEDV and regurgitation in subjects with and without MFS 114
6.5. Discussion 116
6.5.1. Aspects of methodology 117
6.6. Conclusions 120
7.1. Summary of findings 122
7.2. Mechanisms of aortic disease in Marfan syndrome 123
7.3. Clinical application of 4D flow 125
REFERENCES 126

LIST OF ABBREVIATIONS

AA	Ascending aorta
AIIRB	Angiotensin II receptor antagonist
ANOVA	Analysis of variance
AoD	Aortic dissection
ARB	Angiotensin II receptor antagonist
AT/AT1/AT2	Angiotensin receptor type 1 / type 2
BAV	Bicuspid aortic valve
BMI	Body mass index
BMP	Bone Morphogenic Protein
BP	Blood pressure
BRC	Biomedical Research Centre
BSA	Body surface area
CFD	Computational fluid dynamics
CI	Confidence interval (95% unless specified)
CMR	Cardiovascular magnetic resonance
DDA	Distal descending aorta
DICOM	Digital Imaging and Communications in Medicine
ECG	Electrocardiogram
EMT	Endothelial-to-mesenchymal transition
ERK 1/2	Extracellular signal-regulated kinases
FBN1	Fibrillin-1
GRAPPA	Generalized auto-calibrating partially parallel acquisitions
HV	Healthy volunteers
IRAD	International Registry of Aortic Dissection
JNK	c-Jun N-terminal kinases
LAP	Latency associated peptide
LTBP	Latency-associated peptide binding protein
LV	Left ventricle
LVEDV	Left ventricular end-diastolic volume
LVEF	Left ventricular ejection fraction
LVESV	Left ventricular end systolic volume
MAPK	Mitogen-activated protein kinases
MFS	Marfan syndrome
MR	Mitral regurgitation
MRI	Magnetic resonance imaging
mRNA	Messenger ribonucleic acid
OSI	Oscillatory shear index
PAA	Proximal ascending aorta
PC-MRA	Phase-contrast magnetic resonance angiogram
PC-MRI	Phase-contrast magnetic resonance imaging
PD	Pressure difference
PDA	Proximal descending aorta
RAAS	Renin-angiotensin-aldosterone system
RV	Right ventricle
RVEDV	Right ventricular end diastolic volume
RVEF	Right ventricular ejection fraction
RVESV	Right ventricular end systolic volume
SoV	Sinuses of Valsalva
SSFP	Steady-state free-precession imaging
SV	Stroke volume

TE	Echo time
TF	Transcription factors
TGFβ	Transforming growth factor beta
TR	Repetition time
VENC	Velocity-encoding range
WSS	Wall shear stress

LIST OF FIGURES

CHAPTER 1

Figure 1.1: Model of normal regulation of TGFβ by microfibrils and perturbations associated with microfibrillar deficiency in MFS

Figure 1.2: Early diastolic still frame from an SSFP cine acquisition in a modified, oblique coronal slice position, of a patient with MFS, showing dilation of the sinuses of Valsalva and a central jet of aortic regurgitation

Figure 1.3: Principles of phase-contrast imaging

Figure 1.4: Anatomical data arising from a 4D flow acquisition can be visualised either as magnitude data or as a phase-contrast magnetic resonance angiogram

Figure 1.5: Data acquisition for time-resolved, phase-contrast flow acquisitions with 3-directional velocity encoding

CHAPTER 3

Figure 3.1: Velomap tool (Matlab)

Figure 3.2: The Ensight visualisation platform

Figure 3.3: Definition of aortic segments and positioning of planes for particle traces and streamlines

Figure 3.4: Prevalence of flow disturbance by aortic region in subjects with MFS and in healthy subjects

Figure 3.5: Prevalence of major flow disturbance by aortic region in subjects with MFS and in healthy subjects

Figure 3.6: Still frames from an animation showing time-resolved 3-dimensional velocity encoded (4D flow) images of the aorta of a patient with Marfan syndrome and a healthy volunteer

CHAPTER 4

Figure 4.1: Clip Plane orientation for flow and wall shear stress quantification

Figure 4.2: Anatomical distribution of wall shear stress interrogation planes in an oblique sagittal view of the aorta

Figure 4.3: Flowtool user interface

Figure 4.4: Correlation between direct measurement of aortic dimensions, and segmentation-derived estimates of aortic dimensions

Figure 4.5: Bland-Altman analysis of measured compared to estimated aortic dimensions

Figure 4.6: Bland-Altman analysis of intra-observer reproducibility

Figure 4.7: Mean temporally-averaged and spatially-averaged vectorial WSS at five anatomical areas of interest for subjects with MFS compared to healthy subjects

Figure 4.8: Mean WSS by aortic dimensions at the sinuses of Valsalva among healthy subjects

Figure 4.9: Mean WSS by aortic dimensions at the sinuses of Valsalva among subjects with MFS

CHAPTER 5

Figure 5.1: Input velocity field of a healthy volunteer projected on streamlines and estimated pressure projected on fluid domain boundary at various points in the cardiac cycle

Figure 5.2: Overview of the methodology for the computation of the spatio-temporal maps of relative pressure in the aorta

Figure 5.3: Schematic representation of the temporal transients of pressure in the aorta

Figure 5.4: Average temporal evolution of the aortic pressure difference between the sinotubular junction and the descending aorta (at a distance of 250 mm from the aortic root) in three healthy volunteers, decomposed in its three components: unsteady, convective and viscous

Figure 5.5: Average spatial evolution of the aortic pressure difference in the three healthy subjects in systole

Figure 5.6: Spatio-temporal pressure maps in the six subjects analysed

Figure 5.7: Detailed anatomical inspection of the convective pressure in four of the subjects under study, showing velocity streamlines coloured by pressure

Figure 6.1: Relationship between stroke volume difference and LVEDV in subjects A: with MFS and B: with mitral regurgitation and with no features of MFS

LIST OF TABLES

CHAPTER 3

Table 3.1: Baseline characteristics of subjects

Table 3.2: Proportion of analysable segments

Table 3.3: Inter-rater agreement

CHAPTER 4

Table 4.1: Number of analysable segments by region and overall, for subjects with Marfan syndrome and healthy subjects

CHAPTER 5

Table 5.1: Summary of qualitative characteristics observed in the pressure differences (PD) in the aorta, and its components, in healthy and diseased subjects

Table 5.2: Unsteady pressure indexes in healthy and diseased subjects

CHAPTER 6

Table 6.1: Baseline characteristics of subjects

Table 6.2: Ventricular parameters in MFS and healthy subjects

CHAPTER 1

INTRODUCTION AND AIMS

1.1. OVERVIEW

Marfan syndrome (MFS) is an inheritable disorder of connective tissue, which predisposes to aortic dilation, dissection and rupture; to valvular heart disease; perhaps to heart muscle disease; and to premature but often preventable death from cardiovascular causes (1). There is marked variability in the severity of the condition between affected individuals (even within affected families) and this is reflected in a highly variable degree of cardiovascular involvement (2).

Cardiovascular magnetic resonance (CMR) allows detailed phenotyping of inherited and acquired cardiovascular diseases (3). Novel CMR approaches have the potential to further our understanding of aspects of the pathophysiology of MFS. In particular, advances in phase-contrast magnetic resonance acquisition and analysis uniquely allow the reliable estimation of blood velocity everywhere within the entire thoracic aorta in 3D, and throughout the cardiac cycle, such that many aspects of aortic blood flow and pressure can be visualised and quantified in a single acquisition (4).

Application of advanced CMR imaging techniques may provide novel insights into the mechanisms of cardiovascular disease in MFS, elucidate factors underlying the variability which is characteristic of the condition, and identify candidate risk markers which predict risk of progressive disease and/or complications in future longitudinal studies and clinical trials (5).

1.2. MARFAN SYNDROME

1.2.1. EPIDEMIOLOGY AND CLINICAL FEATURES

MFS is the commonest inheritable connective tissue disorder, affecting approximately 1 in 5,000 people, and almost always caused by a mis-sense mutation in the fibrillin-1 (FBN1) gene on the long arm of chromosome 15 (6-9), which encodes a component of extra-cellular microfibrils, which have a complex role in maintaining tissue architecture and in regulating local tissue signalling in a number of diverse tissues throughout the body. Approximately one-third of sufferers carry a de-novo mutation, and the trait is inherited in an autosomal dominant pattern with high penetrance. Affected patients may have manifestations in a number of organ systems, with the cardiovascular, ocular, musculoskeletal, pulmonary and integumentary systems most prominently involved.

1.2.2. HISTORICAL BACKGROUND

Marfan syndrome (OMIM #154700) is named after Antoine Bernard Marfan (1858–1942), who described a 5-year-old girl with severe skeletal abnormalities (10). Although this patient has subsequently been thought to have features more suggestive of congenital contracture arachnodactyly (OMIM #121050) (11,12), many more cases of what came to be known as Marfan syndrome were described in the early twentieth century. Early attention was paid only to the musculoskeletal manifestations, but its pleiotropic nature began to be recognised with the recognition of ocular lens dislocation in 1914 by Börger. Case reports of serious cardiovascular complications, including aortic aneurysm and aortic dissection, first appeared in 1943, and cardiovascular features in over 100 patients were described by McKusick in 1955 (1), emphasising the high prevalence, wide range and marked variability of cardiovascular abnormalities of the disease. Developments in cardiovascular imaging, particularly echocardiography, confirmed the very high prevalence and marked variation in the severity of the cardiovascular phenotype, even within affected members of the same family.

1.2.3. DIAGNOSIS

Diagnostic criteria for heritable disorders of connective tissue (including MFS) were defined by expert consensus in 1986 (13). A widely accepted revision to the diagnostic criteria "The revised Ghent nosology" was proposed in 1996 (14), taking account of developments in the molecular genetics of MFS, and these criteria were further revised in 2010 (15).

MFS is a clinical diagnosis requiring the presence of specific combinations of features in several organ systems (14,15). Cardiovascular imaging is mandatory whenever the disease is suspected, and at least annually thereafter (16). The diagnosis may require specialised investigations, including spinal and pelvic imaging, and genetic testing in selected cases, but identification of a FBN1 variant is neither necessary nor sufficient to make the diagnosis.

1.2.4. MOLECULAR PATHOGENESIS

The molecular pathogenesis of MFS was elusive for many decades, with many candidate genes and gene products being proposed and subsequently refuted (17,18). The microfibril was suspected of involvement, and in 1986 a new connective tissue protein fibrillin was discovered by Sakai and colleagues (19), and was shown to be a major component of microfibrils. Immunohistochemical methods showed that fibrillin was deficient or absent in the skin, cultured dermal fibroblasts or both of patients with MFS, but not in healthy subjects or in patients with other connective tissue disorders. A candidate gene approach localised the genetic defect to a region on the long arm of chromosome 15 (9,20) and the genetic basis of the condition was finally elucidated in 1991 with confirmation of the precise location of the defect, partial sequencing of the FBN1 gene, and demonstration of a de-novo mis-sense mutation in two families each with a single affected offspring, but unaffected parents. Subsequent studies fully sequenced the gene, and have now identified over 1,000 pathogenic mutations in families worldwide.

The fundamental defect which underlies the pleiotropic manifestations of MFS is a defect in the FBN1 gene product, the fibrillin-1 protein, which is a component of 10–12 nm extracellular calcium-binding microfibrils, occurring either in association with elastin or in elastin-free bundles (19,21). These microfibrils have an important structural role in diverse tissue types, but also have a regulatory role, particularly in controlling the local and circulating levels of Transforming Growth Factor Beta (TGFβ) and Bone Morphogenetic Protein (BMP), thus being key determinants of signalling through these ubiquitous signalling pathways (22,23).

In recent years, there has been enormous progress in our understanding of how defects in the fibrillin-1 protein give rise to arterial wall deficiency. In brief, it is now clear that normal extra-cellular fibrillin-rich microfibrils indirectly bind and sequester TGFβ in its inactive form (i.e. bound covalently to Latent TGFβ-Binding Protein (LTBP) via non-covalent association with Latency-Associated Peptide (LAP)), and so contribute to the regulation of local and circulating TGFβ levels and thus TGFβ signalling, the control of which is essential for normal vascular smooth muscle cell, fibroblast and endothelial cell function (Figure 1.1) (21). In MFS, abnormal fibrillin-1 fails to bind TGFβ, resulting in increased circulating levels and excessive and deleterious downstream TGFβ signalling in multiple cell types (21). Evidence from animal models (24,25) and human studies (26,27) converge on the central importance of dysregulated TGFβ signalling in many of the manifestations of MFS and related disorders, and at least in mice and probably also in humans, as being the principal cause of aortic disease (28). The importance of this new model of MFS is not least that TGFβ signalling (unlike fibrillin-1) is a potential pharmacological target, and specifically that angiotensin II plays a key role in activating downstream TGFβ signalling in epithelial cells (29) and vascular smooth muscle cells (30,31). These findings provide an explanation for the dramatic, beneficial effects of the angiotensin II receptor antagonist, losartan, on aortic structure in mice (24) and (in uncontrolled studies) in humans (26), and the rationale for a number of controlled trials of AIIRBs planned or underway internationally (32-35).

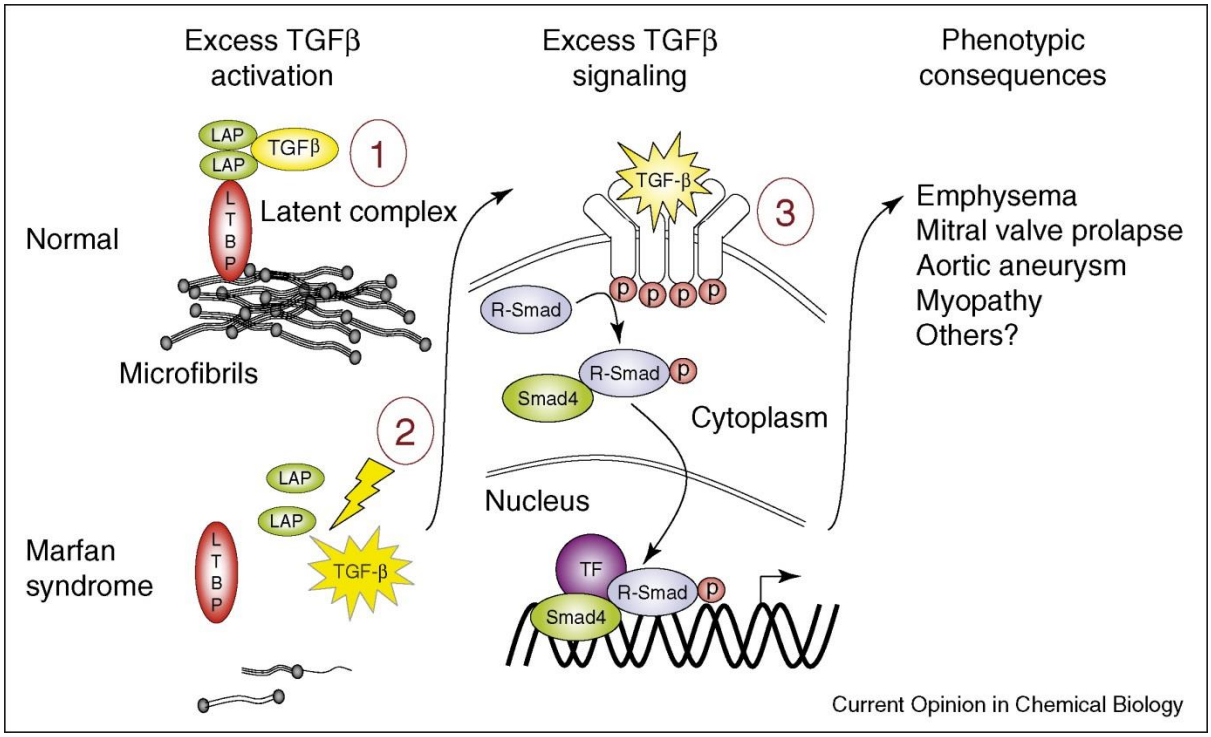

Figure 1.1: Model of normal regulation of TGFβ by microfibrils and perturbations associated with microfibrillar deficiency in MFS. Extracellular microfibrils normally bind the large latent complex of TGFβ, composed of the mature cytokine (TGFβ), latency-associated peptide (LAP) and one of three latent TGFβ binding proteins (LTBPs) (1). This interaction suppresses the release of free and active TGFβ. In the absence of sufficient functional microfibrils (e.g. owing to deficiencies of fibrillin-1, an important component of the microfibril, such as occur in MFS), failure of matrix sequestration of the large latent complex leads to increased total TGFβ and promiscuous activation of TGFβ (lightning bolt) by multiple mechanisms (2). Free and active TGFβ (star burst) interacts with its cell surface receptor (3), resulting in downstream phosphorylation (P) of the receptor-activated smad proteins (R-Smads 2 and 3), which can (in their phosphorylated form) bind to Smad4 and translocate from the cytoplasm to the nucleus, where, in combination with transcription factors (TFs), they mediate TGFβ-induced transcriptional responses. Genes downstream of TGFβ induce a number of the phenotypic consequences in MFS (although probably not all consequences) including developmental emphysema, myxomatous changes of the mitral valve and mitral valve prolapse, aortic aneurysm formation and skeletal muscle myopathy. Selective AT1 receptor blockade is believed to rescue these phenotypes by decreasing the expression of TGFβ, by decreasing expression of TGFβ receptor, by decreasing the

expression of activators of TGFβ such as thrombospondin-1, and by increasing the availability of AT to bind to AT2 receptors with potentially beneficial effects on vascular smooth muscle cell behaviour. Reproduced (with modifications to the figure legend) by permission of Elsevier, from Ramirez and Dietz et al, *Current Opinion in Genetics and Development* (23).

Figure 1.2: Early diastolic still frame from an SSFP cine acquisition in a modified, oblique coronal slice position, of a patient with MFS, showing dilation of the sinuses of Valsalva and a central jet of aortic regurgitation (courtesy of Dr Saul Myerson).

1.2.5. CARDIOVASCULAR MANIFESTATIONS OF MARFAN SYNDROME

There are a number of cardiovascular manifestations of MFS. Dilation of the ascending aorta, particularly at the sinuses of Valsalva, gives rise to 'flask-shape' dilation, which is often progressive, is the most characteristic cardiovascular feature, and is present to some extent in most patients (Figure 1.2). Dissection of the aorta, sometimes with rupture to the adventitia and beyond, is the most important complication and remains the commonest cause of premature death in MFS. Intimal tears (more correctly called intimo-medial tears) usually originate in the ascending aorta, typically at the sinuses of Valsalva, but there is increasing recognition that the proximal descending thoracic aorta and the abdominal aorta may also be the site of aortic dissection, either as a first aortic complication or following aortic root surgery (36). The proximal pulmonary arteries can be dilated in MFS, but dissection is rare, and the clinical significance of this finding is uncertain (37). Other arteries are only rarely the site of an intimo-medial tear in dissections. Mitral leaflet thickening and redundancy, perhaps with abnormalities of the sub-valvular apparatus, both contribute to a high prevalence of mitral valve prolapse, which can give rise to mitral regurgitation for which mitral valve surgery may be required (38). The tricuspid valve may be similarly affected, but in isolation does not usually require intervention. Increased left ventricular dimensions, volumes and function have been variably reported by a number of authors using a variety of imaging techniques (including CMR), but the existence of a specific Marfan cardiomyopathy remains controversial. In particular, currently reported studies have not always described methods for rigorously excluding subjects with regurgitant valve lesions and/or shunting.

1.2.6. PROGNOSIS

The natural history of MFS in historical series, prior to the widespread availability of prophylactic medical and surgical therapy for aortic root disease, was bleak, with a reported median age at death of 34 years (39). Recent series have found much better survival rates (40), reflecting improved recognition of mild cases, a higher proportion of sufferers diagnosed as a result of cascade screening of affected relatives (who tend to be more mildly affected than probands), and the advent of medical

treatment and surgical replacement of the aortic root, and improved awareness by patients and improved recognition and treatment of acute aortic dissection clinicians.

Risk stratification of patients with MFS is based on (i) absolute maximum aortic dimensions; (ii) rate of aortic dilation; and (iii) the presence or absence of a family history of aortic dissection at normal or only modestly increased aortic dimensions (41). In general, patients are offered prophylactic surgery if the aortic root measures ≥50mm; if the rate of aortic expansion is ≥5mm per year; or if the aortic dimension is ≥45mm in a patient with a family history of aortic dissection at an aortic dimension at <50mm. A number of other approaches to risk stratification have been proposed, including lower thresholds in women (42), setting surgical thresholds based on indexation of aortic dimensions to body-surface area (42), estimates of central aortic pressure or augmentation index based on radial artery applanation tonometry (43), and aortic pulse wave velocity based on magnetic resonance imaging approaches (44), but none have been evaluated in prospective studies, and they have not been widely accepted in clinical practice.

1.2.7. CURRENT ROLE OF CARDIOVASCULAR IMAGING

Cardiovascular imaging is mandatory whenever the diagnosis of MFS is known or suspected, and should be undertaken annually in affected subjects. In the management of MFS, accurate knowledge of cardiovascular anatomy and function derived from imaging studies contributes to diagnosis, risk stratification and prognostication, and influences lifestyle, occupational, contraceptive and pregnancy advice. It also allows screening of at-risk family members, identification of patients likely to benefit from medical therapy, identification of patients in whom aortic and/or valvular surgery is required, and detailed pre-operative and post-operative evaluation of such patients. Imaging is essential for the detection and classification of aortic dissection. Imaging is also used for the evaluation of eligibility, and as the primary endpoint for numerous randomised clinical trials and an international prospective meta-analysis (45).

1.2.8. CURRENT ROLE OF CARDIOVASCULAR MAGNETIC RESONANCE IN PATIENT MANAGEMENT

CMR is a powerful and versatile technique (46) which has particular strengths in the evaluation of cardiovascular disease in MFS (47), and which is beginning to emerge as the optimal imaging strategy for specific types of patients with MFS, and to ascertain certain types of information (41).

Patients with MFS often have severe chest wall and spinal deformities, which can limit echocardiographic windows, and CMR can provide comprehensive imaging in these patients. Patients with MFS may require repeated imaging of the entire thoracic aorta at frequent intervals throughout life, beginning in childhood or early adulthood, and so are particularly at risk of high levels of cumulative ionising radiation exposure from other modalities (e.g. computed tomography).

Moreover, CMR can provide incremental information, not readily available using other techniques, particularly regarding aortic elasticity and the pattern of blood flow within the great vessels, and quantitative measures of blood flow and vessel wall parameters, which may provide insight into disease mechanisms, and may be used as markers of future disease progression. CMR cannot be used in all patients, and those with implanted devices or pacemakers, or those with severe claustrophobia, may not be able to undergo CMR.

1.2.9. THERAPEUTIC OPTIONS

Therapy in MFS can be medical or surgical. Beta-blockers are used in the prevention of aortic dilation in subjects with MFS. A single randomised, open-label study reported reduced rate of aortic growth among subjects allocated to propranolol treatment compared to those allocated placebo (48). Limitations of this study were its small sample size, and the possibility of bias owing to the open-label trial design. A meta-analysis concluded that there was little evidence to support the use of beta-blockers in MFS (49). Angiotensin converting enzyme-inhibitors reduced measures of arterial stiffness in a small study (50).

The emerging role of TGFβ has focused attention on angiotensin receptor antagonists (ARBs) as a potential therapy for the aortic disease of MFS. ARBs are thought to downregulate Type 1 Angiotensin Receptor signalling through a range of mechanisms, and the ARB losartan had a dramatic effect on aortic dimensions in a mouse model of MFS (24), and in an uncontrolled retrospective study in humans (26). Ten randomised trials (32,33,51-56), and a prospective individual-patient data meta-analysis of all of these trials of ARB therapy (45) are currently underway worldwide, to evaluate the effectiveness of ARBs therapy in MFS, but have not yet been completed.

Options for surgical therapy for the prevention of aortic dissection in MFS include aortic valve and aortic root replacement with a composite valve-graft conduit (CVG replacement), and uncommonly, homograft aortic root replacement or allograft porcine aortic root replacement. These procedures all involve sacrifice of the native aortic valve. The CVG replacement is a reproducible operation, with a low risk of serious complications and a durable outcome in large case series from experienced centres. The limitations of the technique are the need for lifelong anticoagulation (in the case of mechanical CVG replacement), or the need for re-do surgery for homograft or allograft deterioration (in the case of homograft CVG, homograft aortic root replacement and allograft porcine aortic root replacement). Aortic valve sparing surgery was developed to address these limitations, and has developed along two parallel lines, with the Yacoub remodelling procedure (57) and the David re-implantation procedure (58) both being used. Both procedures are technically demanding, and perhaps less predictable durability of repair compared to CVG procedures, but have been shown to have low peri-operative mortality, and provide generally durable repairs for the majority of patients. Some iterations of the Yacoub re-modelling procedure were found to be associated with significant post-operative aortic regurgitation, and the approach is generally avoided if the annulus reaches 30mm, where the sub-annular suture line of the David procedure is said to provide some protection from this complication at higher annulus diameters. Recent advances in aortic surgery, particularly augmented by computer-aided design, rapid-prototyping and advances in surgical technique, mean that patient-specific, customised aortic external support devices are now becoming available (59), with promising medium-

term results, but are currently being evaluated only in subjects with aortic root diameters <50mm, and have not been extensively tested in subjects with aortic root diameters greater than 50mm.

1.2.10. NEED FOR IMPROVED IMAGING STRATEGIES FOR RISK STRATIFICATION

Currently recommended thresholds for prophylactic aortic root replacement do not capture all patients at risk of ascending aortic dissection and rupture, with aortic dissection below current guidelines being well recognised. Recent data from the international registry of aortic dissection (IRAD which is a prospective registry of patients with aortic dissections and not a prospective registry of MFS *per se*) suggest a significant proportion of subjects with MFS and aortic dissection had aortic dimensions below currently recommended thresholds at the time of, or immediately prior to, sustaining aortic dissection (Isselbacher, personal communication). Historical observational studies demonstrate that many patients are advised to undergo surgery on the basis of current treatment thresholds, in whom surgery could have been safely deferred (had it been possible to ascertain their risk more precisely), and are therefore exposed to the risks of surgery and often the need for lifelong aortic surgery at a younger age. Dissection of the proximal *descending* aorta accounts for up to 20% of dissections in subjects with MFS, and is not reliably predicted by aortic size (36). This proportion is likely to increase as the proportion of patients undergoing prophylactic aortic root surgery increases. Finally the emergence of a wider range of medical and surgical therapeutic strategies available to clinicians increases the need to make rational decisions about the magnitude of the risk posed to an individual, and thus to identify those patients most likely to benefit from more or less aggressive therapy.

New hypotheses regarding the fundamental molecular mechanisms by which mutations in fibrillin-1 give rise to aortic dilation have identified a number of pharmacological targets for which a number of promising candidate therapies for the prevention of aortic disease have been and will continue to be identified (51,60-62). Furthermore, evolving surgical therapies require evaluation to ensure that the risks and benefits of the emerging approaches are favourable (59).

1.3. CARDIOVASCULAR MAGNETIC RESONANCE

CMR is a powerful set of techniques, based on the nuclear magnetic resonance principle which allows the evaluation of many aspects of cardiovascular function, using a range of imaging (3) and spectroscopic (63) tools. CMR is now widely used for many indications in clinical practice, and is particularly valuable for the evaluation of novel therapies (5). It is non-invasive and well-tolerated by the vast majority of subjects. The technique itself carries no known risks (as long as safety precautions are followed), and specifically does not require the use of ionising radiation (unlike CT and nuclear methods). CMR is extremely versatile, and this versatility arises from the very wide range of pulse sequences available. A limited number of sequences are typically required to answer specific questions and these can often be completed in a single study lasting ~30–45 minutes. CMR provides a quantitative assessment of many aspects of cardiovascular structure and function, such as left and right ventricular function, valve function, vascular function and blood flow. It can determine the presence and extent of myocardial scar, fibrosis and oedema and can quantitatively evaluate myocardial perfusion, metabolism, and myocardial tissue characteristics.

1.3.1. BASIC PRINCIPLES OF CARDIOVASCULAR MAGNETIC RESONANCE

A full discussion of the principles of CMR is beyond the scope of this work and is provided elsewhere (64). Isotopes with an odd number of protons and/or neutrons have a property called spin. When placed in an external magnetic field B0, spins align in such a way as to produce a magnetic field, called the net magnetisation vector. In a magnetic resonance experiment, an incident radiofrequency pulse is applied to a sample, causing perturbation of the net magnetisation vector. Subsequently, the sample generates a magnetic field, which oscillates in the radiofrequency range, which is detected by radiofrequency coils. The frequency of this signal is called the Larmor frequency, and is determined by the gyromagnetic ratio for the species, and the external magnetic field. Since the Larmor frequency varies with field strength, by applying a non-uniform, but known, magnetic field (a spatial magnetic field gradient), information can be derived concerning the spatial location of a signal.

1.3.2. PHASE-CONTRAST PRINCIPLE

The physical principles underlying the phase-contrast phenomenon are described in detail elsewhere (65). A simplified description follows. Precessing spins can precess in phase or out of phase with each other. When precessing spins move through a magnet field gradient, the frequency of precession changes, resulting in a phase-shift in the emitted signal of a magnitude proportional to the strength of the gradient and to the velocity of the moving spin, and in a direction dependent upon the direction of the gradient and of the movement. Phase-contrast imaging techniques exploit this principle to allow visualisation and quantification of blood vessels and blood flow by generating contrast between flowing blood and stationary tissues by manipulating the phase of magnetisation, such that the net magnetisation from stationary spins is zero, and the phase of the moving spins is non-zero.

In phase difference images, the signal is linearly related to the velocity of the moving spins, with spins of greater velocity giving rise to a larger signal than spins with a lower velocity. Both flow-sensitive and flow-compensated images are acquired for each acquisition. The non-flow encoded image is digitally subtracted from each of the flow-encoded images, to eliminate phase accumulations from sources other than velocity, yielding a high contrast image, giving true phase images (Figure 1.3). A particular advantage of the phase-contrast technique is that the technique does not destroy the signal relating to magnitude (anatomical) information (Figure 1.4). Thus anatomical information can be reconstructed from the acquired data. In addition, a further advantage of the phase-contrast method is that by combining the data from both the magnitude and phase images, a so-called phase-contrast angiogram can be obtained, containing useful anatomical data.

Flow imaging used in clinical practice typically has a single velocity encoding direction, usually planned perpendicular either to the vessel or to the flow jet of interest (which will often, but not always, be coaxial). Three-directional velocity (or flow) encoding requires a velocity encoding gradient to be acquired in each of three mutually orthogonal planes in separate TR intervals. In addition, a fourth non-flow encoded acquisition is acquired, as a reference image.

The sequence used for 4D flow is a gradient echo sequence, which allows short echo times, and short repetition times, so speeding up acquisitions (Figure 1.5) (4). The gradient echo pulse sequence uses very low flip angles (e.g. 7–15 degrees), and RF pulse spoiling to reduce the time required for recovery of longitudinal magnetisation, so reducing TR. During each cardiac cycle only a subset (n_k) of all required (N) phase encoding steps are collected. The procedure has to be repeated for a total of N/n_k heartbeats to acquire the full dataset (4). This process is called k-space segmentation, and the important implication is that the final dataset is composed of data averaged over many heartbeats, typically several hundred. The scan time is therefore given by the expression: n x TR x NSA x #SE x #PE, where n is the number of acquisitions (=4 in a 3D dataset), TR is the repetition time, NSA is the number of signal averages, PE is the number of phase encoding steps and SE is the number of slice-encoding values. Various methods are employed to reduce acquisition time. The non-flow encoded image is digitally subtracted from each of the flow-encoded images, to eliminate phase accumulations from sources other than velocity, yielding a high contrast image.

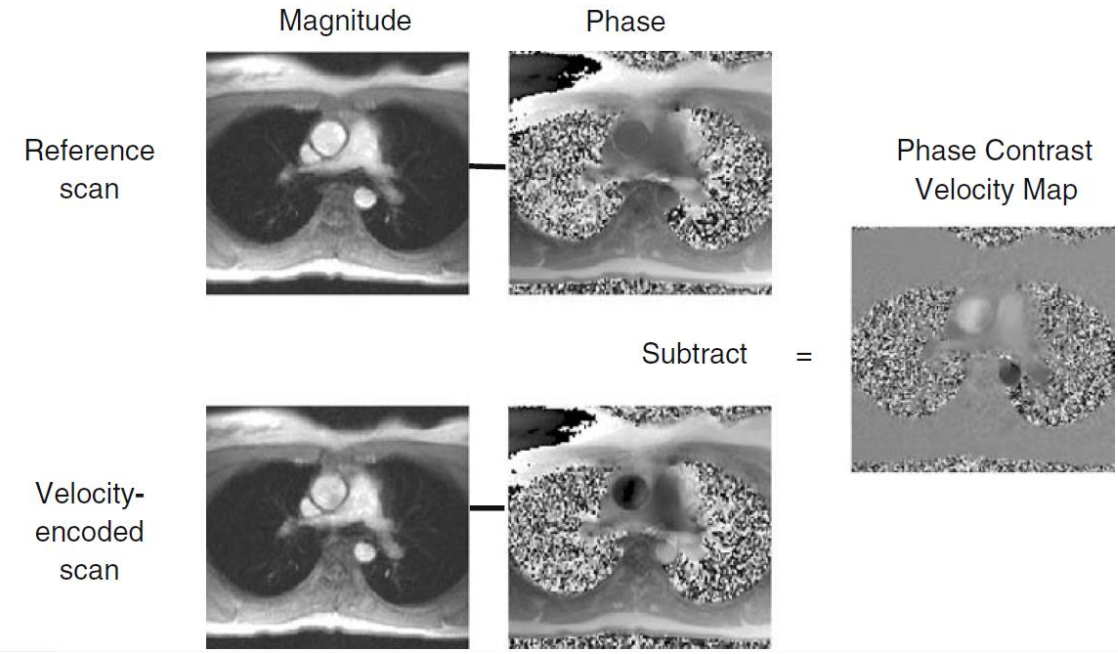

Figure 1.3: Magnitude and phase images are reconstructed from the reference scan (top row) and also from the velocity-sensitive scan (bottom row). The phase images are subtracted to make the phase-contrast image (velocity map). Reproduced with permission from Gatehouse, Keegan, Crowe et al European Radiology (65).

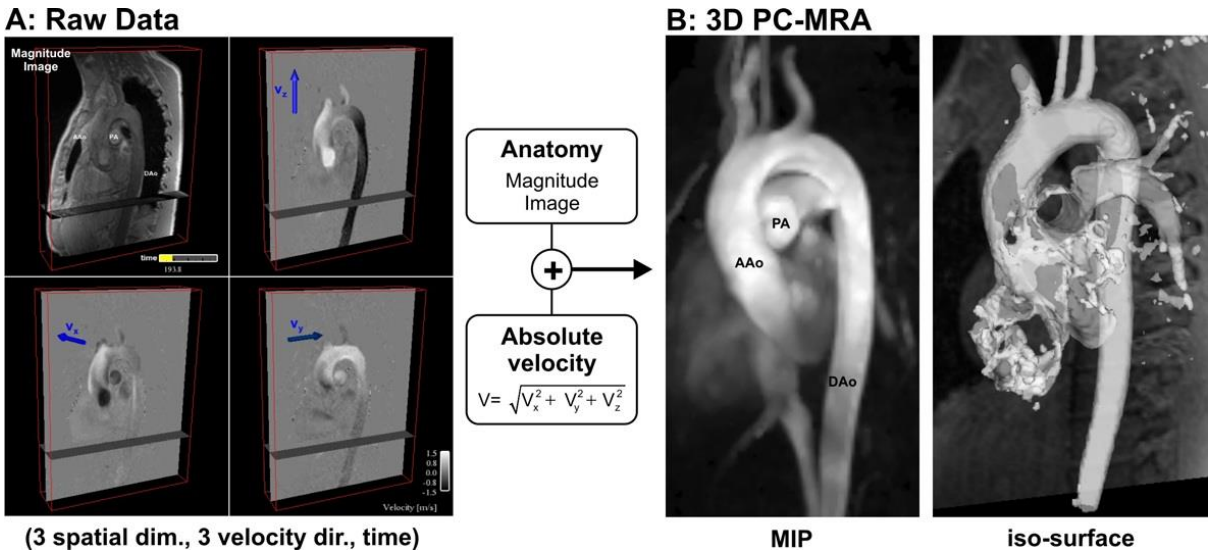

Figure 1.4: Anatomical data arising from a 4D flow acquisition can be visualised either as magnitude data (Figure A, top left, Mag) or as a phase-contrast magnetic resonance angiogram, PC-MRA, which is based on the root mean square sum of the velocities in each voxel, with manual thresholding. This can be viewed as a maximum intensity projection (MIP) or as a semi-transparent 3D iso-surface, alone or in combination with flow data. Reproduced by permission (with modifications) from Markl, Kilner and Ebbers (4).

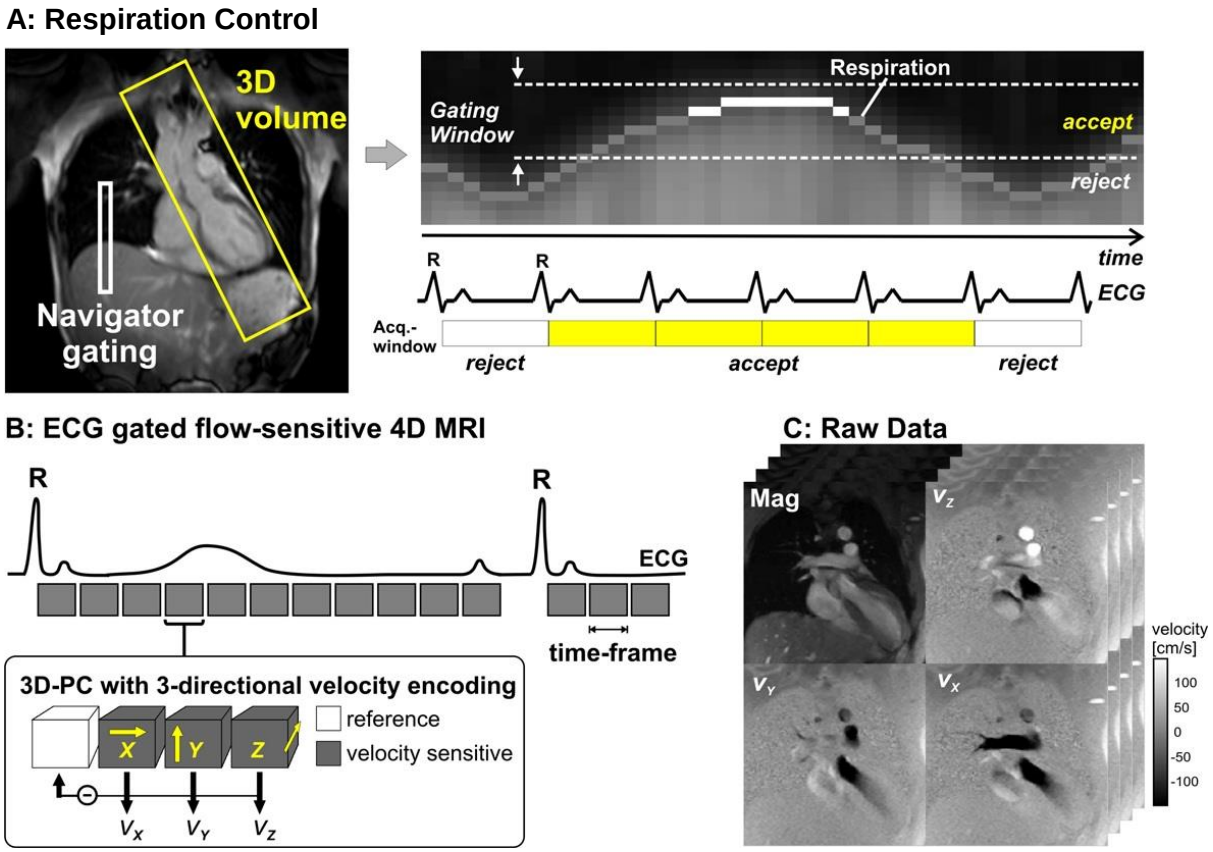

Figure 1.5: Data acquisition for time-resolved, phase-contrast flow acquisitions with 3-directional velocity encoding. Figure A: a 3D field of view is defined (here, over the left ventricle and ascending aorta), and a CMR navigator is positioned over the diaphragm, with a defined acceptance window within which data will be accepted, to allow respiratory gating. Respiratory gating also allows adaptive k-space re-ordering to reduce acquisition time (not shown). Figure B: Acquisitions are synchronised to the ECG using prospective gating. For each time-frame, a flow compensated acquisition and three flow sensitive acquisitions are performed with interleaving. Figure C: Datasets comprise anatomical or magnitude (Mag) data and velocity data (represented by grey scale intensity) encoded in 3 spatial directions and by time in the cardiac cycle (not represented here, but can be imagined as a further set of similar stacks of images). Reproduced by permission (with modifications) from Markl, Kilner and Ebbers (4).

In many CMR applications, sufficient data for high-contrast, high-resolution cine imaging can be acquired in a single breathhold. 4D flow datasets, however, require data to be acquired over many cardiac cycles and so must be acquired during free-breathing. In order to overcome artefacts relating to respiratory motion which would otherwise severely compromise image quality, a number of respiratory motion compensation strategies have been implemented, including respiratory navigator gating, respiratory bellows or self-gating. Respiratory navigator gating is most widely used, and was the method employed in this work using the method described by Markl et al (66). Navigator gating makes frequent measurements of the position of the diaphragm throughout the acquisition (typically once per cardiac cycle in end-diastole) and uses this data in real-time to inform the data acquisition and offline to inform the reconstruction process, such that data is only accepted when the respiratory cycle is within a narrow window defined around end-expiration. Adaptive k-space re-ordering (in which phase encoding is based on the position of the respiratory cycle) has improved scan efficiency, and so reduces scan time without substantial deterioration in image quality. Advances in respiratory compensation have been an important factor in making the implementation of 4D flow in clinical research studies feasible.

Phase-contrast techniques generally have modifiable sensitivity to particular velocity ranges, which allows discrimination of velocities within a defined range. A consequence is that velocities which fall outside of the range specified will be misrepresented in the image, and so careful selection of the appropriate velocity encoding range, or appropriate post-acquisition adjustment, is required to optimise images. Where the calculated, cross-sectional area of the evaluated vessel is known, flow can be calculated from the expression: flow = area x average velocity.

Visualisation of time-varying flow in 3-spatial dimensions requires 3D visualisation platforms, requiring high-performance graphics capabilities and multi-core processors. These platforms have been modified for this application from software developed for use in the automotive and aerospace industries.

While it is quite possible, in principle, to depict the entire velocity field, it is not generally meaningful or desirable to do so, as the information content is greater than can be appreciated by the human visual system. Thus it is necessary to seek a trade-off between identifying important flow features and overwhelming the viewer with large data-loads. This is made possible by the use of a number of visualisation tools including vector arrows, streamlines and pathlines. These tools allow different approaches to evaluating the same dataset, and each can allow optimal visualisation of particular types of flow. A further tool, the spatio-temporal relative pressure map, is introduced in this work, and provides a concise summary of the time-resolved pressure field for relatively straightforward visualisation.

A number of studies have described and quantified aspects of flow in the normal human thoracic aorta using 4D flow techniques. These studies describe mild (usually right-handed) helical flow, and mild early diastolic retrograde flow particularly in the ascending aorta and aortic arch (summarised in (4). Several studies have described a number of derived parameters allowing the potential for understanding the forces and characteristics of the arterial wall. In particular, wall shear stress (WSS) (67,68) and pulse wave velocity (69) have been estimated based on 4D flow datasets. These studies show marked regional variation in WSS in different aortic locations (70), with potential implications for the distribution of aortic disease (68). Studies of healthy older subjects have found modest differences in blood flow pattern and WSS distribution (71).

4D flow characteristics have been defined in a number of pathological entities affecting the aorta, including atherosclerosis, aortic aneurysms, aortic dissection and aortic coarctation, bicuspid aortic valve disease and after surgical repair of the aortic root. A particularly important study used pathline visualisation of aortic datasets to demonstrate a potential mechanism by which atherosclerotic plaque in the proximal descending aorta could be carried into the carotid arteries, and could thus be a potential source of embolic stroke in otherwise cryptogenic stroke (72).

1.4. AIMS

The aims of this work were (i) to describe the flow patterns seen in subjects with Marfan syndrome, compared to healthy adult subjects; (ii) to define the pattern and distribution of wall shear stress in these patients; (iii) to apply a novel method for the non-invasive estimation of relative pressure to aortic flow datasets; (iv) to extend the relative pressure estimation to allow the isolation of components of pressure estimation; (v) to evaluate biventricular volumes and function in Marfan syndrome and to relate these to degree of shunting or valvular regurgitation.

We sought to test the following hypotheses:

(i) to determine whether the flow patterns seen in subjects with Marfan syndrome, differed from those of healthy adult subjects and to estimate the anatomical distribution and extent of any differences;

(ii) to determine whether wall shear stress differed between subjects with MFS and healthy volunteer adult subjects;

(iii) to determine whether a novel method for the non-invasive estimation of relative pressure estimation could be used to identify differences in pressure distributions and in the isolation of pressure components to aortic flow datasets;

(iv) to determine whether biventricular volumes and function differ in unselected patients with MFS in Marfan syndrome

CHAPTER 2

METHODS

2.1. ETHICS

The study was conducted in accordance with the principles of the Declaration of Helsinki (73). A favourable ethical opinion was obtained from the Oxfordshire regional ethics committee (reference 07/H0604/150) and the study design was peer-reviewed by the Oxford BRC Heart (now Cardiovascular) theme. All participants gave written informed consent.

2.2. SUBJECT RECRUITMENT

Subjects with MFS were identified from the Oxford inherited aortic diseases clinic. The diagnosis of MFS was made according to the Ghent criteria (1996) (14), and physical findings were confirmed in all cases by a cardiologist, geneticist, rheumatologist and/or ophthalmologist, each experienced in the diagnosis of MFS. Healthy subjects were recruited by advertising at sites in the University of Oxford.

2.3. STUDY ELIGIBILITY

Potential subjects were eligible for the study if they were aged 16 years or older; had capacity to give informed consent; and were willing to undergo study procedures. Subjects were ineligible if they were unable to undergo study procedures (in particular, if they had contra-indications to CMR). Subjects with MFS were additionally required to have a definite diagnosis of MFS according to the 1996 Ghent criteria (14). Healthy subjects were included only if they had no known or suspected cardiovascular disease.

2.4. STUDY DESIGN

The study design is that of an observational case-control study. Subjects were recruited in three categories:

(i) Subjects with MFS and no prior history of cardiovascular surgery or dissection

(ii) Age-, sex- and height-matched healthy subjects

(iii) Subjects with MFS and complex aortic disease, defined as prior aortic root and/or aortic valve surgery and/or prior aortic dissection

Each subject completed a medical questionnaire, underwent a physical examination including anthropometric measures, and underwent a CMR acquisition using a 1.5T CMR system, followed by a further CMR acquisition using a 3T system, at the same study visit.

2.5. STUDY PROTOCOL

Each subject underwent study procedures in a particular sequence on a single morning between 8am and 12 noon, following an overnight fast (clear fluids were permitted). All subjects were asked to refrain from smoking, consuming caffeine, and vigorous exertion for 24 hours prior to the study visit. Subjects with MFS treated with beta-blockers were asked to withhold these medications for 72 hours prior to the study visit.

Relevant parts of the medical notes of subjects with MFS were reviewed (with consent) to confirm study eligibility, and to extract relevant clinical information, including the results (where available) of genetic testing.

Each subject completed a medical questionnaire and underwent a physical examination by a medical practitioner. Height, weight, arm span, and upper body segment were measured. Arm span:height and upper segment:lower segment ratios were calculated. Body Mass Index (BMI) was calculated using the Quetelet index (74) and body surface area (BSA) was calculated using the method of Du Bois (75). Systolic and diastolic blood pressures were measured with an oscillatory sphygmomanometer at the right arm with the patient in the supine position for 5 minutes prior to blood pressure measurement.

2.6. CMR DATA ACQUISITION

2.6.1. CMR HARDWARE

CMR imaging was performed on a 1.5T CMR system (Avanto, Siemens, Erlangen) and on a 3T CMR system (Trio, Siemens, Erlangen), including a high performance gradient system (maximum amplitude 40mT/m, slew rate 200mT/m/ms, 200 µs rise time) and an 8-channel cardiac coil.

2.6.2. CMR PROTOCOLS

CMR at 1.5T was performed for measurement of left and right ventricular volumes, function and mass, aortic dimensions, distensibility, aortic pulse wave velocity and quantification of aortic regurgitation. A multichannel spine coil was used. After localisers, HASTE imaging was performed in the Transverse, Coronal and Oblique sagittal planes (in the plane of the aorta). Planes were defined perpendicular to the thoracic aorta at the level of the pulmonary artery, and 12–14cm below this plane, immediately below the diaphragm at the level of the abdominal aorta. Steady-state free procession (SSFP) cine images were acquired at these image positions, and 2D flow sequences were also acquired at these levels. Blood pressure was measured during each cine acquisition using a CMR compatible oscillatory sphygmomanometer. SSFP cine images of the heart in long axis and short axis views were acquired for calculation of biventricular volumes, mass and function.

2.6.3. VENTRICULAR VOLUMES AND FUNCTION

Ventricular volumes and function data were acquired at 1.5T. After pilot imaging, a stack of SSFP short axis cine images was acquired from the atrioventricular groove to the cardiac apex, perpendicular to the ventricular long axes. Acquisitions were performed during held end-expiration, using retrospective vectorcardiographic gating. Sequence settings were: echo time 1.5 ms, repeat time = 47.8 ms, field of view 236 × 360 mm, read matrix 111, phase matrix 256, slice thickness 7 mm, with a 3 mm gap between slices, 25 frames per cardiac cycle (typical temporal resolution of 50 ms depending on heart rate), flip angle 56°. Left and right ventricular endocardial contours were

manually segmented based on the short axis stack of cine images, at each slice position, at end-diastole and end-systole using ARGUS software (Siemens, Erlangen, Germany). Left ventricular basal slices were included in the segmentation if more than 50% of the lumen was surrounded by myocardium, and papillary muscles were excluded from the ventricular volume. This segmentation was used to quantify left and right ventricular end-diastolic and end-systolic volumes, and to calculate ejection fraction, stroke volume and stroke volume difference.

2.6.4. PHASE-CONTRAST CMR ACQUISITIONS

Time-resolved, phase-contrast CMR imaging with 3-directional velocity encoding was acquired using a 3T CMR system (Trio, Siemens, Erlangen) using the general approach described by Markl et al (66). The pulse sequence used was a fast, flow-sensitive, radiofrequency-spoiled gradient-echo pulse sequence, which after reconstruction generates an anatomical (magnitude) image and three phase-contrast images (each with an orthogonal velocity encoding direction), in Digital Imaging and Communications in Medicine (DICOM) format for each slice position, and for each time-point in the cardiac cycle. The 3D acquisition volume slab was positioned in a double oblique, modified sagittal orientation, to include the entire thoracic aorta. An adaptive diaphragm navigator was positioned over the most superior point of the right hemi-diaphragm, to allow diaphragm navigator gating, using a 6 mm end-expiration acceptance window. Electrocardiographic monitoring with prospective gating was used to acquire 90% of the RR interval, beginning at the R-wave. Sequence parameters were as follows: TR 5–7 ms, TE 2.378 ms (2–4 ms), flip angle 7–15 degrees, typical field of view 320 mm(read)/240 mm(phase), slab thickness 80–120 mm, matrix size 256 (phase) x 192 (read), in-plane velocity-encoding (VENC) 1.5 m/sec, through-plane velocity-encoding (VENC) 1.5 m/sec. Parallel imaging (Generalised Autocalibrating Partially Parallel Acquisitions, GRAPPA) was used with an acceleration factor of 2. Typical spatial resolution was 2.66 x 1.33 x 3.2 mm, the temporal resolution was 38.4 ms. Acquisition times were 15–35 minutes per subject.

2.6.5. PHASE-CONTRAST DATA PRE-PROCESSING AND VISUALISATION

Reconstructed DICOM images were corrected for aliasing, eddy currents arising in static tissue, and background noise in low-signal volumes, to generate a reliable velocity field, using custom-made software. 3D visualisation of volume-rendered datasets was performed on a commercially available engineering visualisation platform (Ensight, CEI, North Carolina), customised for the evaluation of phase-contrast datasets.

2.6.6. PHASE-CONTRAST DATA POST-PROCESSING

Details of specific post-processing steps of phase-contrast data are described in the relevant chapter.

2.7. STATISTICAL METHODS

2.7.1. DESCRIPTIVE STATISTICS

Statistical analysis was performed in SPSS (version 19). Continuous variables were expressed as means with standard deviations and/or 95% confidence intervals. Categorical data were expressed as a proportion or as a percentage with 95% confidence intervals. The distribution of each variable was evaluated for symmetry using a histogram, and for normality using a normal plot. Normality was adjudicated formally using the Shapiro-Wilk W test. When normally distributed, the assumption of equal variances was then tested using the F test (i.e. the variance ratio test).

2.7.2. PARAMETRIC TESTS

Where all distributional assumptions necessary for the conduct of parametric tests were met, hypothesis testing for statistical significance was performed using independent samples two-tailed t-tests. T-tests were used in cases where a single observation was made in two groups. Where more than two sets of observations were made, the one-way analysis of variance (ANOVA) method was used. Where assumptions regarding equal variance between groups were violated, but data were otherwise

suitable for parametric analysis, the Welch test (modified t-test for use with unequal variance) was used.

2.7.3. NON-PARAMETRIC TESTS

Where distributional assumptions necessary for the use of parametric tests were violated, non-parametric tests were used as follows: Mann-Whitney tests for independent samples; Wilcoxon matched pairs signed rank sum tests for paired samples; Kruskal-Wallis tests for more than 2 observations on the same individual. In all cases a (two-tailed) p value of <0.05 was deemed statistically significant.

CHAPTER 3

AORTIC BLOOD FLOW DISTURBANCE IN MARFAN SYNDROME

3.1. ABSTRACT

3.1.1. BACKGROUND

MFS is the commonest inherited connective tissue disease, affecting around 1 in 5,000 people, and conferring a dramatically increased risk of potentially life-threatening aortic aneurysm, dissection and rupture, which principally arise at or near the sinuses of Valsalva or, less commonly, the proximal descending aorta. Departures from smooth, laminar blood flow (i.e. blood flow disturbance) may influence progression of aortic dilation, dissection and rupture. This work seeks to characterise the prevalence, severity and distribution of blood flow disturbance in the aorta of unselected patients with MFS.

3.1.2. METHODS

31 subjects with MFS with no prior aortic surgery or aortic dissection, and 25 healthy subjects matched for age, sex and height, underwent time-resolved phase-contrast CMR with 3-directional velocity encoding (4D flow CMR) of the thoracic aorta from the aortic valve to the diaphragm at 3T. After pre- and post-processing, resultant blood flow was visualised as pathlines and streamlines, using interactive 3D visualisation software, and disturbances of blood flow Disturbances (i.e. departures from smooth, laminar forward blood flow), scored according to pre-defined, reproducible criteria.

3.1.3. RESULTS

Disturbances of aortic blood flow were much more prevalent in subjects with MFS than in healthy subjects (41 ± 8% of analysable segments showing any flow disturbance in subjects with MFS, compared to 19 ± 7% of analysable segments in healthy subjects, $p<0.0005$). Where present, blood flow disturbance was, on average, more severe in subjects with MFS than in healthy subjects (median flow disturbance score 3 for MFS v 1 for healthy subjects, $p<0.0005$). The aortic regions most commonly and most severely affected in MFS were the sinuses of Valsalva, and the proximal descending aorta.

3.1.4. CONCLUSIONS

4D flow CMR demonstrates that MFS is associated with a high prevalence of aortic blood flow disturbance, and the regions most commonly affected are the sinuses of Valsalva and the proximal descending aorta. These regions coincide with those showing significant aortic dilation among affected subjects compared to healthy subjects, and correspond to those known from epidemiological studies to be most prone to dissection. These data suggest a possible novel mechanism for the regional variation seen in the progression of aortic dilation and/or dissection in MFS.

3.2. INTRODUCTION

MFS is the commonest inherited connective tissue disease, affecting around 1 in 5,000 people, and conferring a dramatically increased risk of potentially life-threatening aortic dilation, dissection and rupture, which principally arise at or near the sinuses of Valsalva, or less commonly, the proximal descending aorta. The haemodynamic forces to which the vulnerable aorta in MFS are exposed are key determinants of aortic disease progression and, perhaps, risk of rupture (43). Advances in CMR hardware and sequences, coupled with increasing sophistication of image processing and 3D visualisation tools, now allow the acquisition and visualisation of time-resolved datasets encoding the entire velocity field of the thoracic aorta (4D flow CMR) (4,76). The aim of this work was to use these techniques to characterise the prevalence, severity and distribution of blood flow disturbance, which underlie these forces, in the aorta of patients with MFS. The hypothesis was that flow disturbance would be greatest in those regions of the aorta known to be at highest risk of aortic dissection (the sinuses of Valsalva and the proximal descending aorta).

3.3. METHODS

3.3.1. SUBJECTS

All subjects gave written informed consent, and all study-related procedures were approved by a research ethics committee.

31 consecutive patients with MFS, strictly defined according to the 1996 Ghent criteria (14), were recruited from the inherited connective tissue disease clinic at the John Radcliffe Hospital, Oxford, between 2007 and 2011. Inclusion criteria were: MFS defined according to the Ghent criteria; age 16 or above; willing and able to give informed consent; no history of aortic dissection or surgery. Exclusion criteria were: contra-indications to MRI. 25 healthy volunteers, matched to patients by age, sex and height, were screened for cardiovascular disease by history, examination and 12-lead ECG.

3.3.2. STUDY PROTOCOL

All subjects underwent study protocols as described in the general methods section. In brief, all subjects underwent study procedures in a single morning, after an overnight fast. Patients taking beta-blockers were asked to withhold these medications for 72 hours prior to the study. All other medications were continued.

3.3.3. CMR DATA ACQUISITION AND PRE-PROCESSING

4D flow CMR data acquisition was undertaken at 3T using a time-resolved phase-contrast CMR sequence with 3-directional velocity encoding, and pre-processed as described in the general methods section. Raw 4D flow data were exported to an offline workstation in DICOM format, where they underwent file format conversion (to case file format) and correction for aliasing owing to high velocities, eddy currents arising in static tissue (e.g. skeletal muscle), and background noise in low-signal volumes (e.g. lung), using custom-made software previously developed in Matlab (Figure 3.1).

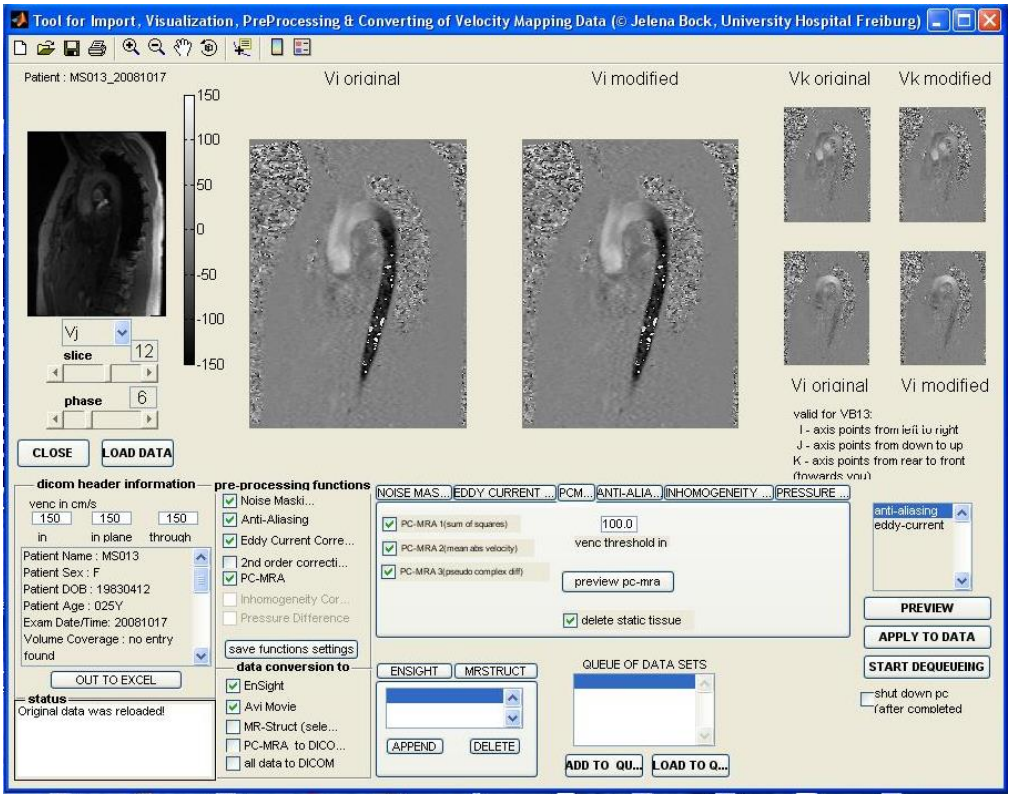

Figure 3.1: Velomap tool (Matlab) with data loaded, before pre-processing algorithms are applied. Note the presence of aliasing, static tissue inhomogeneity due to eddy currents and speckle appearance of empty pixels due to the random phase-shift of low amplitude noise. An average quality dataset was selected for this image to demonstrate the aliasing artefact (white specs within the otherwise dark descending aorta) prior to correction. The velomap tool was used to reduce noise in analysed datasets, to correct for potential inaccuracies in the measured velocity acquisitions, and to convert the dicom file format into a format compatible with visualisation tools.

Noise reduction algorithms were applied to exclude regions of low signal intensity (such as the lungs and air outside the subject) to reduce processing time, and to remove noise. Noise masking algorithms were based on a user-defined threshold of signal intensity of magnitude images, and on variations in velocity-time standard deviations. Automated anti-aliasing algorithms were applied to correct for aliasing (i.e. where measured local velocities were higher than the acquired venc), by identifying and correcting pixels whose signal intensity was substantially greater than those of its immediate neighbours.

Phase-contrast data is subject to a number of potential sources of error, including eddy currents, concomitant-gradient (or Maxwell) terms and departures of the gradient field from linear behaviour. Eddy currents arise as a result of rapid switching of the velocity encoding gradient, inducing magnetic flux in electrical conductors in the scanner, giving rise to spatially varying phase errors in the images. Concomitant gradient terms arise as a result of the phenomenon of non-linear concomitant gradients arising from the magnetic field gradient, and gradient field inhomogeneities relate to intrinsic distortions in the gradient field owing to imperfect gradient coil design and construction.

Spatial magnetic field inhomogeneities were corrected in the first instance by the subtraction of the phase-insensitive acquisition from the phase-sensitive acquisition. Eddy current correction was performed using the velomap tool as follows: regions were segmented into static tissue and non-static tissue (i.e. blood flow and noise) on the basis of a threshold intra-pixel velocity-time standard deviation. Pixels having a low standard deviation were regarded as being static. An estimate of the spatial inhomogeneity in the magnetic field was then derived based on the static tissue alone, and this correction was applied to each time-frame to provide an adjusted data-set.

3.3.4. DATA POST-PROCESSING

Converted and pre-processed data were visualised on a commercially available engineering visualisation platform (Ensight, CEI, North Carolina) (Figure 3.2). Vessel lumen thresholding and segmentation was performed manually on the phase-contrast magnetic resonance angiogram in Ensight. Algorithms were applied to confine velocity evaluation to the volume of interest (i.e. that enclosed within the selected threshold volume). Square clip-grids, typically 12–25 cm^2, were applied to the aorta at 7 pre-defined locations based on anatomical features of the phase-contrast angiogram (aortic valve, sino-tubular junction, mid-ascending aorta at the level of the pulmonary arteries, proximal arch at the point of attachment of the head and neck vessels, distal arch at the point of attachment of the head and neck vessels, proximal descending aorta at the level of the pulmonary arteries, and distal (thoracic) descending aorta at the level of the aortic valve). These formed the borders of 6 aortic regions, and the basis for streamlines and pathlines to evaluate forward and

backward flow from that grid over each time-frame, and for the subsequent evaluation of blood and vessel properties at that slice position.

3.3.5. AORTIC VISUALISATION AND EVALUATION

The aorta was segmented into 6 regions on the basis of anatomic features (Figure 3.3). Each segment was evaluated as analysable or not analysable. A segment of aorta was defined as analysable if the whole of the segment was within the acquired volume, with flow clearly seen entering, leaving and within the segment, and in which the observer was confident that flow features could be identified. In all other circumstances, the segment was said to be non-analysable.

Analysable segments were rated as normal or abnormal (defined as the presence of turbulent flow vortices) and, where abnormal, extent of abnormality was classified on a 4-point scale determined by the extent of radial involvement of the aorta as follows: 0 = no flow disturbance; 1 = minor flow disturbance affecting less than 25% of the luminal diameter; 2 = moderate flow disturbance affecting 25–50% of luminal diameter; 3 = marked flow disturbance occupying >50% of luminal diameter.

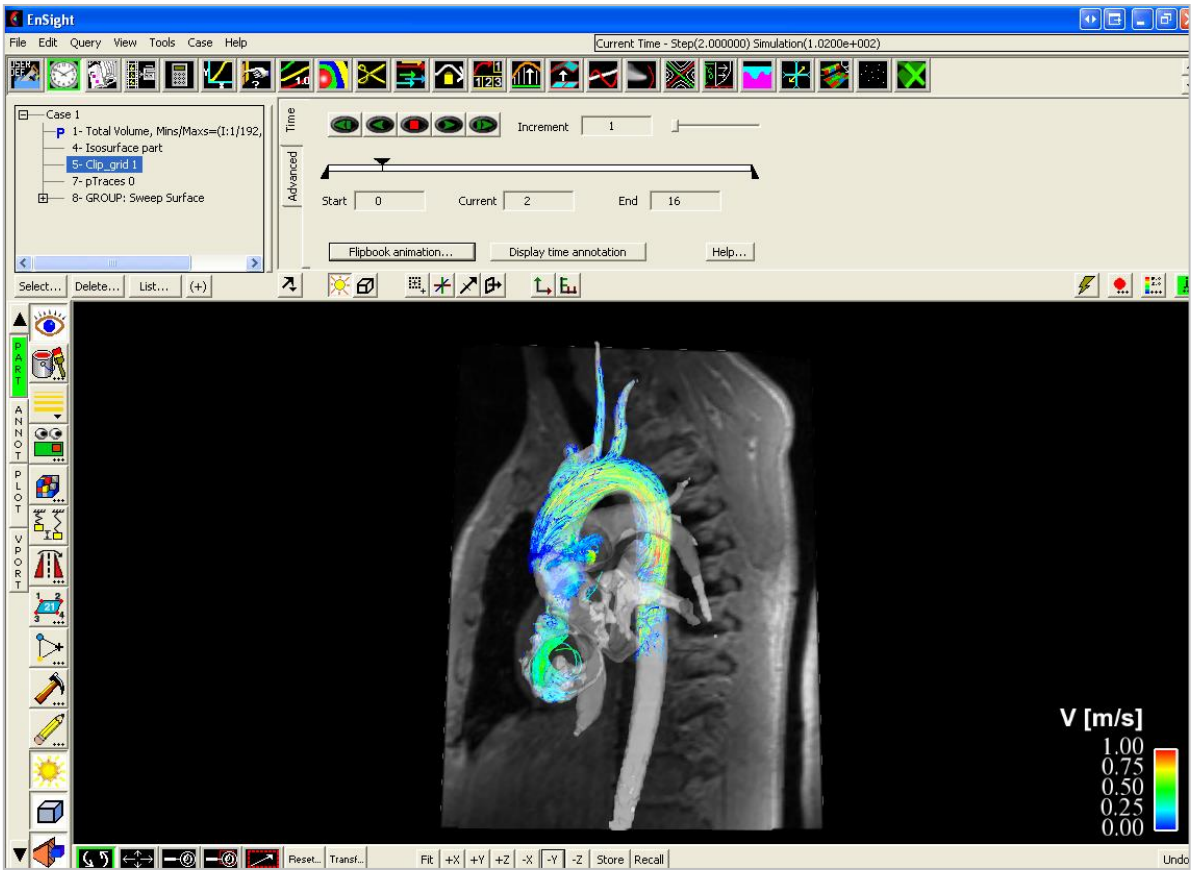

Figure 3.2: The Ensight visualisation platform with magnitude and flow data loaded, showing a still frame of a particle trace animation, projected from a plane defined at the ascending aorta at the level of the pulmonary arteries. Velocities are encoded as colour, with the velocity values represented shown in the bottom right corner.

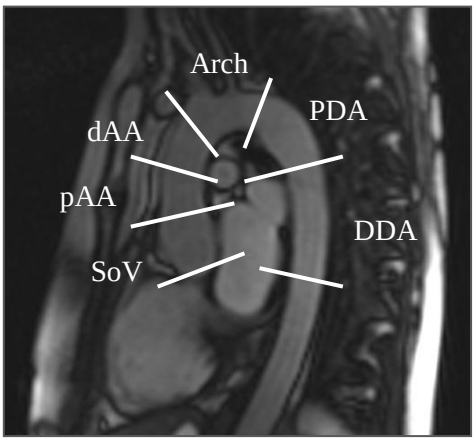

Figure 3.3: Definition of aortic segments and positioning of planes for particle traces and streamlines. SoV=sinuses of Valsalva; pAA=proximal ascending aorta; dAA=distal ascending aorta; Arch=aortic arch; PDA=proximal thoracic descending aorta; DDA distal thoracic descending aorta.

Each dataset was evaluated by a single observer, experienced in 3D aortic flow visualisation, and blinded to patient identity and unaware of whether the subject was affected or unaffected by MFS. To improve concealment, only the velocity field was reviewed, with no anatomical information being available to the observer at the time of rating of the flow pattern.

3.3.6. INTRA-OBSERVER REPRODUCIBILITY METHODS

12 datasets were randomly selected for reproducibility analysis of flow disturbance classification. Flow patterns were classified in each aortic segment by two independent observers, each unaware of the scores given by the other observer. Agreements and disagreements were tabulated, and the inter-observer agreement (i.e. the proportion of segments which were given the same classification by each observer), Kappa values and weighted Kappa values were calculated.

3.4. RESULTS

3.4.1. BASELINE CHARACTERISTICS

There were no significant differences between groups in age, gender distribution, height or weight. Aortic dimensions were significantly different at the sinuses of Valsalva and at the proximal descending aorta, but not at other locations (Table 3.1).

3.4.2. ANALYSABLE SEGMENTS

Overall, 88±3% of segments were analysable, with a non-significant trend to a higher proportion of analysable segments in healthy subjects (93±4% of segments analysable) than in subjects with MFS (83±5% of segments analysable), p for difference = 0.09 (Table 3.2).

3.4.3. INTER-RATER AGREEMENT

The inter-rater reliability for the two raters was found to be high (Weighted Kappa = 0.90 (+/- 95% CI 0.11) $p<0.0005$, Table 3.3).

3.4.4. PREVALENCE OF ANY FLOW DISTURBANCE

28/31 (90±11%) of subjects with MFS showed disturbance of flow (of any degree) in one or more aortic segments, compared to 18/25 (72±17%) in healthy subjects. In subjects with MFS, the total number of analysable segments showing any flow disturbance (i.e. flow score >0) was 64/155 (41±8%), compared to 26/139 (19±7%), in healthy subjects ($p<0.0005$). The anatomical distribution of flow disturbance differed markedly by aortic region. The distribution of any flow disturbance is shown in Figure 3.4.

Table 3.1: Baseline characteristics of subjects.

	Marfan	**Control**	**P-value for difference**
Number of subjects	31	25	-
Age (years)	36 (± 12)	34 (±15)	0.81
Gender M/F	13M/18F	17M/8F	0.052
Height (m)	1.84 (±0.10)	1.82 (±0.08)	0.35
Weight (kg)	77 (±16)	81 (±12)	0.44
BMI (kg/m^2)	23±5	24±3.5	0.2
BSA (m^2)	1.84 (±0.51)	2.01 (±0.17)	0.72
Aortic dimension SOV (cm)	4.1 (±0.6)	3.3 (±0.4)	**<0.0005**
Aortic dimension AA (cm)	2.9 (±0.5)	2.8 (±0.5)	0.54
Aortic dimension Arch (cm)	2.2 (±0.3)	2.2 (±0.3)	0.68
Aortic dimension PDA (cm)	2.3 (±0.4)	2.1 (±0.3)	**0.035**
Aortic dimension DDA (cm)	2.2 (±0.5)	2.1 (±0.5)	0.34
LVEF (%)	65	64	0.29

Table 3.2: Proportion of analysable segments.

	Marfan	**Healthy subjects**	**Marfan**	**Healthy subjects**
SOV	27/31	24/25	87%	96%
Prox AA	27/31	24/25	87%	96%
Dist AA	27/31	24/25	87%	96%
Arch	24/31	22/25	77%	88%
Prox DA	26/31	22/25	84%	88%
Dist DA	24/31	23/25	77%	92%
Overall	**155/186**	**139/150**	**83%**	**93%**
Totals	**294/336**		**88%**	

Table 3.3: Inter-rater agreement (agreements shown in bold).

		Observer 1				
	Score	0	1	2	3	Total
Observer 2	0	**64**	0	0	0	64
	1	3	**1**	0	0	4
	2	0	0	**5**	0	5
	3	0	0	0	**11**	11
	Total	67	1	5	11	84

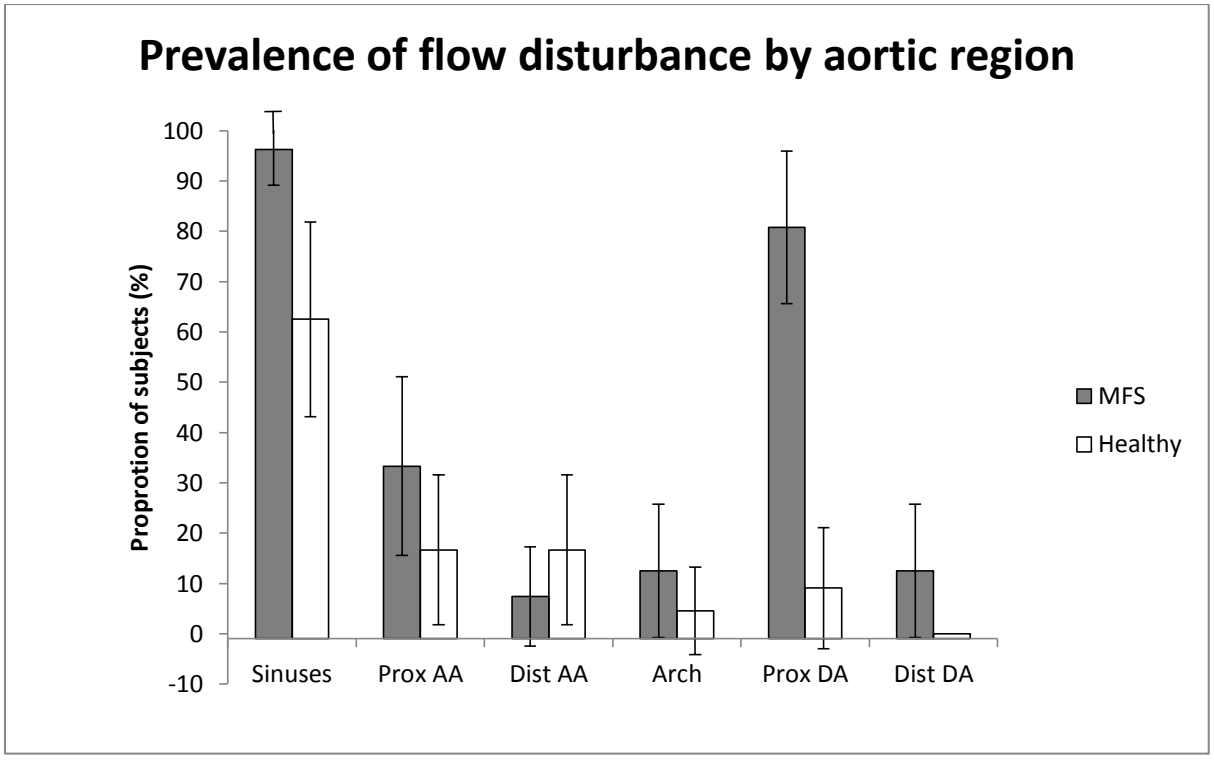

Figure 3.4: Prevalence of flow disturbance (defined as >25% aortic lumen involved) by aortic region in subjects with MFS (shaded), and in healthy subjects (unshaded). Error bars represent 95% confidence intervals. MFS= Marfan syndrome

3.4.5. PREVALENCE OF MAJOR FLOW DISTURBANCE

The proportion of subjects showing major flow disturbance (defined as flow disturbance occupying more than 25% of the aortic lumen) in one or more aortic segments was 27/31 (87±12%) in subjects with MFS compared to 7/25 (28±18%) in healthy subjects ($p<0.0005$). In subjects with MFS, 61/155 (39±8%) of analysable segments were affected by major flow disturbance, compared to 9/139 (7±4%) of analysable segments in healthy subjects ($p<0.0005$). The anatomical distribution of major flow disturbance was similar to that demonstrated for any flow disturbance, and is shown in Figure 3.5. When analysed by aortic region, the sinuses of Valsalva showed the highest prevalence of flow disturbance, followed by the proximal descending aorta, among both healthy subjects and subjects with MFS. Flow disturbance was more prevalent in subjects with MFS than in healthy subjects in each of these regions. Examples of flow disturbance in subjects with MFS and in healthy subjects are shown in Figure 3.6. There were no significant differences in the prevalence of flow disturbance, or of major flow disturbance (howsoever defined) among subjects with MFS and healthy subjects at any other aortic region evaluated (proximal ascending aorta, aortic arch, or distal descending aorta). Major flow disturbance (defined as flow disturbance involving >50% of the aortic lumen) was much more prevalent in subjects with MFS than healthy controls. The absolute threshold selected did not influence this finding.

Overall, among all analysed segments, the median flow disturbance rating was 2 for subjects with MFS and 0 for healthy subjects. Among segments showing flow disturbance (much more numerous among subjects with MFS), the median flow disturbance rating was 3 among disturbed flow segments in subjects with MFS compared to 1 among disturbed segments in healthy subjects.

Mean aortic root size at the sinuses of Valsalva was 4.1 cm among subjects with MFS, compared to 3.3 among healthy subjects ($p<0.0005$). No significant differences in prevalence or severity of aortic flow disturbance were found between males and females, or with age, weight, or height, among healthy subjects or subjects with MFS.

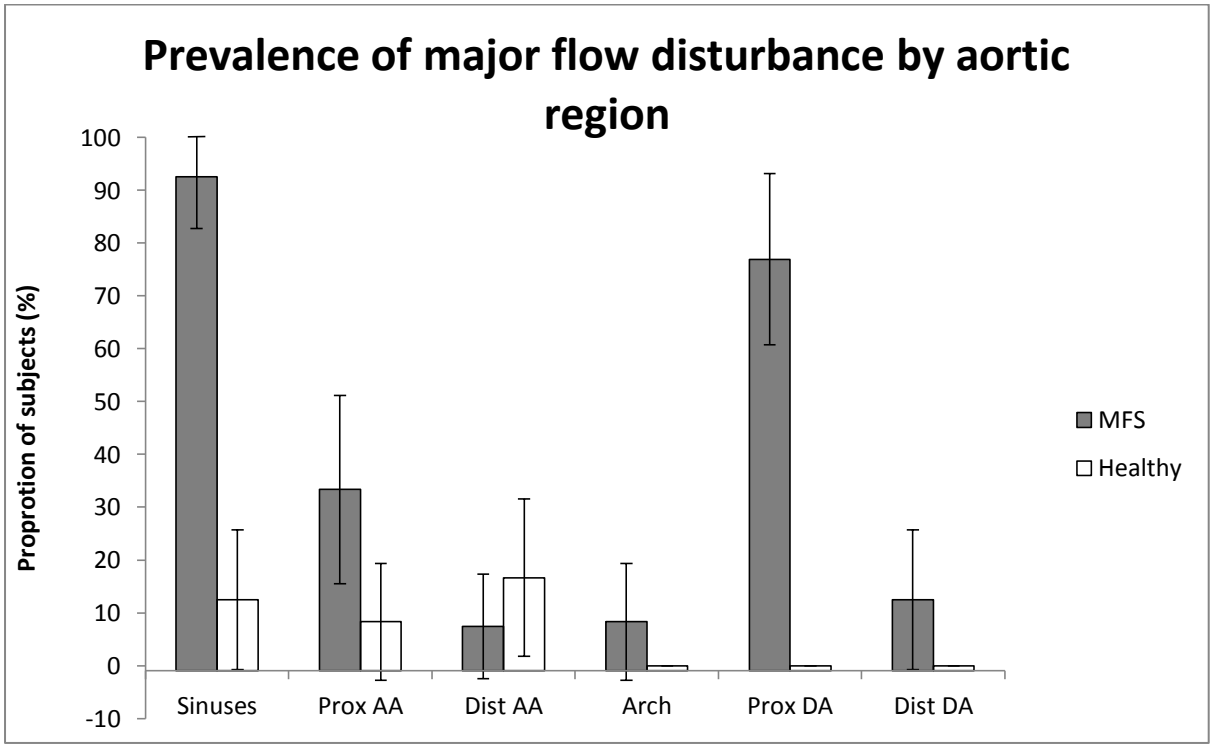

Figure 3.5: Prevalence of major flow disturbance (defined as >50% aortic lumen involved) by aortic region in subjects with MFS (shaded), and in healthy subjects (unshaded). Error bars represent 95% confidence intervals. MFS=Marfan syndrome

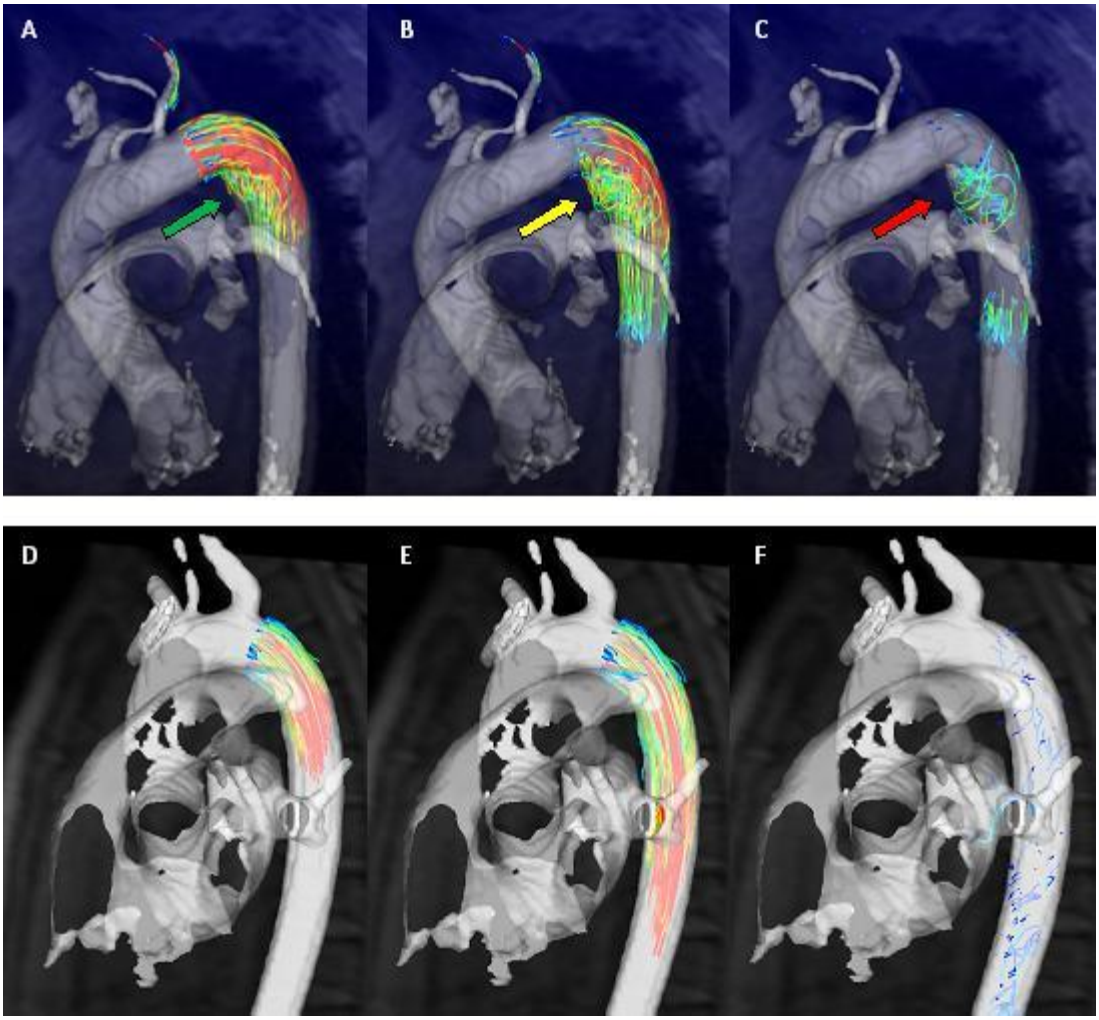

Figure 3.6: Still frames from an animation showing time-resolved 3-dimensional velocity encoded (4D flow) images of the aorta of a patient with Marfan syndrome (top row, A–C), and a healthy volunteer (bottom row, D–F). Arrows highlight turbulent, complex vortex formation in the proximal descending aorta at 224ms (green arrow), 510ms (yellow arrow) and 674ms (red arrow) after ventricular systole in the subject with Marfan syndrome. There is smooth laminar flow at the same sites in the healthy subject at equivalent timepoints. The differences in 4D flow images seen here may be due to the anatomical angulation seen in the MFS patient, which is absent in the healthy volunteer.

3.5. DISCUSSION

3.5.1. SUMMARY OF FINDINGS

This work describes the use of phase-contrast CMR with 3-directional velocity encoding to demonstrate a higher prevalence of aortic flow disturbance in unselected patients with Marfan syndrome compared to age-, sex- and height-matched healthy controls. Where present, the flow disturbance seen is of greater severity. The distribution of flow disturbance within the aorta is non-uniform, with the sinuses of Valsalva and the proximal descending aorta being the regions prone to significant differences in flow disturbance. The thresholds used to determine severity of flow disturbance did not appear to influence the direction of the findings.

Regions of the aorta with the highest prevalence of flow disturbance, and with the most severe flow disturbance where present, were also the regions found to be significantly enlarged in subjects with MFS compared to healthy subjects, and co-localised to those areas known from epidemiological studies to be prone to aortic dissection. These findings suggest a novel mechanism for the progression of aortic dilation and/or aortic dissection, and may provide a new method for risk stratification of patients with MFS when evaluated in longitudinal studies. Findings in healthy subjects were broadly comparable to those of previous studies, and in patients with MFS were consistent with earlier case reports and smaller case series and case-control studies. Greiger et al have recently reported the distribution of flow disturbance in the aorta in a smaller study of predominantly paediatric patients with MFS (77). They found flow disturbances in the sinuses of Valsalva and proximal descending aorta, although these authors found a somewhat lower prevalence of flow disturbance in their subjects, likely because they were studying subjects earlier in the disease process than the subjects reported here. This study supports our finding of high levels of flow disturbance in subjects with MFS in a distribution consistent with the pattern of aortic dilation and dissection.

3.5.2. ASPECTS OF STUDY METHODOLOGY

The approach provides unique insights into the blood flow pattern seen in MFS, but a number of limitations are recognised. Firstly, the acquisition technique aggregates data from several hundred cardiac cycles into one cardiac cine, and cannot detect flow disturbances or eddies on spatial or temporal scales below the spatial and temporal resolution of the technique. The technique is, therefore, unable to detect beat-to-beat instabilities of flow, or true turbulence, which, by definition, shows random flow and flow instabilities on all temporal and spatial scales. While methods to improve and apply approaches to detecting, localising and quantifying turbulence are in development, and are an active area of research for our group, it may, in fact, be the repetitive disturbances of flow which are likely to be of most importance in determining progression of aortic dilation or dissection.

Secondly, the method used for adjudicating presence and extent and severity of flow disturbance relies upon visual assessments, using a semi-quantitative grading system. While there is excellent agreement between experienced users of the software platform on which flow is visualised, this may not extend to less experienced users, so limiting clinical applicability in the short term. Quantitative methods for determining severity of disturbance of flow are in development but are not yet sufficiently robust for use in clinical studies.

Thirdly, this is a cross-sectional study, and cannot therefore elucidate a cause and effect mechanism for aortic dilation and dissection. It is likely that geometry and flow interact in a complex way, with minor changes in geometry causing disturbances of flow which alter the haemodynamic regimen to which the intrinsically vulnerable aorta is exposed. This question could be addressed by longitudinal studies of aortic geometry and flow, based on the cohort described in this work.

Finally, the acquisition and post-processing times of datasets at the time of data collection were too long to allow routine use of this technology at present. New developments in CMR hardware (particularly expanded use of high field 3T and 7T CMR scanners); CMR software, including

sequence acceleration; and semi-automated or fully automated post-processing platforms are now becoming available, which are likely to make the technique feasible as part of a clinical protocol in selected patients at specialised CMR centres in the near future.

3.5.3. MECHANISMS

The fundamental aortic abnormality in MFS is near complete deficiency of fibrillin-1 protein in the media of the aortic wall, owing to mutations in the FBN-1 gene. Once thought to have an exclusively structural role in the aortic wall, it is now thought that the deleterious effects of fibrillin-1 deficiency are mediated, at least in part, by the failure of fibrillin-1 to sequester and regulate circulating levels of TGFβ. This dysregulated TGFβ can thus contribute to disordered cellular behaviour in the aortic wall. These biochemical and cellular events are now being understood in much greater detail, but how these cellular processes lead to decreased aortic wall compliance, dilation and dissection is not understood. In particular, the inability to resist the haemodynamic forces imposed upon the aorta seems to be an important part of the pathophysiology of macroscopic events in MFS, and reduction of rate of aortic loading is thought to play a part in the protective effects of beta-blockade in these patients. Despite the central importance of loading of the aorta, little attention has been paid to how mild to moderate dilation of the aorta alters blood flow, and how this impacts upon the flow patterns seen.

The contribution of abnormal flow patterns to aortic complications is unknown. Three mechanisms are proposed, by which blood flow may impact upon rate of progression and/or risk of rupture: Firstly, abnormal flow patterns, arising as a consequence of aortic anatomic or functional changes, may themselves produce abnormal loads on an inherently vulnerable aorta. Secondly, chaotic flow patterns are likely to increase wall shear stress, which may be relevant to the initiation and propagation of intimo-medial dissection flaps. Thirdly, the presence of significant flow abnormalities in the aorta may interfere with the propagation of incident and reflected pulse waves.

3.6. CONCLUSIONS

MFS is associated with a high frequency of aortic blood flow disturbance, and those regions most commonly affected are the sinuses of Valsalva and the proximal descending aorta. The co-localisation of regions of abnormal flow with regions known to be most prone to aortic dissection suggests possible novel mechanisms for progressive aortic dilation and dissection at these sites in these patients. These mechanisms require further study to determine their role in disease progression and risk stratification, and as therapeutic targets.

CHAPTER 4

AORTIC WALL SHEAR STRESS IN MARFAN SYNDROME

4.1. ABSTRACT

4.1.1. BACKGROUND

Wall shear stress (WSS) is the shearing force per unit area experienced by a vessel wall as a consequence of the relative movement of an adjacent viscous fluid, such as blood. Computational models highlight the potential importance of WSS in determining aneurysm progression and/or rupture, but reliable measurement of WSS in vivo has historically been challenging. Advances in time-resolved, phase-contrast CMR with 3-directional velocity encoding now allow the estimation of aortic WSS and its components, based on near-wall spatial velocity gradients. This work describes the estimation of aortic WSS in adult subjects with MFS compared to healthy subjects.

4.1.2. METHODS

31 subjects with MFS and 25 healthy subjects of similar age, gender distribution and height underwent time-resolved, phase-contrast CMR acquisition of the thoracic aorta, with 3-directional velocity encoding. Mean (temporally-averaged and spatially-averaged) WSS was estimated from near-wall spatial velocity gradients at five anatomically-defined locations of clinical relevance: the sinuses of Valsalva (SOV), the ascending aorta (AA), the mid-aortic arch (Arch), the proximal descending aorta (PDA) and the distal descending aorta (DDA).

4.1.3. RESULTS

Baseline characteristics were not significantly different between subjects with MFS and healthy subjects, except aortic dimensions, which were significantly different at the SOV (4.1 cm MFS v 3.3 cm healthy subjects, $p<0.0005$) and at the PDA (2.3 cm MFS v 2.1 cm healthy subjects, $p=0.035$), but not at other aortic locations. WSS analysis showed good intra-observer reproducibility. Subjects with MFS had lower mean WSS at all five anatomical positions compared to healthy subjects. WSS reductions were: SOV 15%; AA 12%; Arch 17%; PDA 18%; and DDA 14% ($p<0.05$ for each). In healthy subjects, increased aortic diameter at the SOV was associated with increased mean WSS

(Pearson's R=0.64, p=0.001), but in subjects with MFS, no such relationship was seen (R=0.27, p=0.2).

4.1.4. CONCLUSIONS

Mean WSS is reduced by 12–18% in the aorta of subjects with MFS compared to healthy subjects. WSS is positively correlated with aortic dimension in healthy subjects, but not in subjects with MFS.

4.2. INTRODUCTION

The aorta is subject to shearing forces arising as a result of the movement of viscous blood along its lumen. The magnitude and direction of these forces vary throughout the cardiac cycle, and at different anatomical locations in the aorta. This shearing force per unit area can be quantified as the wall shear stress (WSS).

Wall shear stress represents the tangential force per unit area of flowing blood on the endothelial surface of the blood vessel, and is defined mathematically for Newtonian fluids as:

$$WSS = \rho \cdot \frac{\delta V}{\delta r}$$

where ρ represents the viscosity of blood, V the velocity of blood, r the radius of the vessel, and in which δV/ δr represents the near-wall spatial velocity gradient at any instant.

WSS is a vector quantity having both magnitude and direction, and can be resolved into axial and circumferential components which can be estimated from near-wall spatial velocity gradients. 4D flow CMR uniquely allows the interrogation of such gradients – and therefore segmental WSS – at unlimited locations of interest anywhere within the large field of view prescribed during acquisition.

WSS is reduced in atherosclerosis (67), increased in coarctation of the aorta (78,79), and asymmetric in bicuspid aortic valve-associated aortopathy (79)and may be an important determinant of aneurysm progression, and may have a role in the initiation of rupture. We sought to use the velocity field to estimate WSS at specific pre-defined anatomical locations in the aorta, and to compare these in subjects with MFS to matched healthy volunteer controls.

4.2.1. AIM

The aim of this work is to estimate WSS at well-defined anatomical positions throughout the cardiac cycle, in healthy subjects, and in patients with MFS, based on time-resolved phase-contrast CMR with 3-directional velocity encoding.

4.3. METHODS

4.3.1. SUBJECTS AND PROTOCOL

31 subjects with MFS and no prior aortic dissection or aortic surgery, and 25 healthy subjects, underwent time-resolved phase-contrast CMR with 3-directional velocity encoding, as described in the general methods section. Baseline characteristics of subjects are shown in Table 3.1.

4.3.2. WALL SHEAR STRESS ANALYSIS

Planes for WSS analysis were placed at 5 aortic locations of interest (the sinuses of Valsalva (SOV), the ascending aorta at the level of the pulmonary artery (AA), the mid-aortic arch (Arch), the proximal descending aorta (PDA) and the distal descending aorta (DDA)), as shown in Figures 4.1 and 4.2. Planes were positioned at anatomical landmarks based on the Phase-Contrast Magnetic Resonance Angiogram (PC-MRA) in Ensight without reference to the flow field. WSS analysis was undertaken using the flowtool programme in Matlab (mathworks), Figure 4.3. The principles underlying this tool and its validation against both phantoms and in vivo have been described previously (80). Briefly, after export of the velocity vectors to the flowtool programme, interactive manual segmentation of the aortic lumen was undertaken for each frame at each anatomical location, with cubic B-spline interpolation. Vectorial WSS and its components in the axial and circumferential directions were estimated directly from the near-wall spatial velocity gradients derived from the measured 3-directional velocity field using a deformation tensor. Mean absolute WSS magnitude was measured for each anatomical location for each patient.

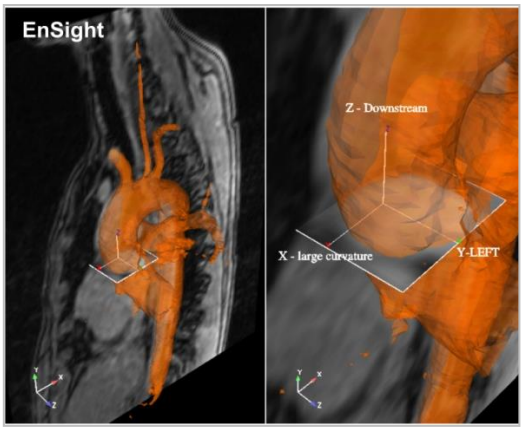

Figure 4.1: Clip Plane orientation for flow and wall shear stress quantification (courtesy of Michael Markl).

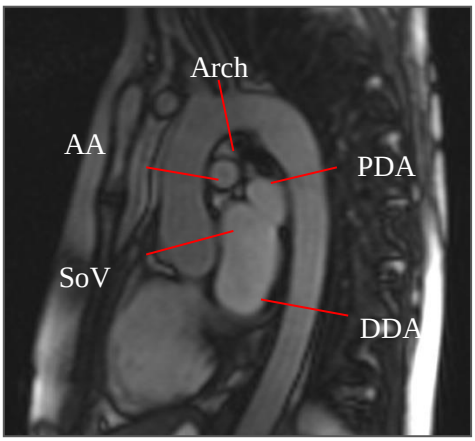

Figure 4.2: Anatomical distribution of wall shear stress interrogation planes in an oblique sagittal view of the aorta.

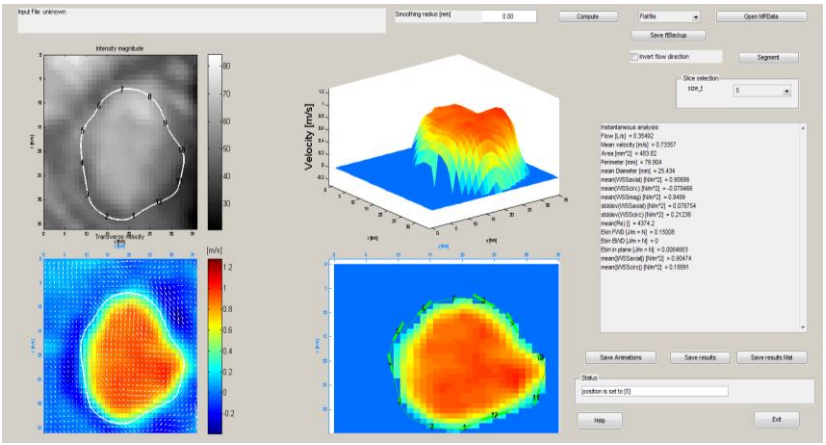

Figure 4.3: Flowtool user interface, showing segmentation of the aorta using both magnitude (top left) and flow (bottom left) to derive a flow profile (top middle) and wall shear stress measures (bottom middle and right).

4.3.3. DEFINITION OF AN ANALYSABLE SEGMENT

A segment was defined as analysable if the observer could clearly define the whole of the perimeter of the vessel in flowtool. The determination as to whether the segment was analysable was made prior to quantifying WSS or other flow-based metrics, and all datasets deemed analysable were included in the final analysis. Numbers of analysable segments for subjects with MFS and healthy subjects are given in Table 4.1.

4.3.4. ACCURACY OF SEGMENTATION

Accuracy of segmentation was confirmed by comparison of derived minimum aortic diameter estimates from the flowtool segmentation to diastolic measures of aortic diameters from cines at the same anatomical locations. Discrepancies of >3 mm were re-evaluated in flowtool to confirm accuracy of segmentation. The error in segmentation was estimated by comparing flowtool estimated diameters with cine estimated diameters.

4.3.5. REPRODUCIBILITY OF WSS ESTIMATION

WSS estimation shows good intra-observer, inter-observer and scan-scan reproducibility (80,81). To confirm reproducibility in our workflow, 24 planes were analysed twice by the same observer with > 1 week between analyses and Bland-Altman analysis was performed.

Table 4.1: Number of analysable segments by region and overall, for subjects with Marfan syndrome and healthy subjects.

	Marfan	**Healthy subjects**	**Marfan**	**Healthy subjects**
SOV	25/31	23/25	81%	92%
AA	28/31	24/25	90%	96%
Arch	27/31	24/25	87%	92%
PDA	25/31	23/25	81%	92%
DDA	25/31	24/25	81%	96%
Overall	**130/155**	**118/125**	**84%**	**94%**
Totals	**248/280**		**89%**	

4.4. RESULTS

4.4.1. BASELINE CHARACTERISTICS

There were no significant differences across a range of baseline characteristics between subjects with MFS and healthy subjects (Table 3.1), except aortic dimensions at the SOV (4.1 v 3.3 cm, $p<0.0005$) and at the PDA (2.3 v 2.1 cm, $p=0.035$).

4.4.2. ANALYSABILITY OF IMAGING PLANES

Overall, 248 (of a possible 280) imaging planes were considered analysable, representing 89% of slices (Table 4.1). All analysable segments were included in the analysis.

4.4.3. ACCURACY OF SEGMENTATION

Segmentation-derived and cine-derived estimates of aortic diameter at corresponding aortic locations were highly correlated ($R=0.94$, $p<0.0005$, Figure 4.4). Mean differences between the methods were very small (mean difference 0.5 mm, 95%; CI 0.05–0.095 mm, 95% Limits of agreement are ±5.5 mm, Figure 4.5), and were similar to those reported previously. Segmentation-derived techniques tended to slightly over-estimate lumen size.

4.4.4. REPRODUCIBILITY OF WSS ESTIMATES

WSS analysis showed high intra-observer reproducibility (Figure 4.6).

4.4.5. MEAN WSS AT AORTIC LOCATIONS

Subjects with MFS had, on average, lower mean WSS at each anatomical position analysed (SOV 15%, $p=0.007$; AA 12%, $p=0.024$; Arch 17%, $p=0.006$; PDA 18%, $p=0.012$; DDA 14%, $p=0.025$, Figure 4.7). In healthy subjects, increased aortic diameter at the SOV was associated with increased

mean WSS (Pearson's R=0.64, p=0.001, Figure 4.8), but in subjects with MFS, no such relationship was seen (R=0.27, p=0.2, Figure 4.9).

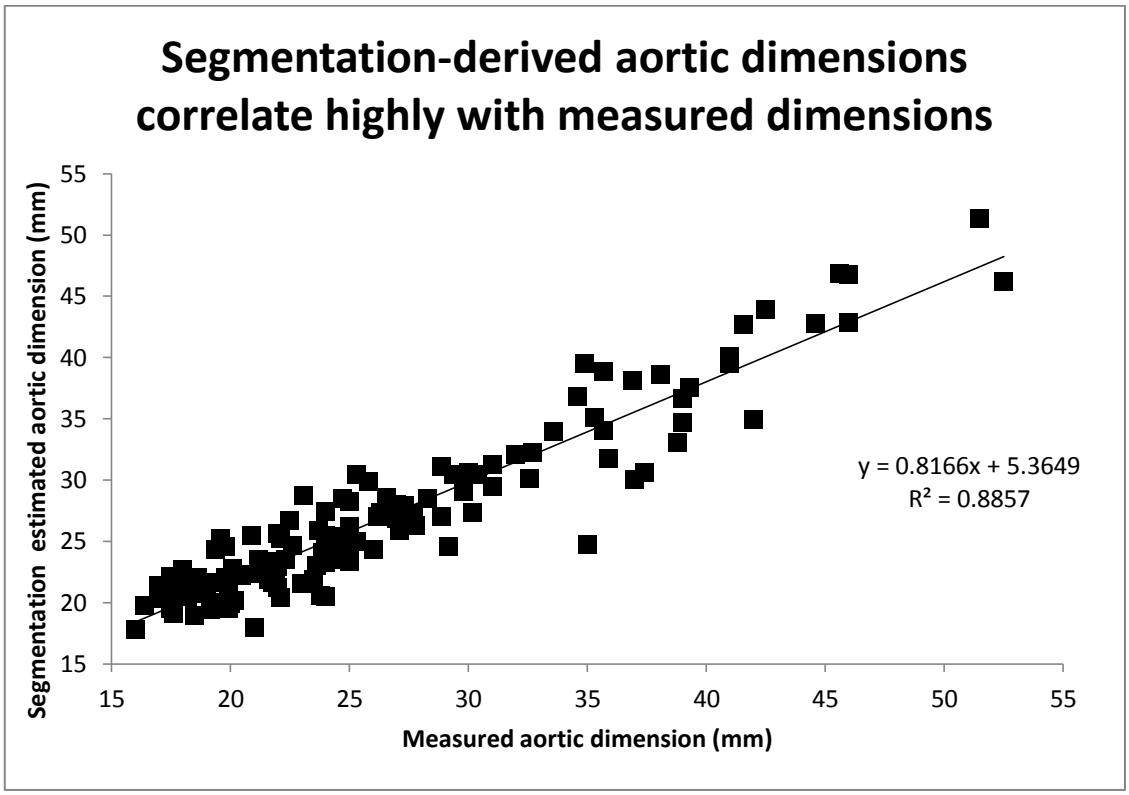

Figure 4.4: Correlation between direct measurement of aortic dimensions, and segmentation-derived estimates of aortic dimensions.

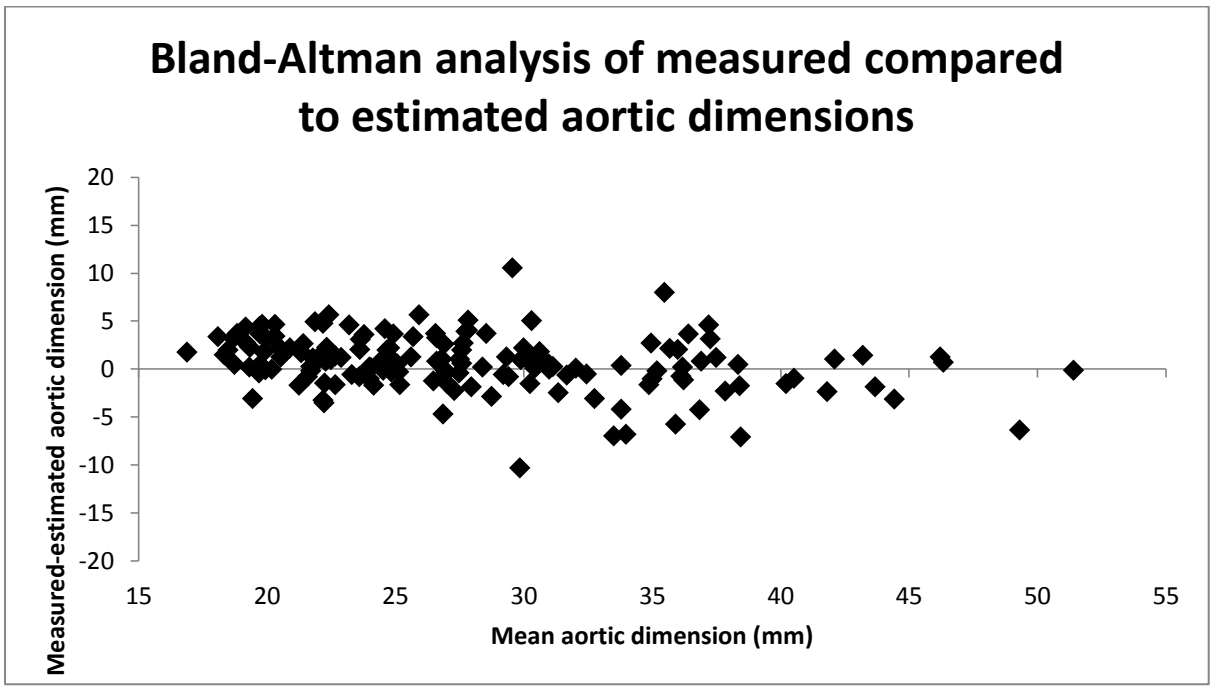

Figure 4.5: Bland-Altman analysis of measured compared to estimated aortic dimensions.

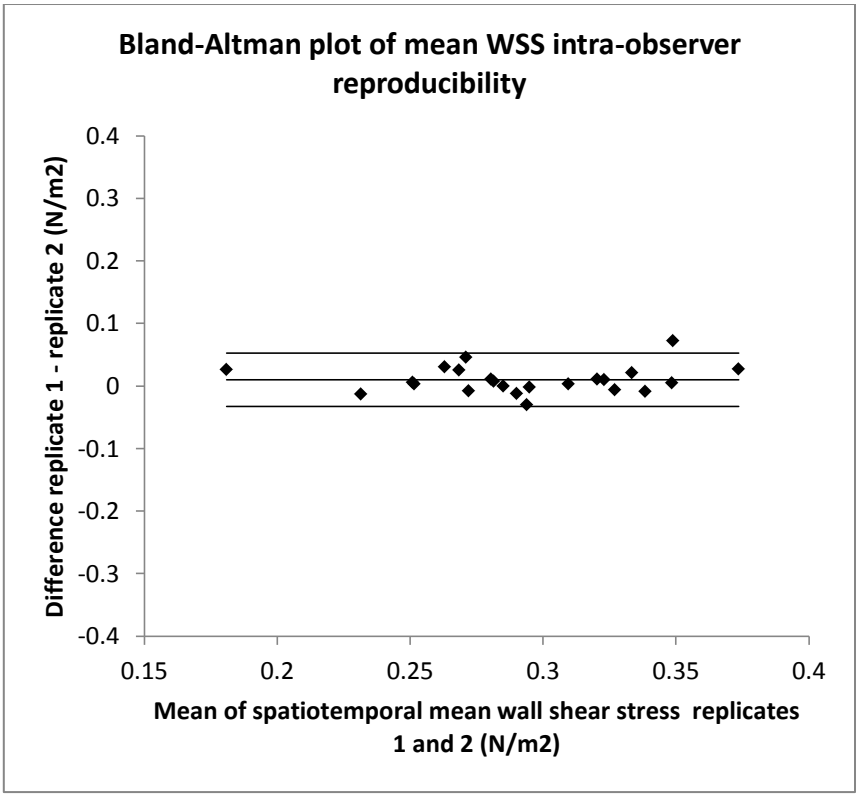

Figure 4.6: Bland-Altman analysis of intra-observer reproducibility.

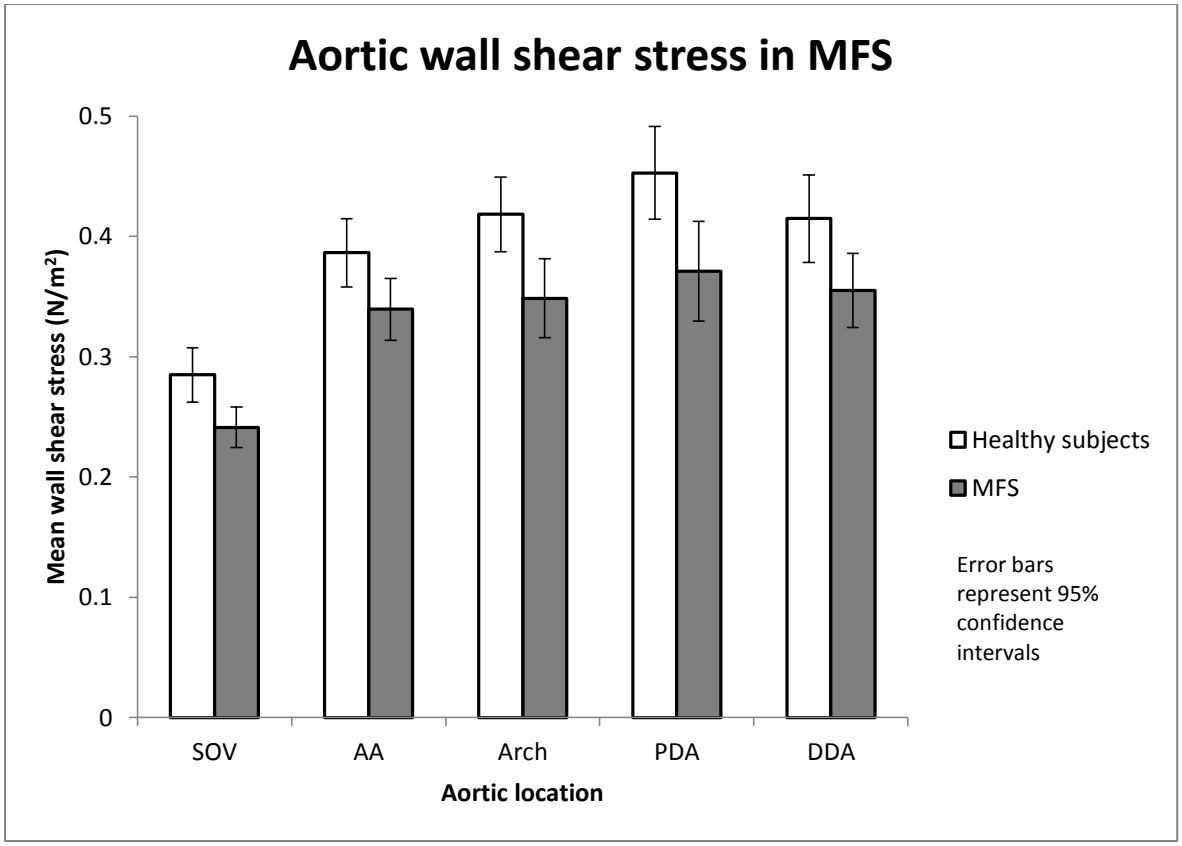

Figure 4.7: Mean temporally-averaged and spatially-averaged vectorial WSS at five anatomical areas of interest for subjects with MFS (Marfan syndrome, n=31), compared to healthy subjects (n=25) (SOV: sinuses of Valsalva; AA: ascending aorta at the level of the pulmonary artery; Arch: mid-aortic arch; PDA: proximal descending aorta; DDA: distal descending aorta).

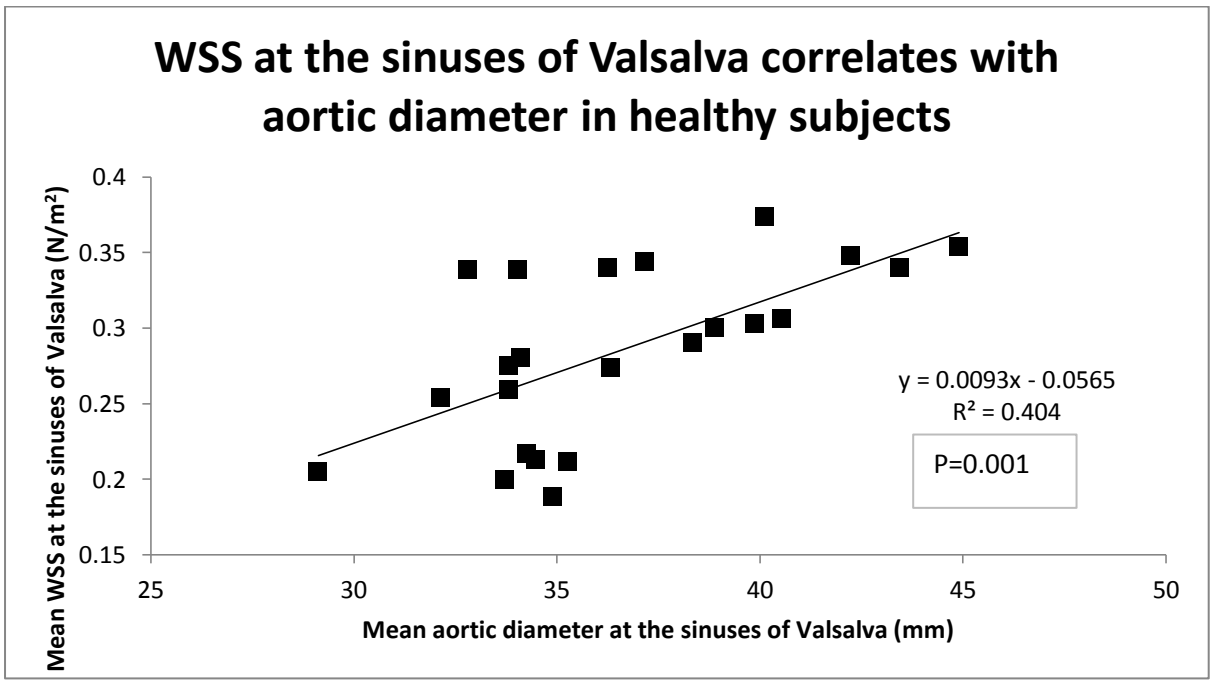

Figure 4.8: Mean wall shear stress (WSS) by aortic dimensions at the sinuses of Valsalva among healthy subjects.

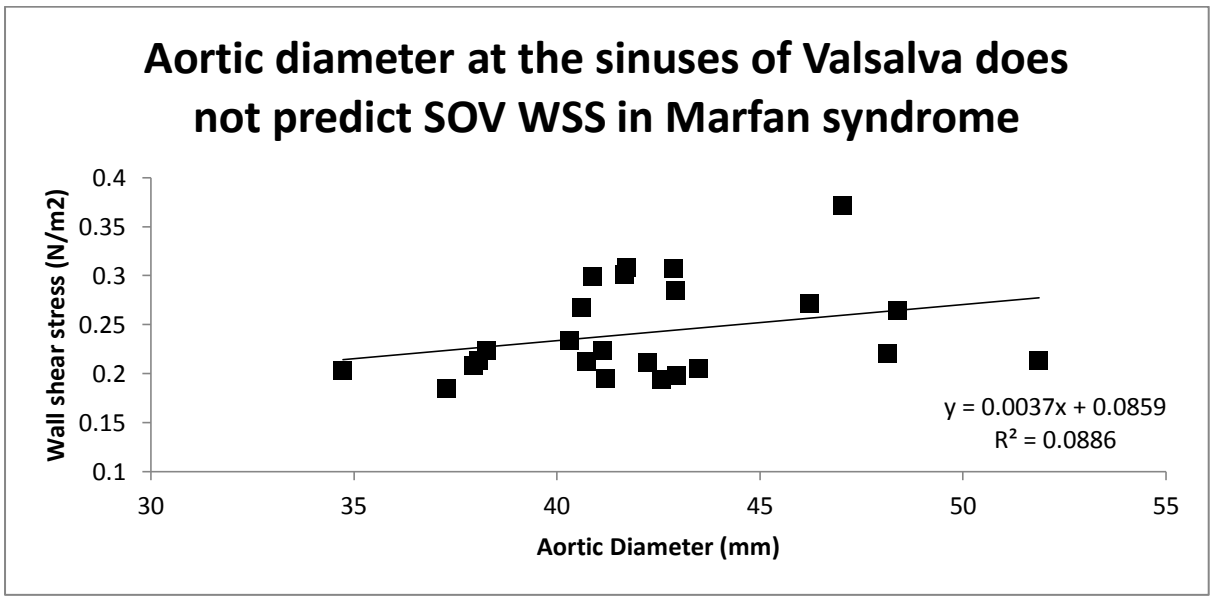

Figure 4.9: Mean wall shear stress (WSS) by aortic dimensions at the sinuses of Valsalva (SOV) among subjects with Marfan syndrome.

4.5. DISCUSSION

This work demonstrates lower levels of mean aortic WSS in a sample of subjects with MFS compared to an age-, sex- and height-matched sample of healthy subjects. These findings were consistent irrespective of anatomical location evaluated, and suggest a generalised reduction of WSS.

There is now a significant body of literature supporting the importance of WSS and its related variable, OSI, in vascular function (82). Shear affects endothelial cell membrane and cytoskeletal function, gene expression, signalling and turnover and alignment (82,83). It alters adhesion molecule expression and so may influence the recruitment of inflammatory cells into the vascular wall (84). Some of these data derive from animal models, and it should be noted that theoretical allometric approaches predict significantly increased WSS in small mammals compared to humans (e.g. 20-fold) (83).

WSS exerts a potentially disruptive force on the wall of the aorta, and locally or transiently high levels of WSS may play a role in the progression of aortic dilation or in the initiation and propagation of aortic dissection. Moreover, in vitro studies have demonstrated that variations in WSS within the physiological range alters gene expression of several mediators of vascular dysfunction in endothelial cells and both directly and indirectly on vascular smooth muscle cells and fibroblasts, with low WSS in particular being associated with up-regulation of pro-atherosclerotic and pro-aneurysmal mediators (85). The TGFβ pathway, which is now thought to be central to the pathogenesis of aortic disease in MFS (86), is sensitive to WSS in vitro, and the mechanism of TGFβ alteration may relate to the activation of the intra-cellular Mitogen-activated protein kinase (MAPK) group of proteins, such as ERK 1/2, p38 and JNK, which are all activated in vitro by WSS alterations (87), or to WSS related changes in Smad signalling (88). Computational modelling of aneurysm behaviour in a range of aneurysmal states has suggested that aneurysm formation associates with low WSS (89).

WSS can be derived using a number of methods which have been validated in vitro and in vivo (90) and has been characterised in vivo in healthy volunteers using 2D phase-contrast flow imaging in the aorta; pulmonary (91), carotid, femoral and brachial arteries (92); and in the inferior vena cava at rest and during exercise (93), and has been shown by similar methods to be altered in the aorta of patients with atherosclerosis (82) and bicuspid aortic valve disease (94). CFD models predict a lowering of aneurysm shoulder stress (89).

Stalder et al first described the method used here to estimate WSS, and reported synthetic data, error propagation analyses, inter-individual, inter-modality, and inter-observer variability in 19 healthy subjects, and provided validaition of the method compared to 2D methods (95). Markl et al demonstrated scan-rescan repeatability (81), and Frydrychowitz et al reported regional variations in the distribution of WSS within the thoracic aorta in 31 healthy subjects (67). Harloff et al described the WSS distribution in 62 subjects with documented atherosclerosis of the aorta, and correlated low WSS (but not high oscillatory shear index (OSI)) with the localisation of plaques in the aorta (68). Frydrychowitz et al reported elevated WSS levels both near and distant to the site of repair of coarctation of the aorta in 24 subjects (78). Hope et al found asymmetric distribution of WSS in the ascending aorta in patients with bicuspid aortic valve disease (96), whereas Bieging et al found a similar range of patterns of WSS in patients with aneurysmal ascending aortic disease and in healthy patients (97). These studies excluded patients with MFS. Geiger et al evaluated 17 predominantly paediatric patients with MFS, focusing on those with minimal aortic dilation, and found asymmetries of wall shear stress, but normal overall levels of wall shear stress (98). The explanation for these differences likely represent a manifestation of the less severely affected population, at an earlier stage of disease development than those studied in this work.

The method used for estimating WSS makes a number of assumptions which must be remembered when evaluating these data. Firstly, blood is assumed to be a Newtonian fluid. Secondly, the profile of blood flow is assumed to be parabolic. Thirdly, the WSS is estimated based on the near-wall spatial velocity gradient, and not by a measurement made at the blood fluid interface itself.

There was substantial overlap in the magnitudes of WSS seen in subjects with MFS compared to healthy subjects in this work, and so the method will not be useful as a diagnostic test. Furthermore, the study design was cross-sectional, and no causative link between WSS and progression of aortic dilation can be assumed. Further longitudinal studies are required to confirm this finding, and to evaluate its prognostic significance.

The advantages of multi-dimensional flow-based WSS estimation compared to methods using conventional flow imaging (with velocity encoding in only a single direction) is that such methods allow for the estimation of vectorial WSS, not only its axial component. Furthermore, 3-directional volume acquisitions allow for an unlimited number of planes to be prescribed anywhere within the aorta without increasing acquisition time, and planes can be prescribed with great care because the analysis is performed off-line.

4.6. CONCLUSIONS

WSS estimation from near-wall velocity gradients is reproducible. Mean WSS is reduced in the aorta of subjects with MFS compared to healthy subjects of similar age, gender distribution and height. The association between increased aortic dimension and increased WSS seen in the sinuses of Valsalva in healthy subjects was not seen in subjects with MFS.

CHAPTER 5

AORTIC RELATIVE PRESSURE AND ITS COMPONENTS IN HEALTH AND DISEASE

5.1. ABSTRACT

5.1.1. BACKGROUND

A comprehensive description of the relative spatiotemporal pressure gradients which drive blood flow has been an important goal of haemodynamics over six decades. Advances in phase-contrast magnetic resonance imaging (PC-MRI), coupled with novel computational methods, now make possible the visualisation and quantification of the spatio-temporal distribution of these pressure gradients in the human aorta in health and disease, and, uniquely, its physical components. This chapter describes the development of such an approach, and its application to the aorta in healthy volunteers, in selected patients with established changes in aortic geometry.

5.1.2. METHODS

Six subjects (three healthy subjects, and three subjects with severe derangements of aortic geometry relating to MFS, bicuspid aortic valve disease and repaired Type A aortic dissection) underwent 4D flow CMR acquisition and specialised post-processing using a novel algorithm to allow visualisation and offline quantification of overall relative aortic pressure distributions, and the three physical components of relative pressure, the temporal, spatial and viscous components. Cases were selected to maximise the differences between healthy subjects and subjects with aortic diseases.

5.1.3. RESULTS

Pressure distributions for healthy subjects were similar in all three healthy subjects, and agreed with previously published values using a different method of pressure estimation. Subjects with aortic disease showed markedly different aortic pressure distributions compared to healthy subjects, and each diseased subject showed characteristic differences in the pressure field. Disturbances in aortic geometry (e.g. angulation, dilation) and in the flow field (e.g. regions of high vorticity) were each associated with disturbances of pressure. An analysis of the physical components of aortic pressure (temporal, spatial and viscous) found that overall pressure was predominantly related to temporal

acceleration (mean pressure difference between ascending and descending aorta, 15 mmHg, at peak acceleration in healthy subjects), with a smaller, but potentially important contribution made by the spatial accelerations (mean pressure difference 3 mmHg at peak velocity in healthy subjects between the same reference points).

5.1.4. CONCLUSIONS

A finite-element computational approach to 4D flow datasets can be used to visualise and quantify relative spatiotemporal pressure in the aorta in health and in selected aortic diseases, and allows for the isolation and separate evaluation of the physical components of relative pressure, with potential implications for mechanisms of disease and planning of therapy.

5.2. INTRODUCTION

Considerable progress has been made in understanding the biological processes of the aortic wall which predispose to a tendency to develop aortic aneurysms in aortic disease in general, and particularly so in MFS (86). Time-resolved, phase-contrast CMR with 3-directional velocity encoding (4D flow CMR) now allows for a detailed understanding of the patterns of blood flow disturbance in these conditions, such that a picture can be built up of the loads to which the aorta must respond.

The regional distribution and temporal changes in aortic pressure in human subjects are not well understood, particularly in aneurysmal aortic disease, and may play a particularly important role in driving progression of aortic aneurysm, and are likely to be critical in initiating complications such as dissection and rupture. Understanding the nature and origin of these pressure changes may lead to new insights into the mechanisms of aneurysm growth, dissection and rupture, may provide novel approaches to risk stratifying patients, and may inform the development of novel therapies for patients who are likely to experience complications.

The pressure in a viscous fluid, such as blood, can be considered to arise as a consequence of two types of forces acting upon the fluid, inertial forces and viscous forces. The inertial forces are those forces which arise as a result of the momentum inertia of blood, whereas the viscous forces arise as a result of the internal resistance to flow characteristic of all viscous fluids, including blood. In the vessels of the human cardiovascular system under normal circumstances, other forces acting on blood, such as the gravitational component, can reasonably be neglected. The inertial forces can themselves be meaningfully resolved into two further components: those that cause the temporal, or time-varying acceleration of the blood (*unsteady* acceleration, sometimes called *transient* acceleration), and those that cause the spatial changes of the flow (*convective* acceleration). Pressure is therefore decomposed into three components: unsteady, convective and viscous.

PC-MRI with 3-directional velocity encoding has emerged over the last decade as a valuable approach to the comprehensive visualisation and quantification of blood flow within a large 3D field of interest, such as the entire thoracic aorta (76). Flow patterns, derived from velocity fields, have been shown to vary with anatomical location and extent across a range of cardiac and vascular diseases (4). The velocity field, when coupled with established values for the density and viscosity of blood, provide, in principle, all of the information necessary to solve the equations which describe the pressure field (*the Pressure Poisson Equation*), and so potentially allow access to the time-resolved cardiovascular pressure field.

5.2.1. AIM

This chapter aims to describe: (1) the development, optimisation and application of a novel computational method which allows the estimation of relative pressure and its components (unsteady, convective and viscous) in the human circulatory system, including methods of data display for these complex datasets; (2) the application of the technique to the thoracic aorta in healthy volunteers to establish sample relative pressure maps in healthy subjects; and (3) the application of the technique to the thoracic aorta of selected individuals with marked abnormalities of aortic geometry.

5.3. METHODS

5.3.1. COMPUTATIONAL METHODS

The numerical solution to the Pressure Poisson problem was implemented initially in OpENCMISS, a multi-physics and multi-scale computational infrastructure, and subsequently in CHEART. The numerical model (fully described in Krittian et al (99)), allows the direct computation of cardiovascular pressure relative to a defined reference point, based on 4D flow velocity data input. An overview of the fundamental concept is provided in Figure 5.1 and of the methodology is provided in Figure 5.2. The analysis of blood flow velocity, captured by PC-MRI, enables the calculation of the pressure differences by solving Newton's second law applied to fluid motion, i.e. the Navier-Stokes equation. The solution of this equation in each of the frames of the PC-MRI sequence is assembled to produce the spatio-temporal maps. Pressure values in this study are obtained with respect to a reference point located at the descending aorta, 250 mm from the sinotubular junction.

5.3.2. CASE SELECTION

Three healthy volunteers (HV1–3) with no known cardiovascular disease were selected for pressure estimation to develop, optimise and apply the pressure estimation method. Subject characteristics were as follows: HV1 21-year-old male; HV2 23-year-old female; HV3 28-year-old male.

Three subjects with particularly marked abnormalities of aortic geometry were selected to test the ability of the pressure estimation method to identify and characterise aortic pressure differences in marked aortic disease. Patient characteristics are as follows: Subject 4 is a 55-year-old male with a bicuspid aortic valve (BAV) and an aneurysm of the ascending aorta (maximum aortic dimensions 4.6 cm at the level of the pulmonary artery, peak blood velocity 1.4 m/s). Subject 5 is a 39-year-old male, who sustained a Type A aortic dissection (AoD) 2 years previously, for which he underwent immediate aortic valve and aortic root replacement with a mechanical valved conduit. The dissected distal ascending aorta and dissected aortic arch were not treated surgically, giving rise to a 'double

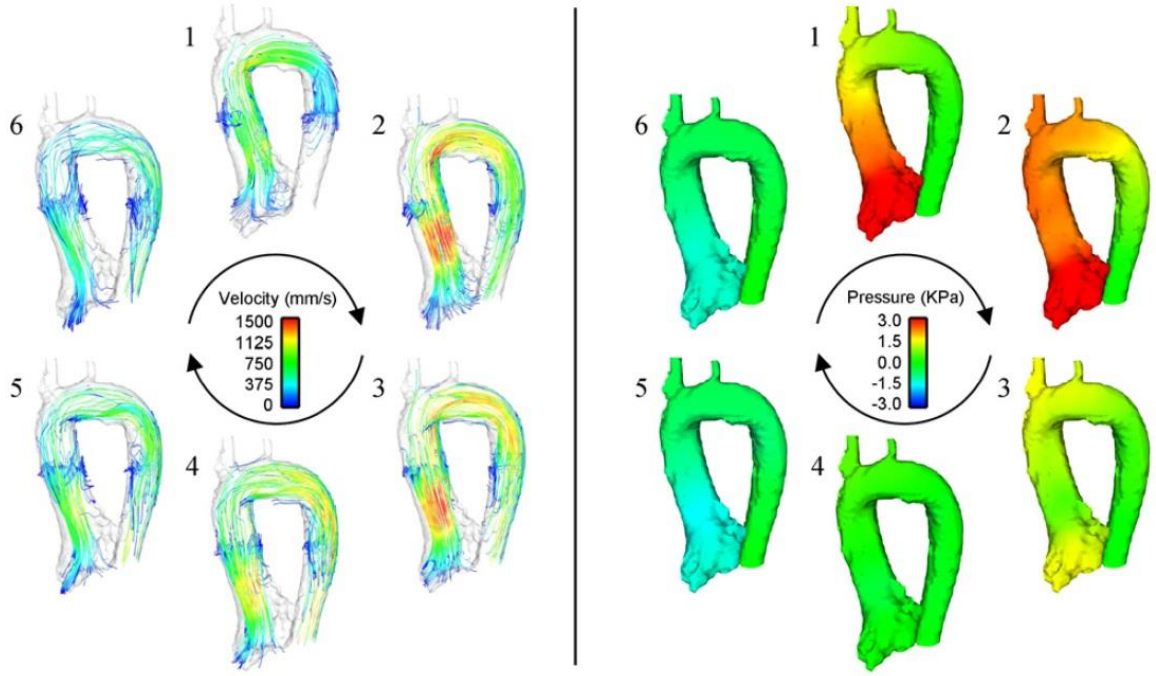

Figure 5.1: Input velocity field of a healthy volunteer projected on streamlines (left) and estimated pressure projected on fluid domain boundary (right), at various points in the cardiac cycle (from Krittian et al, 2012 (99), reproduced with permission).

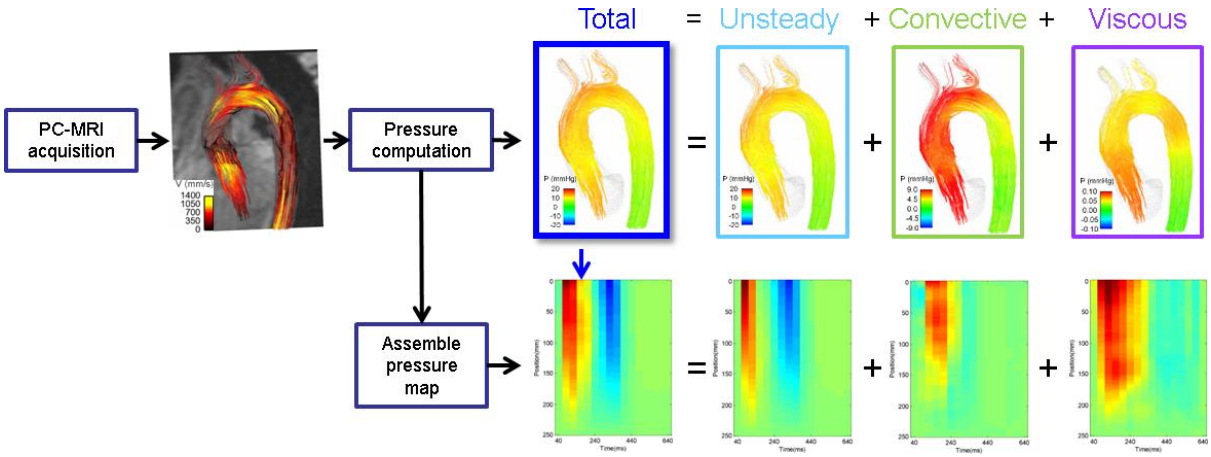

Figure 5.2: Overview of the methodology for the computation of the spatio-temporal maps of relative pressure in the aorta. The top of the illustration represents the data workflow from a single frame, frame 4, which constitutes the fourth column in the spatio-temporal map, as indicated by the blue arrow.

barrelled' distal ascending aorta and arch. The false lumen re-enters the true lumen at the proximal descending aorta. Subject 6 is a 49-year-old female with MFS. She had no prior surgical treatment and was treated with beta-blockers. The sinuses of Valsalva were mildly dilated at 4.0 cm and the proximal descending aorta was also mildly dilated at 3.2 cm.

5.3.3. CMR DATA ACQUISITION

Each subject underwent PC-MRI as described in the general methods section.

5.3.4. CMR DATA PRE-PROCESSING

Data pre-processing was performed in Matlab using the Velomap tool to correct for eddy currents, velocity aliasing and noise masking to generate a reliable flow field as previously described (100). The fluid domain where calculations were to be performed was defined by automated segmentation of the aorta and its major branches by thresholding the average velocity magnitude per voxel, followed by manual segmentation to remove adjacent structures to the aorta.

5.3.5. PRESSURE ESTIMATION

The computational method of estimation of pressure gradients from PC-MRI derived velocity fields based on a finite-element approach is that of Krittian et al (99). In this paper the mathematical and numerical foundations of the pressure estimation process were described. In brief, for an incompressible, laminar Newtonian fluid of density ρ and viscosity μ, the relationship between pressure and flow can be described using the Navier-Stokes Equation:

$$\nabla p = \underbrace{\mu \nabla^2 \boldsymbol{u}}_{viscous} - \underbrace{\rho \frac{\partial \boldsymbol{u}}{\partial t}}_{unsteady} - \underbrace{\rho(\boldsymbol{u} \cdot \nabla)\boldsymbol{u}}_{convective}$$

where p is pressure, u is blood velocity, and t is time, and where the three components of pressure gradients are described. Computations use published values for the density and viscosity of blood for all subjects (ρ = 1.06 kg/m^3, μ = 0.0035 Pa·s). The contribution that each component makes to overall

relative pressure is computed by solving the above equation with each of the fluid forces independently.

5.3.6. VISUALISATION AND CALCULATION OF SPATIO-TEMPORAL MAPS OF RELATIVE PRESSURE

Post-processing of the derived pressure fields in order to obtain a set of spatio-temporal maps of pressure was undertaken as follows: the centreline of the aorta was obtained using a skeletonization algorithm (101). For each frame of the sequence, the average value and standard deviation of pressure is calculated along the centreline of the aorta in evenly spaced points separated by a distance of 1 mm. A disk is defined perpendicular to this centreline at each point and the extent of the segmented fluid domain, and is used to define the set of samples within which the pressure field is linearly interpolated. A schematic representation of relative pressure is provided in Figure 5.3.

5.4. RESULTS

Pressure differences are positive in early systole, negative in late systole, and relatively flat in diastole. Pressure values are primarily caused by the temporal acceleration of blood. A smaller but still important contribution is made by the convective component, but the phase of this waveform is typically approximately 90° out of phase with the unsteady component, and so has an important effect in modifying the shape of the total pressure transient (see Figure 5.4). The pressure difference between the ascending and descending aorta due to the temporal component in healthy subjects was 15 mmHg, compared to 3mmHg for the convective component. The viscous component is negligible compared to the other two components (mean of 0.2 mmHg in this example). A summary of the key general and specific characteristics of the pressure differences in health and disease is provided in Table 5.1.

5.4.1. HEALTHY VOLUNTEERS

The temporal transients of pressure difference show a smooth sinusoidal shape (see Figure 5.4). They show small spatial inhomogeneity in cross section through the aorta (i.e. in the plane perpendicular to the long axes of the aorta/in the short axis of the aorta), in keeping with theoretical expectations (102).

During early systole, blood flow is accelerated, caused by a positive gradient of unsteady pressure (average gradient of 85 mmHg per m of aortic length at the frame with peak acceleration, see Figure 5.5), and during late systole blood is decelerated by a negative gradient (average gradient of -50 mmHg/m at peak deceleration, see Figure 5.5). The acceleration phase has a smaller duration than deceleration (160 ms versus 240 ms). At mid-systole, convective pressure is maximal (average gradient in the aortic arch of 46 mmHg/m, see Figure 5.5), when velocity is maximal and unsteady forces are minimal. Viscous pressure is also maximal at peak systole, and the average gradient at this time is 0.4 mmHg/m.

Table 5.1: Summary of qualitative characteristics observed in the pressure differences (PD) in the aorta, and its components, in the healthy and diseased subjects.

	Total	**Unsteady**	**Convective**	**Viscous**
Meaning	PD between two anatomical points (see Figure 5.3), as if measured by two catheters	Responsible for the temporal acceleration (positive values at early systole) and deceleration (negative values at late systole)	Responsible for the spatial acceleration (changes of direction and vessel tapering). Peaks at maximum velocity	Flow inefficiencies due to blood friction (low signal to noise ratio)
Healthy (HV1–3)	Smooth spatio-temporal transients	Big acceleration and deceleration	Big acceleration at arch (outer curvature)	Losses during systole
Bicuspid valve (BAV)	Delayed and narrow negative peak	Smaller magnitude, delayed deceleration	Drop in pseudo-coarctation. Increase after aneurysm (tapering)	Noise
Dissection (AoD)	Small magnitude	Long and weak deceleration, with peak at the end	Drop at the start of false lumen in systole	Noise
Marfan syndrome (MFS)	Smallest magnitude	'Bi-phasic' deceleration, with two negative peaks	Very small, quite abrupt drops, like in vortex at end of arch	Losses during systole

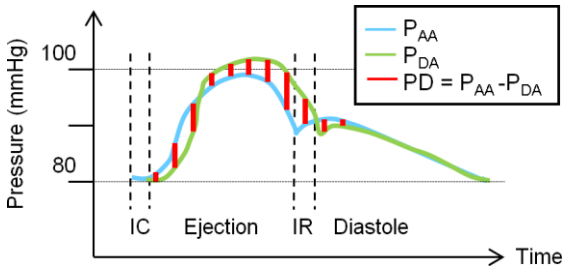

Figure 5.3: Schematic representation of the temporal transients of pressure in the aorta, illustrating the pressure difference (PD) between the ascending (PAA) to the descending aorta (PDA). The analysis of the blood flow velocity enables the computation of PD.

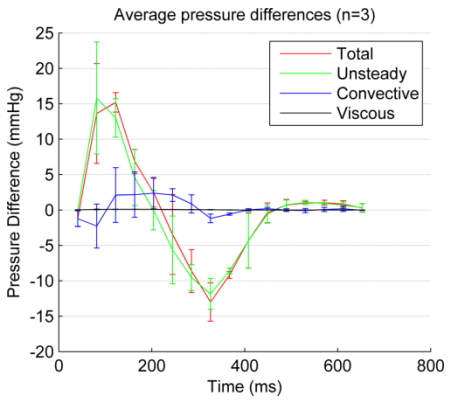

Figure 5.4: Average temporal evolution of the aortic pressure difference between the sinotubular junction and the descending aorta (at a distance of 250 mm from the aortic root) in three healthy volunteers, decomposed in its three components: unsteady, convective and viscous. Confidence intervals indicate mean +/- 1 std.

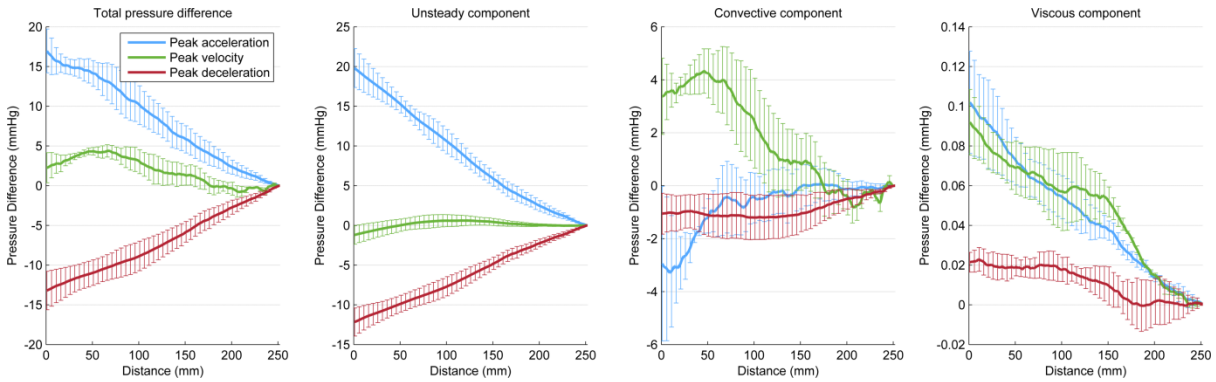

Figure 5.5: Average spatial evolution of the aortic pressure difference in the three healthy subjects in systole. Distances are measured from the sinotubular junction. Confidence intervals indicate mean +/- 1 std.

During diastole, blood is predominantly accelerated towards the descending aorta by a positive gradient of unsteady pressure (average gradient of 4.3 mmHg/m at the first diastolic frame, and 1.9 mmHg/m at the last diastolic frame, see Figure 5.5). At the middle of diastole there is an acceleration of blood from the aortic arch towards the sinotubular junction, with an average gradient of unsteady pressure of -1.8 mmHg/m (see Figure 5.5). Convective and viscous components of pressure have quite low amplitude and a noisy appearance during diastole.

5.4.2. DISEASED SUBJECTS

Diseased subjects showed differences from healthy volunteers and from each other, particularly in the peak value of unsteady gradients, in the duration of the acceleration and deceleration phases, and in the appearance of regional changes in the convective component of pressure. Patients show smaller values of unsteady pressure, with a quicker acceleration and slower deceleration phase (see Table 5.2).

The aneurysm in the BAV subject results in regional changes of both the unsteady and convective components: the unsteady gradient decreases to 15 and -8 mmHg/m at peak acceleration and deceleration respectively, and a drop of convective pressure (see Figure 5.6) of 3 mmHg at the time of peak velocity. The convective drop is caused by a vortical flow in the middle of the aneurysm (see Figure 5.7), and is recovered downstream. A similar vortical pattern is present after a pseudo-coarctation in this BAV subject, where the drop is of 8 mmHg at peak velocity, but in this point the pressure does not return to pre-coarctation values. In the AoD subject the convective pressure experiences a sudden drop of 5 mmHg at peak velocity, without recovery, due to the presence of the entry tear of the dissection (see Figures 5.6 and 5.7). The MFS subject presents the weakest blood acceleration (see Table 5.2) and the smallest convective pressure. It presents a drop and recovery of 1 mmHg in convective pressure at the formation of a vortical flow during late systole and part of diastole (see Figures 5.6 and 5.7). The viscous component of pressure is nevertheless bigger than in the other two diseased subjects, with an average gradient of 0.12 mmHg/m at peak velocity, and with a spatio-temporal pattern similar to the healthy subjects.

Table 5.2: Unsteady pressure indexes in healthy and diseased subjects.

	Peak +P_u (mmHg/m)	**Duration +P_u (ms)**	**Peak -P_u (mmHg/m)**	**Duration -P_u (ms)**
Average healthy (HV1-3)	85.3	160	-49.8	240
Aneurysm (BAV)	47.7	120	-26.0	320
Dissection (AoD)	49.2	120	-20.2	280
Marfan syndrome (MFS)	39.5	120	-20.4	320

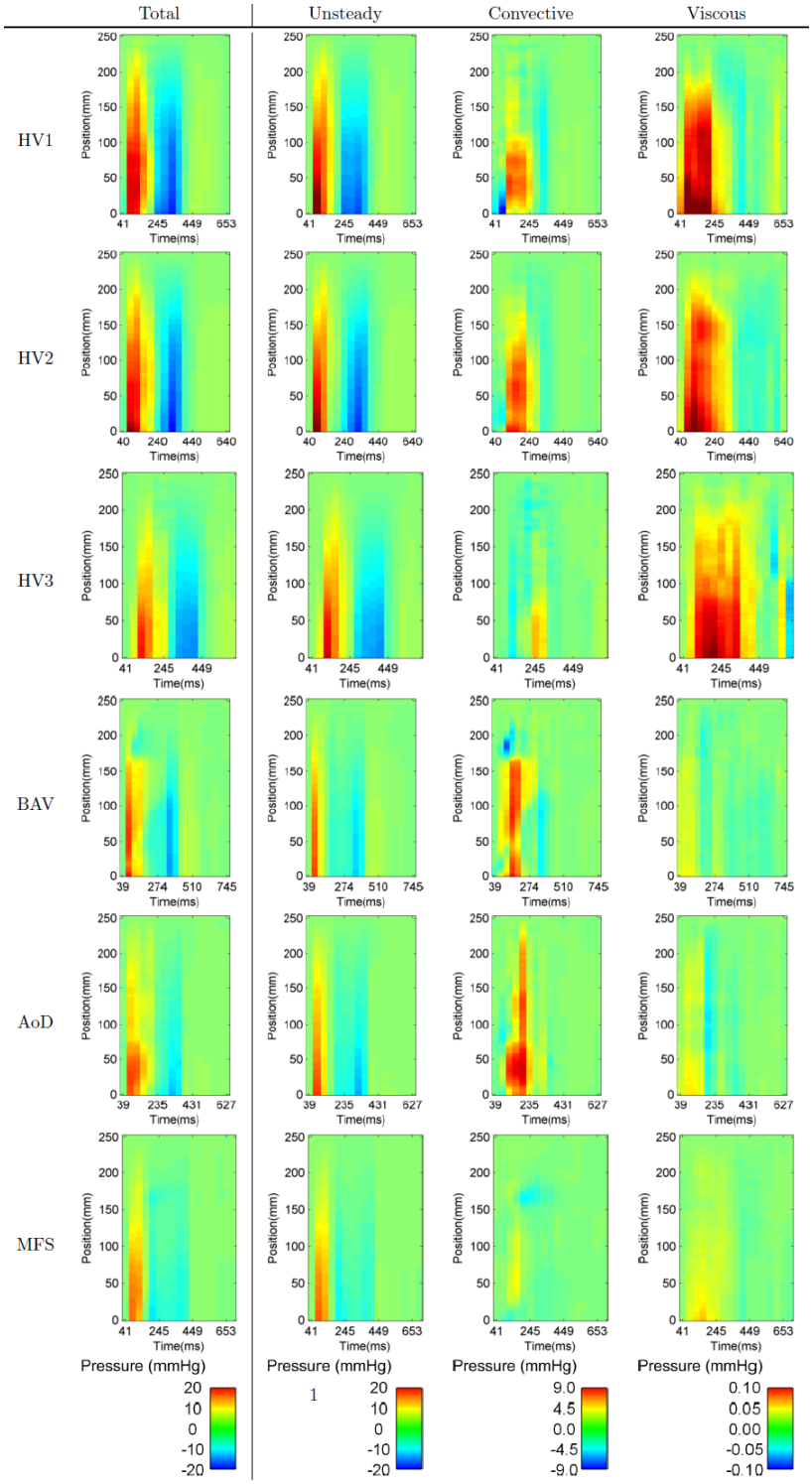

Figure 5.6: Spatio-temporal pressure maps in the six subjects analysed (Healthy, HV1–3, and diseased, bicuspid aortic valve – BAV, dissection – AoD, and Marfan – MFS). Each map shows the average pressure alongside the length of the aorta (Y axis, from sinus of Valsalva at the top of the axis, to the reference point at the descending aorta) through time (X axis). Pressure scale (in mmHg) is different for each component and the same across subjects, as is indicated in the middle of each column.

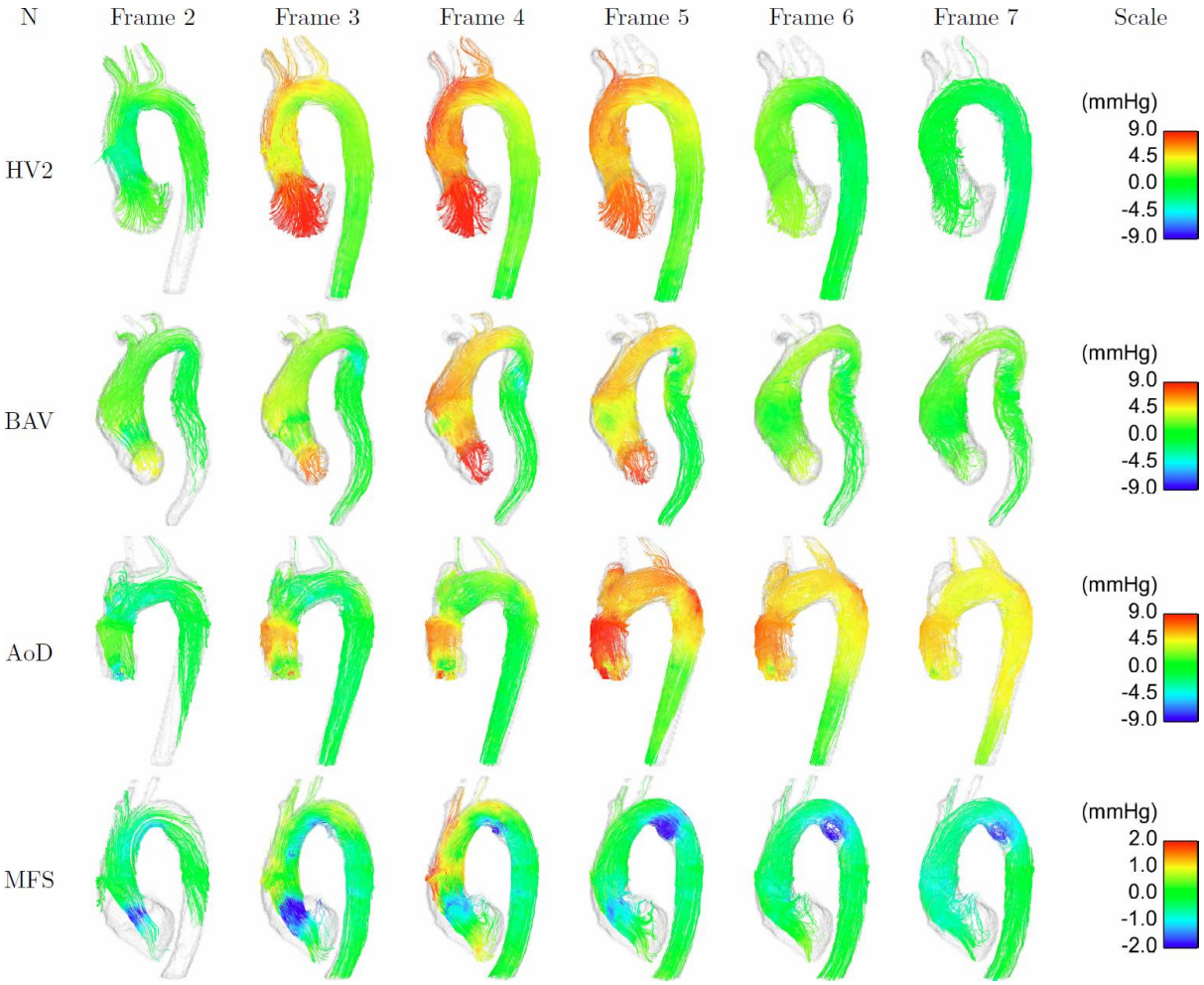

Figure 5.7: Detailed anatomical inspection of the convective pressure in four of the subjects under study, showing velocity streamlines coloured by pressure. The Marfan subject (MFS) shows how vortexes are characterised by a drop of pressure, and the pseudo-coarctation of the bicuspid subject (BAV) shows an abrupt drop of pressure in frames 5 and 6. Note that the colour scale is different for the MFS subject.

5.5. DISCUSSION

5.5.1. SUMMARY OF FINDINGS

This work has contributed to the development, optimisation and application of a computational approach to the estimation of relative pressure (99) in the human cardiovascular system. This approach is comprehensive and robust, and has significant advantages over previous methods. The computational approach has been extended to allow the separation, and thus the distinct characterisation, of the physical components of pressure by mathematically isolating the terms of the Navier-Stokes equation. This required a new approach to the systematic display of aortic relative pressure datasets, solved by the representation of the aortic relative pressure field as a relative pressure map. These methodological developments were then applied to the aorta of healthy subjects, and provided a detailed representation of the spatiotemporal patterns of aortic relative pressure in healthy individuals, which was summarised descriptively. This approach was then applied to three individuals selected for highly abnormal aortic geometry. This group of subjects illustrates the ability of the technique to discriminate, localise and quantify spatial and temporal pressure characteristics, finding differences between healthy and diseased aortas.

5.5.2. ASPECTS OF STUDY DESIGN AND METHODOLOGY

Particular strengths of the approach include: (i) the use of comprehensive, high spatial resolution time-resolved phase-contrast imaging with 3-directional velocity encoding as the basis for pressure estimation, which is not reliant upon traditional assumptions involved in pressure estimation from velocity data such as the modified Bernoulli method (100); (ii) the use of a finite element computational approach which allows a quick, robust and accurate direct calculation of the entire aortic pressure field (99); (iii) the demonstrated capacity of distinguishing and localising (spatially

and temporally), and characterising marked differences in relative pressure and its components between healthy volunteers and diseased patients, with and without prior aortic dissection.

Some potential limitations of the approach should be recognised, which may limit immediate clinical applicability of the approach. 4D flow acquisitions were relatively long (typically 20 minutes), and post-processing and computation times are, at present, too long for routine clinical application. Accelerated acquisition, improved workflows and novel computational solutions and platforms are already reducing these times.

4D flow data are averaged across many heartbeats, and so are insensitive to beat-to-beat instabilities of flow. This can have a potential influence on both large-scale (i.e. recirculation areas) and small-scale fluctuations (i.e. to turbulence). True turbulence is not common in aortic diseases in the absence of severe stenosis, and so is unlikely to affect the pressure estimations to an important degree in the subjects shown, but might have a potential influence in other conditions of interest, such as aortic valvular stenosis and coarctation of the aorta where turbulence is likely. Interesting approaches to the estimation of turbulence intensity have recently been proposed (103), and future work will focus on the implementation of approaches of this type, particularly where turbulence is known or suspected.

The relatively low temporal resolution (approx. 40 ms) acts as a low pass filter on the estimated pressure profiles, and this mainly affects the unsteady component. Convective and viscous components are less affected by temporal resolution and are related more closely to spatial resolution, which is reasonably high in these acquisitions.

5.5.3. RELATIONSHIP TO OTHER METHODOLOGIES

The anatomical arrangement of cardiac chambers and vessels, and their contractile, relaxation, elastic and resistant properties all contribute to the distribution and time-course of pressure within the aorta. The momentum imparted to blood by this circulatory arrangement can itself impact on the aortic wall, and, by interacting with the mechanical properties of the vessel wall, induce geometric changes. The

aorta and its major branches serve a number of functions important to the efficient working of the cardiovascular system. These include a conduit function and a flow-smoothing, or Windkessel, function. Invasive studies in the 1960s showed that the magnitude and shape of the aortic pressure function with time differs from that recorded in peripheral arteries, and that there are regional changes in these features along the length of the aorta, a familiar experience to those undertaking cardiac catheterisations (104).

Catheter-based pressure measurements are, however, only able to describe the pressure waveform at one anatomical location (or at most a few) at a time, and therefore make it difficult to build up a comprehensive picture of the pressure distribution in space and time throughout the entire aorta and throughout the cardiac cycle. In particular, pressure gradients – which are the fundamental drivers of blood flow – are particularly difficult to understand in a comprehensive way using invasive catheters. Furthermore, invasive approaches carry well-described risks of serious complications, particularly in patients with certain aortic diseases or configurations (such as after aortic dissection), and require ionizing radiation for catheter guidance.

Doppler-based pressure difference estimates are widely used and are very useful in many clinical situations. Nevertheless, they are operator dependent, require good acoustic windows, and can normally only estimate spatial pressure gradients along the plane of insonation, and within a narrowly defined region of interest. Such estimates are also highly sensitive to velocity measurement errors due to the exponentiation of velocity terms in these equations.

Central blood pressure estimation from the shape of the peripheral pulse contour has a long history, but an approach in which non-invasively measured radial artery pressures were used as the basis for such estimations was introduced by Kelly (105). Radial artery applanation tonometry was used to generate a peripheral waveform, which was calibrated using non-invasive brachial artery pressure measurements, and transformed using a generalised transfer function. This technique has been evaluated in invasive studies and widely used in research studies. This approach is important as it

emphasises the differences between central and peripheral pressure in humans, but, as currently implemented, does not provide information about relative pressures or pressure gradients within the central circulation. The approaches should be regarded as complementary.

In the field of pressure estimation from PC-MRI, Song et al (1994) computed cardiac pressure fields using an iterative approach by first deriving a 3D velocity field from ultrafast CT images of the heart (106). Iterative methods for pressure estimation based on directly measured velocities using a series of 2D PC-MRI images were introduced by Yang, Kilner et al (107), then extended to true 4D PC-MRI datasets by Tyszka et al (108) and by Ebbers et al (109), and improved to account for any arbitrary domain by Ebbers and Farnebäck (110). This approach has been systematically applied to healthy volunteers and to a small number of patients with coarctation of the aorta by Bock et al (100), who also showed that a more accurate pressure field estimation is achieved by extracting the actual fluid domain from its surrounding imaging space. We have previously proposed a finite-element approach which overcomes several limitations of the iterative method, and also has some theoretical advantages over the finite-difference method (99). We have now applied this technique, with certain technical refinements, to several healthy volunteers and to patients with aortic disease. The reliable estimation of pressure differences based on PC-MRI derived velocity field data has been validated using phantoms (100) and in-vivo in animal models (111). Verification results of our finite-element method approach are reported in Krittian et al (99). The temporal profiles of central aortic blood pressure differences reported in this work agree both qualitatively and quantitatively with previous results published in the literature (100,104).

5.5.4. MECHANISTIC IMPLICATIONS OF FINDINGS

A detailed understanding of the temporal and spatial pressure gradients within the aorta may give insights into vascular diseases more generally. The pressure drop through an aortic coarctation changes through the heart cycle, and depends on fundamental assumptions taken for its computation from either ultrasound or MRI (100). Increased arterial stiffness, common to a number of vascular

diseases and characterised by increased aortic pulse wave velocity and altered wave reflections, has important consequences for the coronary and cerebral circulatory beds, and the way in which incident and reflected pressure waves interact is not fully understood.

The maps of the pressure field decomposition immediately suggest new ways of thinking about aortic pressure. The components of pressure can be interpreted by their different origins. The unsteady component is likely to be heavily influenced by time-varying forces acting externally on the blood – in particular the vigour and timing of left ventricular ejection. The convective component, in contrast, is more likely to be governed principally by spatial variation in external forces acting on blood by changing its flow direction, governed by particular aortic geometry. If this hypothesis is correct, and if – as seems likely – intra-aortic pressure is an important determinant of the location and timing of aortic complications such as aneurysm, dissection and rupture, then one can foresee that the component analysis of aortic pressure could allow treatment strategies in aortic disease to be focused on those components of the pressure distribution which are most likely to be remediable, or to those components which contribute most to disorganisation of total pressure at critical points in the cardiac cycle and at particularly vulnerable anatomic locations.

CHAPTER 6

VENTRICULAR VOLUMES AND FUNCTION IN MARFAN SYNDROME

6.1. ABSTRACT

6.1.1. BACKGROUND

Increased left ventricular volumes, and impairment of left ventricular systolic function, are important prognostic markers across a wide range of cardiovascular diseases, and have been reported in MFS. There have been anecdotal reports of MFS patients who have poor LV / low ejection fraction in the absence of significant AR, and some case series with conflicting findings. It remains uncertain whether such changes occur in the absence of associated valve disease and/or shunt. The relationship between left ventricular volume loading and ventricular size and function in MFS is not understood. Involvement of the right ventricle has not been well characterised.

6.1.2. METHODS

34 subjects with MFS and 70 healthy subjects (37 with, and 33 without, significant mitral regurgitation) underwent cine CMR imaging of the ventricles, with quantitative analysis of left and right ventricular volumes and function. Subjects with MFS were carefully evaluated for the presence of significant shunt or valvular regurgitation, and data were analysed separately for subjects with and without significant shunt or valvular regurgitation. The ventricular response to volume overload was compared between subjects with mitral regurgitation (MR) due to MFS and due to non-MFS related causes.

6.1.3. RESULTS

Among subjects with MFS and no evidence of shunt or significant valvular regurgitation, no subject showed reduced left or right ventricular ejection fraction, and there were no significant differences between these subjects and healthy subjects in left ventricular end-diastolic volume, end-systolic volume or ejection fraction. Right ventricular volumes were not significantly different among subjects with MFS and healthy subjects. There was a small, but only marginally significant, 7% relative

increase in right ventricular ejection fraction in subjects with MFS compared to healthy subjects. There was close correlation between LVEDV and stroke volume difference among subjects with MR with and without MFS. The dependence of LVEDV on stroke volume (SV) difference was greater among subjects with MFS compared to controls. The relationship between LVEDV and SV difference suggests that there may be an enhanced left ventricular response to volume overload in subjects with MFS compared to subjects with volume overload due to other causes.

6.1.4. CONCLUSIONS

Evidence for enlarged left ventricular cavity size or impairment of systolic function was not found among unselected subjects with MFS, when shunt and/or regurgitation was carefully excluded. Subjects with MFS with LV volume loading (principally related to mitral regurgitation) show a close relationship between degree of stroke volume difference and LVEDV. This may, at least in part, explain the tendency to increased LV volumes reported in some other studies. Patients with MFS presenting dilated or impaired ventricles should be carefully evaluated for other causes of cardiomyopathy, and for unrecognised or underestimated regurgitant valve disease. Future research studies in this area should report methods by which shunt and regurgitation were excluded, or how account was taken of the degree of LV response related to valve disease.

6.2. INTRODUCTION

Increased LV cavity size and reduced LV systolic function are powerful predictors of prognosis in asymptomatic populations (112), and across a wide spectrum of cardiovascular disease (113). Increased LV cavity size in systole and diastole, and impairment of LV systolic and diastolic function, have been described in MFS, as have echocardiographic measures of RV systolic function, but the reported prevalence and severity of such findings vary considerably between studies, and the mechanisms by which they arise remain uncertain (2,114-120).

Longitudinal studies of subjects with MFS have shown an appreciable incidence of sudden cardiac death in the absence of demonstrable aortic dissection at post-mortem – 4% over a mean follow-up of 6 years in one series – and all of the patients who died in this way in this series manifested increased BSA-indexed LV end-diastolic dimensions ante-mortem (121). Sudden cardiac death in the absence of aortic dissection, sometimes during exertion (presumed arrhythmic, and perhaps relating to underlying cardiomyopathy), is well described, and can occur late after aortic surgery (122).

Insights into the molecular mechanisms of many aspects of MFS provide a theoretical basis for considering that ventricular impairments related to the fundamental pathophysiology of MFS are at least biologically plausible: the TGFβ receptor is widely expressed within the heart, including by cardiac myocytes and fibroblasts (123), and increased levels of TGFβ1 mRNA have been identified in cardiomyocytes from subjects with dilated cardiomyopathy (124). The close interaction between the renin-angiotensin-aldosterone system (particularly the Angiotensin 1 receptor and its downstream signalling pathways) and TGFβ signalling makes the hypothesis of a potentially treatable cardiomyopathy particularly attractive.

Mitral valve prolapse is extremely common in MFS, affecting up to 85% of patients (125), and is TGFβ dependent in fibrillin-1 deficient mice (126). The presence and severity of mitral regurgitation is not well defined, and its relationship to left ventricular parameters in MFS is not fully understood.

An echocardiographic study suggested an inverse association between the prevalence of mitral valve prolapse and left ventricular dilation (127). Studies of left ventricular volumes and function in MFS have not consistently reported methods for excluding subjects with valvular regurgitation and shunt, and where these methods have been reported, they frequently have not convincingly excluded all patients with regurgitation or shunt.

This work aimed to compare ventricular volumes and systolic function in subjects with MFS, in whom valvular regurgitation and/or shunt had been excluded, compared to matched controls, and to explore the relationship between LV volumes and degree of regurgitation and shunt in subjects with MFS.

6.3. METHODS

6.3.1. SUBJECTS

104 subjects underwent CMR and data were analysed in four groups: subjects with MFS and no evidence of valvular regurgitation or shunt (n=20); subjects with MFS and evidence of valvular regurgitation and/or shunt (n=14); healthy subjects (n=33); and subjects with known mitral regurgitation but no features of MFS (n=37).

Subjects with MFS met the Ghent criteria (1996). Subjects with MFS and healthy subjects were matched for age, gender and height. To explore the relationship between LV volume loading and LV size, subjects with MFS and documented mitral regurgitation were compared with subjects with known mitral regurgitation but no history of MFS. These subjects were recruited to the OxValve study, a large, population-based cohort study of valvular heart disease in an Oxfordshire population.

6.3.2. PROTOCOL

All patients ceased beta-blockade at least 72 hours prior to CMR imaging. Subjects with prior cardiovascular surgery were excluded from the analysis. All patients with echocardiographic features of aortic or mitral valvular regurgitation which was more than mild were excluded from the primary analysis of ventricular volumes and function (but were included in the analysis of subjects with regurgitation and/or shunt). Presence of valvular regurgitation and/or shunt was defined on the basis of the RV/LV stroke volume difference. If this difference exceeded the 95% confidence interval of the mean absolute population difference for controls, patients were excluded.

6.3.3. CMR DATA ACQUISITION

Ventricular volumes and function data were acquired on a 1.5T CMR system. After pilot imaging, a stack of steady-state free precession (SSFP), short axis cine images were acquired from the

atrioventricular groove to the cardiac apex, perpendicular to the ventricular long axes. Acquisitions were performed during held end-expiration, using retrospective electrocardiographic gating. Sequence settings were: echo time 1.5 ms, repetition time = 47.8 ms, field of view 236 × 360 mm, read matrix 111, phase matrix 256, slice thickness 7 mm, with a 3 mm gap between slices, 25 frames per cardiac cycle (typical temporal resolution of 50 ms depending on heart rate), flip angle 56°.

6.3.4. CMR DATA ANALYSIS

Left and right ventricular endocardial contours were manually segmented based on the short axis stack of cine images, at each slice position, at end-diastole and end-systole using ARGUS software (Siemens, Erlangen, Germany). Left ventricular basal slices were included in the segmentation if more than 50% of the lumen was surrounded by myocardium, and papillary muscles were excluded from the ventricular volume. This segmentation was used to quantify left and right ventricular end-diastolic and end-systolic volumes, and to calculate ejection fraction, stroke volume and stroke volume difference.

6.3.5. ASSESSMENT OF SHUNT AND VALVULAR REGURGITATION

Firstly, trans-thoracic echocardiograms were evaluated for each subject with MFS, and subjects were excluded from the primary analysis of ventricular function if any valve showed valvular regurgitation of a degree greater than mild, or if a shunt (of any magnitude) was identified on colour flow Doppler imaging. Secondly, the stroke volume difference for right and left ventricles was calculated from CMR acquisitions. The maximum permitted stroke volume difference was defined as a stroke volume difference greater than the upper limit of the normal reference range of stroke volume difference defined in the healthy population. Any participant with a stroke volume difference exceeding this value (13 ml) was excluded.

6.4. RESULTS

6.4.1. BASELINE CHARACTERISTICS

Baseline characteristics of the groups are shown (Table 6.1).

6.4.2. LEFT AND RIGHT VENTRICULAR VOLUMES AND SYSTOLIC FUNCTION

Among MFS subjects *without* shunt or regurgitation, none showed BSA-indexed LVEDV, BSA-indexed LVESV or LVEF below the lower limit of the 95% population confidence interval. No significant differences were found between such subjects with MFS and healthy subjects in LVEDV, BSA-indexed LVEDV, LVESV, BSA-indexed LVESV, or LVEF (Table 6.2). No significant differences were found between such subjects with MFS and healthy subjects in either RVEDV or BSA-indexed RVEDV. RVEF showed a marginally significant 7% increase among subjects with MFS compared to controls (59% MFS v 55% healthy subjects, p=0.03), driven by a marginally significant 15% reduction in RVESV indexed to BSA (33 ml/m2 MFS v 39 ml/m2 healthy subjects, p=0.03).

6.4.3. RELATIONSHIP BETWEEN LVEDV AND REGURGITATION AND/OR SHUNT

Subjects with MFS and increased stroke volume difference (indicating regurgitation and/or shunt) had higher LVEDV than subjects with MFS and no stroke volume difference (mean LVEDV 190 ml for subjects with regurgitation and/or shunt, v 160 ml for subjects without regurgitation and/or shunt, p=0.03).

Table 6.1: Baseline characteristics of subjects.

	MFS No regurgitation/ shunt	**MFS Regurgitation/shunt**	**Healthy subjects**	**Known mitral regurgitation**
n	20	14	33	37
Age (years)	39	31	36	68
M:F	9:11	6:8	18:15	8:29
Height (cm)	185	186	180	173
Weight (kg)	83.1	76	77	76
BSA (kg/m^2)	2.1	2.0	2.0	1.9

Table 6.2: Ventricular parameters in MFS and healthy subjects shown as means with 95% CI in parentheses.

	Marfan Syndrome		**Healthy Subjects**		
	Mean	**SD**	**Mean**	**SD**	**p-value**
LV					
LVEDV (ml)	157 (152 – 162)	21.5	151 (146 – 156)	29.1	0.46
LVEDV index (ml/m²)	76.4 (74.7 – 78.0)	7.5	77.0 (74.9 – 79.0)	11.9	0.84
LVESV (ml)	59.3 (56.5 – 65.1)	12.8	61.0 (58.3 – 63.7)	15.8	0.68
LVESV index (ml/m²)	28.9 (27.7 – 30.1)	5.5	31.0 (29.8 – 32.2)	7.0	0.26
LVEF (%)	62.3 (60.9 – 63.7)	6.3	60.1 (59.2 – 61.0)	5.1	0.17
LV mass (g)	111 (105 – 117)	26.2	111 (106 – 117)	31.0	0.95
LV mass index (g/m²)	53.6 (51.8 – 55.4)	8.2	56.2 (54.1 – 58.3)	12.1	0.39
RV					
RVEDV (ml)	165 (158 – 173)	33.3	165 (160 – 171)	32.6	1.00
RVEDV index (ml/m²)	80.2 (77.6 – 82.8)	11.8	84.0 (81.9 – 86.0)	11.9	0.27
RVESV (ml)	69.0 (64.1 – 73.9)	22.2	76.5 (73.1 – 79.9)	19.5	0.21
RVESV index (ml/m²)	33.4 (31.4 – 35.5)	9.3	38.8 (37.4 – 40.1)	7.9	**0.03**
RVEF (%)	59.0 (57.2 – 60.8)	8.4	54.7 (53.7 – 55.6)	5.4	**0.03**

6.4.4. RELATIONSHIP BETWEEN LVEDV AND REGURGITATION IN SUBJECTS WITH AND WITHOUT MFS

LVEDV was strongly correlated with LV/RV stroke volume difference both among subjects with MFS (Pearson's r=0.75, p=0.0001, Figure 6.1A) and among subjects with MR but no MFS (Pearson's r=0.61, p<0.0005, Figure 6.1B). The degree of correlation did not differ significantly among subjects with regurgitation with and without MFS, but linear regression of the slopes relating stroke volume difference to LVEDV showed a substantially and significantly steeper slope (larger regression coefficient) among subjects with MFS and regurgitation and/or shunt, compared to those with known mitral regurgitation without MFS (regression coefficient 4.0 among subjects with MFS, compared to 1.9 among subjects with MR but no MFS, p=0.027). Findings were similar when the analysis was confined to subjects with matched degrees of stroke volume difference.

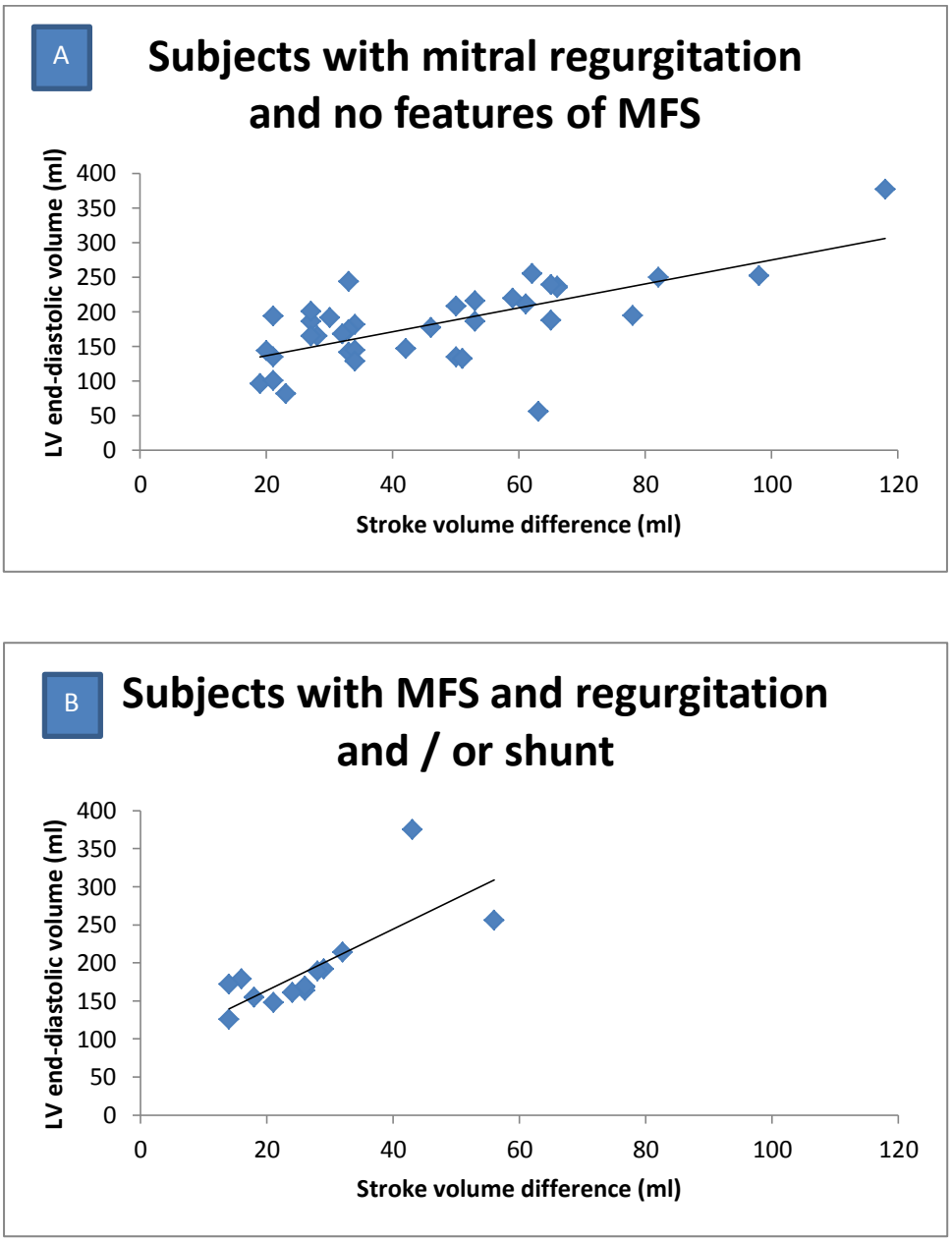

Figure 6.1: Relationship between stroke volume difference and LV end-diastolic volume (LVEDV) in subjects A: with Marfan syndrome (MFS) and B: with mitral regurgitation and with no features of MFS. The scales of the graphs have been selected to allow visual comparison of the degree of dependence of LVEDV on stroke volume between groups.

6.5. DISCUSSION

This work found no evidence for ventricular dilation or impairment of systolic function, and hence for cardiomyopathy, in subjects with MFS in whom valvular regurgitation and shunt had been excluded, and found no significant differences in absolute or BSA-indexed LV volumes or LV function between subjects with MFS and age-, gender- and height-matched controls. Subjects with significant regurgitation and/or shunt, mainly arising as a result of mitral valvular regurgitation as a consequence of mitral valve prolapse, showed increased LVEDV compared to subjects without such regurgitation, and a strong linear relationship was seen between LVEDV and magnitude of stroke volume difference. The dependence of LVEDV on stroke volume difference was more marked in subjects with MFS than for a sample of patients with mitral regurgitation but no features of MFS.

Particular advantages of the methodology used include the use of CMR to quantify LV volumes accurately, rather than using echo estimates of LV volume, which is prone to large exponentiation errors. Stroke volume difference between the right and left ventricles, was used to summarise the degree of both shunt and regurgitation. The advantage of this method is that it is highly reproducible, but the limitation is that it does not allow separation between shunt and regurgitation. Shunt is uncommon among subjects with MFS and was not identified by echocardiography in any subject in this study. Therefore it is likely that differences in stroke volume between LV and RV arose as a result of differences in the severity of mitral regurgitation (aortic regurgitation having been excluded prior to analysis). The interpretation of results allows for this uncertainty.

Savolainen et al (128) evaluated LV dimensions and systolic function by echocardiography in children with MFS without significant valve disease, and found no evidence for LV dilation or impairment of function. Chatrath et al (129) reported similar findings in adults. Meijboom et al (130) found LV dilation in a minority of a large echocardiographically studied cohort, and all three studies reported normal ejection fractions. De Backer et al (114) found reduced ejection fractions (and a trend toward increased volumes) in a small group of MFS patients studied by CMR, and Alpendura et al

(115) found a moderately high prevalence of mild LV systolic dysfunction in patients referred for clinical CMR. De Witte et al (120) observed mild impairments of LV function in their cohort. Kiotsekoglou et al reported impaired LV long axis function (118), LV deformation (116) and LV diastolic function (117), and reduced echocardiographic measures of right ventricular function (119). The interpretation of these studies has been limited by a number of methodological issues, including: small sample sizes of patients, controls or both; limited matching of patients and controls for factors known to influence ventricular dimensions and function; selection bias; incomplete correction for confounding effects of aortic and/or mitral valvular regurgitation or shunting; co-administered beta-blockade, and in some studies the use of echocardiography to estimate volumes and function. The work described here attempts to overcome these limitations using precise CMR methods for the evaluation of volumes and function, in age-, sex- and height-matched groups of patients, in whom beta-blockade was omitted prior to imaging, and in whom significant shunt and regurgitation has been excluded.

The strong relationship between severity of valvular regurgitation estimated by CMR and the degree of LV dilation quantified by CMR derived LVED volumes has recently been described by Uretsky et al (131). The magnitude of the association between LVEDV and regurgitant fraction among subjects with mitral regurgitation described in Uretsky et al was comparable to that described in this work for subjects with mitral regurgitation but without MFS, further supporting the hypothesis that subjects with MFS have larger LVEDV for a given level of regurgitation.

6.5.1. ASPECTS OF METHODOLOGY

The interpretation of these findings should reflect several observations concerning methodology. For the primary analysis, a sample of subjects was defined in whom regurgitant valve lesions were absent. This method, while necessary for the exclusion of valve-related changes in LV volumes, is likely to have defined a sub-group of MFS subjects with particularly mild disease. Conclusions drawn from this mildly affected population may not apply to more severely affected subjects, who could have both

significant valve disease and intrinsic impairment of ventricular function. Nevertheless, the conclusion that MFS subjects without significant valve disease could not be shown to have significantly different LV volumes and function remains valid, as is the assertion that a finding of increased ventricular volumes or apparently impaired systolic function in subjects with MFS should prompt a careful search for other causes, including unrecognised or underestimated regurgitant valve disease and shunt, before such a finding is attributed to MFS alone, particularly in subjects apparently without valvular disease.

A convenience sample of subjects with known mitral regurgitation but no features of MFS was used for the secondary analysis of the dependence of LVEDV on stroke volume difference. These subjects differed in certain baseline characteristics (particularly age) from those with MFS, because of the differing enrolment criteria of the OxValve study from which this population was derived. Results obtained for this secondary analysis could derive from the fact that patients with MFS tend to develop mitral regurgitation at a much younger age than in other conditions which tend to give rise to mitral regurgitation, and that the ventricles are more compliant in response to a volume load when mitral regurgitation begins in childhood or early adulthood. Baseline differences in the population under study may explain these differences but nevertheless can be interpreted as showing that LV volume changes in response to volume loading in subjects with MFS may differ from those commonly seen in mitral regurgitation arising in other contexts.

The analysis of the relationship between the magnitude of regurgitation and/or shunt (estimated by LV/RV stroke volume difference) and LVEDV confirms the importance of carefully identifying and quantifying regurgitation and shunt in clinical or research studies quantifying ventricular volumes and, by extension, ventricular function in MFS. A strong positive correlation between regurgitation severity and LVEDV was found for subjects with and without MFS. This analysis raises the intriguing suggestion that LVEDV may increase by a larger amount for a given degree of stroke volume difference in subjects with MFS and controls. This finding was substantial and statistically significant, and requires verification in other studies, in particular to clarify whether this represents a more

general age-dependent response of the ventricle to LV volume loading, or whether it relates to biological differences in the Marfan ventricle in response to volume loading.

6.6. CONCLUSIONS

This work found no evidence for intrinsic cardiomyopathy in subjects with MFS when valvular regurgitation and shunting were rigorously excluded. Increases in left ventricular volume were found in subjects with MFS in whom mitral regurgitation was present. There was some evidence for an exaggerated left ventricular response to volume loading in subjects with MFS compared to subjects with mitral regurgitation unrelated to MFS, although this finding requires further evaluation in larger studies and may relate to the age of onset of valvular heart disease in subjects with MFS compared to valvular regurgitation due to other causes. Increased ventricular volumes or impaired function in subjects with MFS should prompt a careful search for other causes. Future studies into ventricular function in MFS should report methods by which shunt and regurgitation were excluded or adjusted for.

CHAPTER 7

CONCLUSIONS AND GENERAL OUTLOOK

7.1. SUMMARY OF FINDINGS

This work describes the application of advanced cardiovascular magnetic resonance imaging techniques to the aorta and heart in MFS. Novel sequences were used to visualise the entire flow field of the thoracic aorta, and these datasets were used to demonstrate the high prevalence of aortic flow disturbance in MFS, and to show the anatomical distribution of regions showing disturbed flow. Regions most commonly affected and most severely affected were those in which intimo-medial tears of aortic dissections are known to be most prevalent. These datasets were then used to allow off-line interrogation of the haemodynamic characteristics of particular aortic regions, specifically WSS. Evidence was found for reduced WSS in subjects with MFS compared to matched healthy volunteer controls.

This work then used these comprehensive flow datasets to demonstrate a novel method for the separation and individual interrogation of the three principal components of pressure as defined in the Navier-Stokes equation, which describes the relationship between pressure and flow. The application of this approach to healthy volunteers, and to patients with known abnormalities of aortic geometry and flow, showed disturbances in overall relative pressure, and in the components of relative pressure, in regions known to be affected by disease.

The demonstration of the relative importance of time-varying, transient (unsteady) components of pressure to the total relative pressure gradients within the aorta focused attention on the volumes and function of the left ventricle in subjects with MFS, which is a key determinant of time-varying aortic pressure differences, and explains the proposed mechanism of action of medical therapy in MFS. Evidence for LV impairment was not found, and LV dilation was only seen in the presence of significant valvular regurgitation or shunt, where there was a marked, and perhaps exaggerated, dependence of LVEDV on degree of stroke volume difference between left and right ventricles.

These findings provide insights into the mechanisms of aortic and cardiac disease in subjects with MFS, provide candidate biomarkers of risk for evaluation in future longitudinal studies, and provide potential targets for novel medical and surgical therapies.

7.2. MECHANISMS OF AORTIC DISEASE IN MARFAN SYNDROME

The regional variation in the vulnerability of the aorta to dilation, dissection and rupture is a striking feature of MFS, which has been recognised for many years, but is still not fully understood. The finding that the aorta in MFS is characterised by disturbances in blood flow, reductions in WSS, and changes in relative pressure (at least in a proportion of cases) may have implications for our understanding of the distribution and mechanisms of progression of aortic disease in MFS, as well as the marked inter-individual phenotypic heterogeneity of the condition. The blood flow disturbances and WSS reductions found in this study likely arise, at least in part, as a consequence of early geometric distortions in the MFS aorta. This work proposes that progressive aortic dilation, dissection and rupture are determined by a complex interplay between dysregulated TGFβ-mediated aortic wall signalling, blood flow disturbance, and aortic geometry. Such a model has been proposed for bicuspid aortic valve disease associated aortopathy (79), in which simplistic models characterised by either haemodynamic disturbance or intrinsic aortic dysregulation as the sole cause have been rejected in favour of a more nuanced understanding of the potential for interaction between these factors. Disturbed blood flow regimens impose haemodynamic loads on an inherently vulnerable aorta, and have been shown in vitro to alter numerous aspects of endothelial structure and function including cell shape and cytoskeletal organization, cell growth and apoptosis, cell endocytosis and secretion, and gene expression. The importance of local endothelial dysfunction in determining the regional distribution of aortic disease in MFS is unknown, but recent studies suggest that: (i) a number of transcription factors which are important downstream mediators of TGFβ signalling (e.g. members of the Smad family, ERK 1/2) are biomechanically mediated, for example, by shear-stress responsive promoter elements (87); (ii) endothelium-media interactions play a crucial role in arterial wall homeostasis (85); and (iii) dysregulated endothelial-to-mesenchymal transition (EMT) may be a

particularly important mechanism by which local endothelial dysfunction could lead to the medial 'degeneration' which is the histo-pathological hallmark of MFS (86). The work presented in this thesis suggests a mechanism by which different aortic regions could be differentially sensitive to such dysregulated signalling: endothelium which is responding to differential shear stress signalling may be more vulnerable to dysregulated TGFβ signalling, promoting potentially deleterious EMT. In particular, the often paradoxical nature of TGFβ signalling in aneurysmal disease in vitro (132) could result from directionally opposite TGFβ signalling under different haemodynamic regimens. Future studies linking the haemodynamic findings described in this work to the regional distribution of pathophysiological processes would be of considerable interest, and emerging technology could now allow such studies to be undertaken in small animal models, or in human subjects undergoing aortic surgery.

This work has demonstrated the relative importance of time-varying forces on the overall relative pressure changes in the aorta both in healthy subjects and in those with marked aortic disease. These forces are largely governed by the vigour of left ventricular contraction (as opposed to the spatially-varying forces which are largely governed by aortic geometry). This relative importance of the left ventricle in determining the relative pressure field in the aorta focused attention on left ventricular function in MFS, which has been the subject of a number of conflicting reports in recent years. This work did not find compelling evidence for significant left ventricular cavity dilation, nor impairment of overall systolic function, in subjects with MFS when regurgitation or shunting was carefully excluded. There was a marked increase in LVEDV with increasing degrees of regurgitation, perhaps explaining some of the discrepancies in earlier studies in which methods for excluding regurgitation and shunt were not always clearly described. An exploratory analysis in this work suggested that the response to volume loading in subjects with MFS may be exaggerated compared to populations in whom mitral regurgitation is commonly seen, but further studies including an age-matched control population with mitral regurgitation would be necessary to determine whether this phenomenon is a fundamental feature of MFS, or whether it is a manifestation of the relatively young age at which mitral regurgitation develops in MFS.

7.3. CLINICAL APPLICATION OF 4D FLOW

4D flow CMR is emerging as a powerful tool for the comprehensive evaluation of blood velocity and flow, and a number of derived parameters, including WSS and pressure in the cardiovascular system in a number of research studies. Several obstacles currently limit its suitability for clinical application, including: long acquisition times; complex and time-consuming data processing; and limited data linking qualitative and quantitative findings to pathophysiology and patient outcomes.

Acquisition times are likely to be significantly reduced by developments in hardware, software, and clinical protocols. Hardware developments include the increasing availability of ultra-high field strength (e.g. 7T) CMR systems (133), and advanced coils (134). Software developments include accelerated sequences, which employ, among other techniques, complex k-space under-sampling strategies shown to reduce acquisition time (135). Clinical protocol development will allow optimisation of the trade-off between acquisition time and the extent and detail of data acquired for a particular clinical application. Data processing times have recently been substantially reduced by the introduction of a new generation of post-processing platforms, featuring intuitive graphic user interfaces, and logical workflows (personal communication, A Stalder).

An important determinant of the clinical utility of 4D flow CMR is whether it can be shown to elucidate distinct pathophysiological mechanisms among patients with apparently similar presentations, and whether it can provide information about prognosis, incremental to that which is already available from conventional imaging strategies which are less resource intensive. Studies linking 4D flow CMR to pathophysiological mechanisms and longitudinal studies demonstrating prognosis are essential for the field to gain widespread application in the clinical arena.

Anticipated early clinical applications of 4D flow CMR can be considered to fall broadly into two categories. Firstly, the technique may be of benefit in patients with complex anatomy, in whom flow quantification in multiple locations is required. Here, the use of a 4D flow sequence can allow a single

acquisition, with offline interrogation of flow anywhere within the 4D dataset. Secondly, the technique may allow the risk stratification of patients based on disturbed flow, complex flow, altered WSS, turbulence and pressure, where such parameters can be shown in longitudinal studies to associate with risk.

In summary, it is anticipated that reduced acquisition times, semi-automated post-processing, and optimised clinical protocols for acquisition and processing will make this technique a feasible adjunct to the anatomical and functional imaging CMR techniques currently available, initially in selected patient groups at specialised centres. Further clinical studies defining the role of the technique in different patient groups are necessary to define the patient groups most likely to benefit from this enhanced imaging approach.

REFERENCES

(1) McKusick VA. The cardiovascular aspects of Marfan's syndrome: a heritable disorder of connective tissue. Circulation 1955 Mar;11(3):321-342.

(2) De Backer J. The expanding cardiovascular phenotype of Marfan syndrome. Eur J Echocardiogr 2009 Mar;10(2):213-215.

(3) Karamitsos TD, Neubauer S. Cardiovascular magnetic resonance: a powerful diagnostic and prognostic tool in modern cardiology. Prog Cardiovasc Dis 2011 Nov-Dec;54(3):179-180.

(4) Markl M, Kilner PJ, Ebbers T. Comprehensive 4D velocity mapping of the heart and great vessels by cardiovascular magnetic resonance. J Cardiovasc Magn Reson 2011 Jan 14;13:7.

(5) Pitcher A, Ashby D, Elliott P, Petersen SE. Cardiovascular MRI in clinical trials: expanded applications through novel surrogate endpoints. Heart 2011 Aug;97(16):1286-1292.

(6) Canadas V, Vilacosta I, Bruna I, Fuster V. Marfan syndrome. Part 1: pathophysiology and diagnosis. Nat Rev Cardiol 2010 May;7(5):256-265.

(7) Canadas V, Vilacosta I, Bruna I, Fuster V. Marfan syndrome. Part 2: treatment and management of patients. Nat Rev Cardiol 2010 May;7(5):266-276.

(8) Dietz HC, Cutting GR, Pyeritz RE, Maslen CL, Sakai LY, Corson GM, et al. Marfan syndrome caused by a recurrent de novo missense mutation in the fibrillin gene. Nature 1991 Jul 25;352(6333):337-339.

(9) Dietz HC, Pyeritz RE, Hall BD, Cadle RG, Hamosh A, Schwartz J, et al. The Marfan syndrome locus: confirmation of assignment to chromosome 15 and identification of tightly linked markers at 15q15-q21.3. Genomics 1991 Feb;9(2):355-361.

(10) Marfan AB. Un cas de deformation congenitale des quarte membres plus prononcee aux extremites caracterisee par l'allongement des os avec un certain degre d'amincissement
,
. Bull Mem Soc Med Hop Paris 1896;13:220-226.

(11) Beals RK, Hecht F. Congenital contractural arachnodactyly. A heritable disorder of connective tissue. J Bone Joint Surg Am 1971 Jul;53(5):987-993.

(12) Hecht F, Beals RK. "New" syndrome of congenital contractural arachnodactyly originally described by Marfan in 1896. Pediatrics 1972 Apr;49(4):574-579.

(13) Beighton P, de Paepe A, Danks D, Finidori G, Gedde-Dahl T, Goodman R, et al. International nosology of heritable disorders of connective tissue, Berlin, 1986. Am J Med Genet 1988;29(3):581-594.

(14) De Paepe A, Devereux RB, Dietz HC, Hennekam RC, Pyeritz RE. Revised diagnostic criteria for the Marfan syndrome. Am J Med Genet 1996 Apr 24;62(4):417-426.

(15) Loeys BL, Dietz HC, Braverman AC, Callewaert BL, De Backer J, Devereux RB, et al. The revised Ghent nosology for the Marfan syndrome. J Med Genet 2010 Jul;47(7):476-485.

(16) Hiratzka LF, Bakris GL, Beckman JA, Bersin RM, Carr VF, Casey DE,Jr, et al. 2010 ACCF/AHA/AATS/ACR/ASA/SCA/SCAI/SIR/STS/SVM guidelines for the diagnosis and management of patients with Thoracic Aortic Disease: a report of the American College of Cardiology Foundation/American Heart Association Task Force on Practice Guidelines, American Association for Thoracic Surgery, American College of Radiology, American Stroke Association, Society of Cardiovascular Anesthesiologists, Society for Cardiovascular Angiography and Interventions, Society of Interventional Radiology, Society of Thoracic Surgeons, and Society for Vascular Medicine. Circulation 2010 Apr 6;121(13):e266-369.

(17) Kainulainen K, Savolainen A, Palotie A, Kaitila I, Rosenbloom J, Peltonen L. Marfan syndrome: exclusion of genetic linkage to five genes coding for connective tissue components in the long arm of chromosome 2. Hum Genet 1990 Feb;84(3):233-236.

(18) Blanton SH, Sarfarazi M, Eiberg H, de Groote J, Farndon PA, Kilpatrick MW, et al. An exclusion map of Marfan syndrome. J Med Genet 1990 Feb;27(2):73-77.

(19) Sakai LY, Keene DR, Engvall E. Fibrillin, a new 350-kD glycoprotein, is a component of extracellular microfibrils. J Cell Biol 1986 Dec;103(6 Pt 1):2499-2509.

(20) Kainulainen K, Pulkkinen L, Savolainen A, Kaitila I, Peltonen L. Location on chromosome 15 of the gene defect causing Marfan syndrome. N Engl J Med 1990 Oct 4;323(14):935-939.

(21) Ramirez F, Dietz HC. Extracellular microfibrils in vertebrate development and disease processes. J Biol Chem 2009 May 29;284(22):14677-14681.

(22) Ramirez F, Rifkin DB. Extracellular microfibrils: contextual platforms for TGFbeta and BMP signaling. Curr Opin Cell Biol 2009 Oct;21(5):616-622.

(23) Ramirez F, Dietz HC. Marfan syndrome: from molecular pathogenesis to clinical treatment. Curr Opin Genet Dev 2007 Jun;17(3):252-258.

(24) Habashi JP, Judge DP, Holm TM, Cohn RD, Loeys BL, Cooper TK, et al. Losartan, an AT1 antagonist, prevents aortic aneurysm in a mouse model of Marfan syndrome. Science 2006 Apr 7;312(5770):117-121.

(25) Neptune ER, Frischmeyer PA, Arking DE, Myers L, Bunton TE, Gayraud B, et al. Dysregulation of TGF-beta activation contributes to pathogenesis in Marfan syndrome. Nat Genet 2003 Mar;33(3):407-411.

(26) Brooke BS, Habashi JP, Judge DP, Patel N, Loeys B, Dietz HC,3rd. Angiotensin II blockade and aortic-root dilation in Marfan's syndrome. N Engl J Med 2008 Jun 26;358(26):2787-2795.

(27) Matt P, Schoenhoff F, Habashi J, Holm T, Van Erp C, Loch D, et al. Circulating transforming growth factor-beta in Marfan syndrome. Circulation 2009 Aug 11;120(6):526-532.

(28) Matt P, Habashi J, Carrel T, Cameron DE, Van Eyk JE, Dietz HC. Recent advances in understanding Marfan syndrome: should we now treat surgical patients with losartan? J Thorac Cardiovasc Surg 2008 Feb;135(2):389-394.

(29) Wolf G, Mueller E, Stahl RA, Ziyadeh FN. Angiotensin II-induced hypertrophy of cultured murine proximal tubular cells is mediated by endogenous transforming growth factor-beta. J Clin Invest 1993 Sep;92(3):1366-1372.

(30) Fukuda N, Hu WY, Kubo A, Endoh M, Kishioka H, Satoh C, et al. Abnormal regulation of transforming growth factor-beta receptors on vascular smooth muscle cells from spontaneously hypertensive rats by angiotensin II. Hypertension 1998 Feb;31(2):672-677.

(31) Khan R, Sheppard R. Fibrosis in heart disease: understanding the role of transforming growth factor-beta in cardiomyopathy, valvular disease and arrhythmia. Immunology 2006 May;118(1):10-24.

(32) Detaint D, Aegerter P, Tubach F, Hoffman I, Plauchu H, Dulac Y, et al. Rationale and design of a randomized clinical trial (Marfan Sartan) of angiotensin II receptor blocker therapy versus placebo in individuals with Marfan syndrome. Arch Cardiovasc Dis 2010 May;103(5):317-325.

(33) Gambarin FI, Favalli V, Serio A, Regazzi M, Pasotti M, Klersy C, et al. Rationale and design of a trial evaluating the effects of losartan vs. nebivolol vs. the association of both on the progression of aortic root dilation in Marfan syndrome with FBN1 gene mutations. J Cardiovasc Med (Hagerstown) 2009 Apr;10(4):354-362.

(34) Lacro RV, Dietz HC, Wruck LM, Bradley TJ, Colan SD, Devereux RB, et al. Rationale and design of a randomized clinical trial of beta-blocker therapy (atenolol) versus angiotensin II receptor blocker therapy (losartan) in individuals with Marfan syndrome. Am Heart J 2007 Oct;154(4):624-631.

(35) Radonic T, de Witte P, Baars MJ, Zwinderman AH, Mulder BJ, Groenink M, et al. Losartan therapy in adults with Marfan syndrome: study protocol of the multi-center randomized controlled COMPARE trial. Trials 2010 Jan 12;11:3.

(36) Mimoun L, Detaint D, Hamroun D, Arnoult F, Delorme G, Gautier M, et al. Dissection in Marfan syndrome: the importance of the descending aorta. Eur Heart J 2010 Dec 8.

(37) Nollen GJ, van Schijndel KE, Timmermans J, Groenink M, Barentsz JO, van der Wall EE, et al. Pulmonary artery root dilatation in Marfan syndrome: quantitative assessment of an unknown criterion. Heart 2002 May;87(5):470-471.

(38) Rybczynski M, Mir TS, Sheikhzadeh S, Bernhardt AM, Schad C, Treede H, et al. Frequency and age-related course of mitral valve dysfunction in the Marfan syndrome. Am J Cardiol 2010 Oct 1;106(7):1048-1053.

(39) Murdoch JL, Walker BA, Halpern BL, Kuzma JW, McKusick VA. Life expectancy and causes of death in the Marfan syndrome. N Engl J Med 1972 Apr 13;286(15):804-808.

(40) Silverman DI, Burton KJ, Gray J, Bosner MS, Kouchoukos NT, Roman MJ, et al. Life expectancy in the Marfan syndrome. Am J Cardiol 1995 Jan 15;75(2):157-160.

(41) WRITING GROUP MEMBERS, Hiratzka LF, Bakris GL, Beckman JA, Bersin RM, Carr VF, et al. 2010 ACCF/AHA/AATS/ACR/ASA/SCA/SCAI/SIR/STS/SVM Guidelines for the Diagnosis and Management of Patients With Thoracic Aortic Disease. Circulation 2010 April 06;121(13):e266-e369.

(42) Meijboom LJ, Timmermans J, Zwinderman AH, Engelfriet PM, Mulder BJ. Aortic root growth in men and women with the Marfan's syndrome. Am J Cardiol 2005 Nov 15;96(10):1441-1444.

(43) Jondeau G, Boutouyrie P, Lacolley P, Laloux B, Dubourg O, Bourdarias JP, et al. Central pulse pressure is a major determinant of ascending aorta dilation in Marfan syndrome. Circulation 1999 May 25;99(20):2677-2681.

(44) Groenink M, FAU - de Roos A, de Roos A, FAU - Mulder BJ, Mulder BJ, FAU - Spaan JA, et al. Changes in aortic distensibility and pulse wave velocity assessed with magnetic resonance imaging following beta-blocker therapy in the Marfan syndrome. - Am J Cardiol.1998 Jul 15;82(2):203-8. (0002-9149 (Print); 0002-9149 (Linking)).

(45) Pitcher A, Emberson J, Baigent et al. A prototcol for a prospective, collaborative, meta-analysis of all randomised controlled trials of ARB therapy in Marfan syndrome, based on individual patient data. In preparation .

(46) Pennell DJ. Cardiovascular magnetic resonance. Circulation 2010 Feb 9;121(5):692-705.

(47) De Backer J. Cardiovascular characteristics in Marfan syndrome and their relation to the genotype. Verh K Acad Geneeskd Belg 2009;71(6):335-371.

(48) Shores J, Berger KR, Murphy EA, Pyeritz RE. Progression of aortic dilatation and the benefit of long-term beta-adrenergic blockade in Marfan's syndrome. N Engl J Med 1994 May 12;330(19):1335-1341.

(49) Gersony DR, McClaughlin MA, Jin Z, Gersony WM. The effect of beta-blocker therapy on clinical outcome in patients with Marfan's syndrome: a meta-analysis. Int J Cardiol 2007 Jan 18;114(3):303-308.

(50) Ahimastos AA, FAU - Aggarwal A, Aggarwal A, FAU - D'Orsa KM, D'Orsa KM, FAU - Formosa MF, et al. Effect of perindopril on large artery stiffness and aortic root diameter in patients with Marfan syndrome: a randomized controlled trial. - JAMA.2007 Oct 3;298(13):1539-47. (1538-3598 (Electronic); 0098-7484 (Linking)).

(51) Lacro RV, Dietz HC, Wruck LM, Bradley TJ, Colan SD, Devereux RB, et al. Rationale and design of a randomized clinical trial of beta-blocker therapy (atenolol) versus angiotensin II receptor blocker therapy (losartan) in individuals with Marfan syndrome. Am Heart J 2007 Oct;154(4):624-631.

(52) AIMS Trial. http://www.controlled-trials.com/ISRCTN90011794/marfan. Accessed 05/22, 2011.

(53) Moberg K, De Nobele S, Devos D, Goetghebeur E, Segers P, Trachet B, et al. The Ghent Marfan Trial - A randomized, double-blind placebo controlled trial with losartan in Marfan patients treated with beta-blockers. Int J Cardiol 2011 Jan 14.

(54) Forteza A, Evangelista A, Sanchez V, Teixido G, Garcia D, Sanz P, et al. Study of the efficacy and safety of losartan versus atenolol for aortic dilation in patients with Marfan syndrome. Rev Esp Cardiol 2011 Jun;64(6):492-498.

(55) Radonic T, de Witte P, Baars MJ, Zwinderman AH, Mulder BJ, Groenink M, et al. Losartan therapy in adults with Marfan syndrome: study protocol of the multi-center randomized controlled COMPARE trial. Trials 2010 Jan 12;11:3.

(56) Taiwan Trial. http://clinicaltrials.gov/ct2/show/NCT00651235?term=marfan+angiotensin&rank=4. Accessed 05/22, 2011.

(57) Birks EJ, Webb C, Child A, Radley-Smith R, Yacoub MH. Early and long-term results of a valve-sparing operation for Marfan syndrome. Circulation 1999 Nov 9;100(19 Suppl):II29-35.

(58) David TE, Feindel CM. An aortic valve-sparing operation for patients with aortic incompetence and aneurysm of the ascending aorta. J Thorac Cardiovasc Surg 1992 Apr;103(4):617-21; discussion 622.

(59) Pepper J, John Chan K, Gavino J, Golesworthy T, Mohiaddin R, Treasure T. External aortic root support for Marfan syndrome: early clinical results in the first 20 recipients with a bespoke implant. J R Soc Med 2010 Sep;103(9):370-375.

(60) Pearson GD, Devereux R, Loeys B, Maslen C, Milewicz D, Pyeritz R, et al. Report of the National Heart, Lung, and Blood Institute and National Marfan Foundation Working Group on research in Marfan syndrome and related disorders. Circulation 2008 Aug 12;118(7):785-791.

(61) Hartog AW, Franken R, Zwinderman AH, Groenink M, Mulder BJ. Current and future pharmacological treatment strategies with regard to aortic disease in Marfan syndrome. Expert Opin Pharmacother 2012 Apr;13(5):647-662.

(62) Dietz HC. New therapeutic approaches to mendelian disorders. N Engl J Med 2010 Aug 26;363(9):852-863.

(63) Hudsmith LE, Neubauer S. Magnetic resonance spectroscopy in myocardial disease. JACC Cardiovasc Imaging 2009 Jan;2(1):87-96.

(64) Rodgers CT, Robson MD. Cardiovascular magnetic resonance: physics and terminology. Prog Cardiovasc Dis 2011 Nov-Dec;54(3):181-190.

(65) Gatehouse PD, Keegan J, Crowe LA, Masood S, Mohiaddin RH, Kreitner KF, et al. Applications of phase-contrast flow and velocity imaging in cardiovascular MRI. Eur Radiol 2005 Oct;15(10):2172-2184.

(66) Markl M, Harloff A, Bley TA, Zaitsev M, Jung B, Weigang E, et al. Time-resolved 3D MR velocity mapping at 3T: improved navigator-gated assessment of vascular anatomy and blood flow. J Magn Reson Imaging 2007 Apr;25(4):824-831.

(67) Frydrychowicz A, Stalder AF, Russe MF, Bock J, Bauer S, Harloff A, et al. Three-dimensional analysis of segmental wall shear stress in the aorta by flow-sensitive four-dimensional-MRI. J Magn Reson Imaging 2009 Jul;30(1):77-84.

(68) Harloff A, Nussbaumer A, Bauer S, Stalder AF, Frydrychowicz A, Weiller C, et al. In vivo assessment of wall shear stress in the atherosclerotic aorta using flow-sensitive 4D MRI. Magn Reson Med 2010 Jun;63(6):1529-1536.

(69) Markl M, Wallis W, Strecker C, Gladstone BP, Vach W, Harloff A. Analysis of pulse wave velocity in the thoracic aorta by flow-sensitive four-dimensional MRI: reproducibility and correlation with characteristics in patients with aortic atherosclerosis. J Magn Reson Imaging 2012 May;35(5):1162-1168.

(70) Frydrychowicz A, Berger A, Russe MF, Stalder AF, Harloff A, Dittrich S, et al. Time-resolved magnetic resonance angiography and flow-sensitive 4-dimensional magnetic resonance imaging at 3 Tesla for blood flow and wall shear stress analysis. J Thorac Cardiovasc Surg 2008 Aug;136(2):400-407.

(71) Frydrychowicz A, Berger A, Munoz Del Rio A, Russe MF, Bock J, Harloff A, et al. Interdependencies of aortic arch secondary flow patterns, geometry, and age analysed by 4-

dimensional phase contrast magnetic resonance imaging at 3 Tesla. Eur Radiol 2012 May;22(5):1122-1130.

(72) Harloff A, FAU - Simon J, Simon J, FAU - Brendecke S, Brendecke S, FAU - Assefa D, et al. Complex plaques in the proximal descending aorta: an underestimated embolic source of stroke. - Stroke.2010 Jun;41(6):1145-50.Epub 2010 Apr 29. (1524-4628 (Electronic); 0039-2499 (Linking)).

(73) World Medical Association. Available at: http://www.wma.net/en/30publications/10policies/b3/index.html.

(74) Keys A, Fidanza F, Karvonen MJ, Kimura N, Taylor HL. Indices of relative weight and obesity. J Chronic Dis 1972 Jul 1;25(6):329-343.

(75) DuBois D DE. A formula to estimate the approximate surface area if height and weight be known. Arch Intern Medicine 1916;17:863-871.

(76) Markl M, Frydrychowicz A, Kozerke S, Hope M, Wieben O. 4D flow MRI. Journal of Magnetic Resonance Imaging 2012;36(5):spcone-spcone.

(77) Geiger J, Markl M, Herzer L, Hirtler D, Loeffelbein F, Stiller B, et al. Aortic flow patterns in patients with Marfan syndrome assessed by flow-sensitive four-dimensional MRI. J Magn Reson Imaging 2012 Mar;35(3):594-600.

(78) Frydrychowicz A, Markl M, Hirtler D, Harloff A, Schlensak C, Geiger J, et al. Aortic hemodynamics in patients with and without repair of aortic coarctation: in vivo analysis by 4D flow-sensitive magnetic resonance imaging. Invest Radiol 2011 May;46(5):317-325.

(79) Barker AJ, Markl M. The role of hemodynamics in bicuspid aortic valve disease. Eur J Cardiothorac Surg 2011 Jun;39(6):805-806.

(80) Stalder AF, Frydrychowicz A, Russe MF, Korvink JG, Hennig J, Li K, et al. Assessment of flow instabilities in the healthy aorta using flow-sensitive MRI. J Magn Reson Imaging 2011 Apr;33(4):839-846.

(81) Markl M, Wallis W, Harloff A. Reproducibility of flow and wall shear stress analysis using flow-sensitive four-dimensional MRI. J Magn Reson Imaging 2011 Apr;33(4):988-994.

(82) Shaaban AM, Duerinckx AJ. Wall shear stress and early atherosclerosis: a review. AJR Am J Roentgenol 2000 Jun;174(6):1657-1665.

(83) Weinberg PD, Ross Ethier C. Twenty-fold difference in hemodynamic wall shear stress between murine and human aortas. J Biomech 2007;40(7):1594-1598.

(84) Rossi J, Rouleau L, Emmott A, Tardif J, Leask RL. Laminar shear stress prevents simvastatin-induced adhesion molecule expression in cytokine activated endothelial cells. Eur J Pharmacol 2010 12/15;649(1-3):268-276.

(85) Chiu J, Chien S. Effects of Disturbed Flow on Vascular Endothelium: Pathophysiological Basis and Clinical Perspectives. Physiological Reviews 2011 January 01;91(1):327-387.

(86) Lindsay ME, Dietz HC. Lessons on the pathogenesis of aneurysm from heritable conditions. Nature 2011 May 19;473(7347):308-316.

(87) Brown JD, DiChiara MR, Anderson KR, Gimbrone MA,Jr, Topper JN. MEKK-1, a component of the stress (stress-activated protein kinase/c-Jun N-terminal kinase) pathway, can selectively activate Smad2-mediated transcriptional activation in endothelial cells. J Biol Chem 1999 Mar 26;274(13):8797-8805.

(88) Shepherd RD, Kos SM, Rinker KD. Flow-dependent Smad2 phosphorylation and TGIF nuclear localization in human aortic endothelial cells. Am J Physiol Heart Circ Physiol 2011 Jul;301(1):H98-H107.

(89) Cecchi E, Giglioli C, Valente S, Lazzeri C, Gensini GF, Abbate R, et al. Role of hemodynamic shear stress in cardiovascular disease. Atherosclerosis 2011 Feb;214(2):249-256.

(90) Masaryk AM, Frayne R, Unal O, Krupinski E, Strother CM. In vitro and in vivo comparison of three MR measurement methods for calculating vascular shear stress in the internal carotid artery. AJNR Am J Neuroradiol 1999 Feb;20(2):237-245.

(91) Morgan VL, Graham TP,Jr, Roselli RJ, Lorenz CH. Alterations in pulmonary artery flow patterns and shear stress determined with three-dimensional phase-contrast magnetic resonance imaging in Fontan patients. J Thorac Cardiovasc Surg 1998 Aug;116(2):294-304.

(92) Wu SP, Ringgaard S, Oyre S, Hansen MS, Rasmus S, Pedersen EM. Wall shear rates differ between the normal carotid, femoral, and brachial arteries: an in vivo MRI study. J Magn Reson Imaging 2004 Feb;19(2):188-193.

(93) Cheng CP, Herfkens RJ, Taylor CA. Inferior vena caval hemodynamics quantified in vivo at rest and during cycling exercise using magnetic resonance imaging. Am J Physiol Heart Circ Physiol 2003 Apr;284(4):H1161-7.

(94) Barker AJ, Lanning C, Shandas R. Quantification of hemodynamic wall shear stress in patients with bicuspid aortic valve using phase-contrast MRI. Ann Biomed Eng 2010 Mar;38(3):788-800.

(95) Stalder AF, Russe MF, Frydrychowicz A, Bock J, Hennig J, Markl M. Quantitative 2D and 3D phase contrast MRI: optimized analysis of blood flow and vessel wall parameters. Magn Reson Med 2008 Nov;60(5):1218-1231.

(96) Hope MD, Hope TA, Crook SE, Ordovas KG, Urbania TH, Alley MT, et al. 4D flow CMR in assessment of valve-related ascending aortic disease. JACC Cardiovasc Imaging 2011 Jul;4(7):781-787.

(97) Bieging ET, Frydrychowicz A, Wentland A, Landgraf BR, Johnson KM, Wieben O, et al. In vivo three-dimensional MR wall shear stress estimation in ascending aortic dilatation. J Magn Reson Imaging 2011 Mar;33(3):589-597.

(98) Geiger J, Arnold R, Herzer L, Hirtler D, Stankovic Z, Russe M, et al. Aortic wall shear stress in Marfan syndrome. Magn Reson Med 2012 Nov 20.

(99) Krittian SB, Lamata P, Michler C, Nordsletten DA, Bock J, Bradley CP, et al. A finite-element approach to the direct computation of relative cardiovascular pressure from time-resolved MR velocity data. Med Image Anal 2012 Jul;16(5):1029-1037.

(100) Bock J, Frydrychowicz A, Lorenz R, Hirtler D, Barker AJ, Johnson KM, et al. In vivo noninvasive 4D pressure difference mapping in the human aorta: Phantom comparison and application in healthy volunteers and patients. Magn Reson Med 2011 Mar 24.

(101) Lee, TC, Kashyap RL, Chu CN . Building skeleton models via 3-d medial surface axis thinning algorithms. CVGIP-GRAPHICAL MODELS AND IMAGE PROCESSING 1994.;56(6):462-478.

(102) Canic S, Kim E. "Mathematical analysis of the quasilinear effects in a hyperbolic model blood flow through compliant axi-symmetric vessels. MATHEMATICAL METHODS IN THE APPLIED SCIENCES 2003;26(14):1161-1186.

(103) Dyverfeldt P, Kvitting JP, Sigfridsson A, Engvall J, Bolger AF, Ebbers T. Assessment of fluctuating velocities in disturbed cardiovascular blood flow: in vivo feasibility of generalized phase-contrast MRI. J Magn Reson Imaging 2008 Sep;28(3):655-663.

(104) McDonald DA. The relation of pulsatile pressure to flow in arteries. J Physiol 1955 Mar 28;127(3):533-552.

(105) Karamanoglu M, O'Rourke MF, Avolio AP, Kelly RP. An analysis of the relationship between central aortic and peripheral upper limb pressure waves in man. Eur Heart J 1993 Feb;14(2):160-167.

(106) Song SM, Leahy RM, Boyd DP, Brundage BH, Napel S. Determining cardiac velocity fields and intraventricular pressure distribution from a sequence of ultrafast CT cardiac images. IEEE Trans Med Imaging 1994;13(2):386-397.

(107) Yang GZ, Kilner PJ, Wood NB, Underwood SR, Firmin DN. Computation of flow pressure fields from magnetic resonance velocity mapping. Magn Reson Med 1996 Oct;36(4):520-526.

(108) Tyszka JM, Laidlaw DH, Asa JW, Silverman JM. Three-dimensional, time-resolved (4D) relative pressure mapping using magnetic resonance imaging. J Magn Reson Imaging 2000 Aug;12(2):321-329.

(109) Ebbers T, Wigstrom L, Bolger AF, Engvall J, Karlsson M. Estimation of relative cardiovascular pressures using time-resolved three-dimensional phase contrast MRI. Magn Reson Med 2001 May;45(5):872-879.

(110) Ebbers T, Farneback G. Improving computation of cardiovascular relative pressure fields from velocity MRI. J Magn Reson Imaging 2009 Jul;30(1):54-61.

(111) Lum DP, Johnson KM, Paul RK, Turk AS, Consigny DW, Grinde JR, et al. Transstenotic pressure gradients: measurement in swine--retrospectively ECG-gated 3D phase-contrast MR angiography versus endovascular pressure-sensing guidewires. Radiology 2007 Dec;245(3):751-760.

(112) Yeboah J, Rodriguez CJ, Stacey B, Lima JA, Liu S, Carr JJ, et al. Prognosis of Individuals with Asymptomatic Left Ventricular Systolic Dysfunction in the Multi-Ethnic Study of Atherosclerosis (MESA). Circulation 2012 Nov 2.

(113) Catalano O, Moro G, Perotti M, Frascaroli M, Ceresa M, Antonaci S, et al. Late gadolinium enhancement by cardiovascular magnetic resonance is complementary to left ventricle ejection fraction in predicting prognosis of patients with stable coronary artery disease. J Cardiovasc Magn Reson 2012 May 19;14:29-429X-14-29.

(114) De Backer JF, Devos D, Segers P, Matthys D, Francois K, Gillebert TC, et al. Primary impairment of left ventricular function in Marfan syndrome. Int J Cardiol 2006 Oct 10;112(3):353-358.

(115) Alpendurada F, Wong J, Kiotsekoglou A, Banya W, Child A, Prasad SK, et al. Evidence for Marfan cardiomyopathy. Eur J Heart Fail 2010 Oct;12(10):1085-1091.

(116) Kiotsekoglou A, Saha S, Moggridge JC, Kapetanakis V, Govindan M, Alpendurada F, et al. Impaired biventricular deformation in Marfan syndrome: a strain and strain rate study in adult unoperated patients. Echocardiography 2011 Apr;28(4):416-430.

(117) Kiotsekoglou A, Moggridge JC, Bijnens BH, Kapetanakis V, Alpendurada F, Mullen MJ, et al. Biventricular and atrial diastolic function assessment using conventional echocardiography and tissue-Doppler imaging in adults with Marfan syndrome. Eur J Echocardiogr 2009 Dec;10(8):947-955.

(118) Kiotsekoglou A, Saha SK, Moggridge JC, Kapetanakis V, Bijnens BH, Mullen MJ, et al. Effect of aortic stiffness on left ventricular long-axis systolic function in adults with Marfan syndrome. Hellenic J Cardiol 2010 Nov-Dec;51(6):501-511.

(119) Kiotsekoglou A, Sutherland GR, Moggridge JC, Kapetanakis V, Bajpai A, Bunce N, et al. Impaired right ventricular systolic function demonstrated by reduced atrioventricular plane displacement in adults with Marfan syndrome. Eur J Echocardiogr 2009 Mar;10(2):295-302.

(120) de Witte P, Aalberts JJ, Radonic T, Timmermans J, Scholte AJ, Zwinderman AH, et al. Intrinsic biventricular dysfunction in Marfan syndrome. Heart 2011 Dec;97(24):2063-2068.

(121) Yetman AT, Bornemeier RA, McCrindle BW. Long-term outcome in patients with Marfan syndrome: is aortic dissection the only cause of sudden death? J Am Coll Cardiol 2003 Jan 15;41(2):329-332.

(122) Cameron DE, Alejo DE, Patel ND, Nwakanma LU, Weiss ES, Vricella LA, et al. Aortic root replacement in 372 Marfan patients: evolution of operative repair over 30 years. Ann Thorac Surg 2009 May;87(5):1344-9; discussion 1349-50.

(123) Brand T, Schneider MD. The TGF beta superfamily in myocardium: ligands, receptors, transduction, and function. J Mol Cell Cardiol 1995 Jan;27(1):5-18.

(124) Pauschinger M, Knopf D, Petschauer S, Doerner A, Poller W, Schwimmbeck PL, et al. Dilated cardiomyopathy is associated with significant changes in collagen type I/III ratio. Circulation 1999 Jun 1;99(21):2750-2756.

(125) Judge DP, Rouf R, Habashi J, Dietz HC. Mitral valve disease in Marfan syndrome and related disorders. J Cardiovasc Transl Res 2011 Dec;4(6):741-747.

(126) Ng CM, Cheng A, Myers LA, Martinez-Murillo F, Jie C, Bedja D, et al. TGF-beta-dependent pathogenesis of mitral valve prolapse in a mouse model of Marfan syndrome. J Clin Invest 2004 Dec;114(11):1586-1592.

(127) Lima SD, Lima JA, Pyeritz RE, Weiss JL. Relation of mitral valve prolapse to left ventricular size in Marfan's syndrome. Am J Cardiol 1985 Mar 1;55(6):739-743.

(128) Savolainen A, Nisula L, Keto P, Hekali P, Viitasalo M, Kaitila I, et al. Left ventricular function in children with the Marfan syndrome. Eur Heart J 1994 May;15(5):625-630.

(129) Chatrath R, Beauchesne LM, Connolly HM, Michels VV, Driscoll DJ. Left ventricular function in the Marfan syndrome without significant valvular regurgitation. Am J Cardiol 2003 Apr 1;91(7):914-916.

(130) Meijboom LJ, Timmermans J, van Tintelen JP, Nollen GJ, De Backer J, van den Berg MP, et al. Evaluation of left ventricular dimensions and function in Marfan's syndrome without significant valvular regurgitation. Am J Cardiol 2005 Mar 15;95(6):795-797.

(131) Uretsky S, Supariwala A, Nidadovolu P, Khokhar SS, Comeau C, Shubayev O, et al. Quantification of left ventricular remodeling in response to isolated aortic or mitral regurgitation. J Cardiovasc Magn Reson 2010 May 24;12:32.

(132) Dietz HC. TGF-beta in the pathogenesis and prevention of disease: a matter of aneurysmic proportions. J Clin Invest 2010 Feb 1;120(2):403-407.

(133) Suttie JJ, Delabarre L, Pitcher A, van de Moortele PF, Dass S, Snyder CJ, et al. 7 Tesla (T) human cardiovascular magnetic resonance imaging using FLASH and SSFP to assess cardiac function: validation against 1.5 T and 3 T. NMR Biomed 2012 Jan;25(1):27-34.

(134) Stalder AF, Dong Z, Yang Q, Bock J, Hennig J, Markl M, et al. Four-dimensional flow-sensitive MRI of the thoracic aorta: 12- versus 32-channel coil arrays. J Magn Reson Imaging 2012 Jan;35(1):190-195.

(135) Jung B, Stalder AF, Bauer S, Markl M. On the undersampling strategies to accelerate time-resolved 3D imaging using k-t-GRAPPA. Magn Reson Med 2011 Oct;66(4):966-975.